# Turbo-Like Coding for Spread-Spectrum Communications

A Thesis
Presented to
The Academic Faculty

by

**Hasung Kim**

In Partial Fulfillment
of the Requirements for the Degree
Doctor of Philosophy

School of Electrical and Computer Engineering
Georgia Institute of Technology
September 2004

# Turbo-Like Coding for Spread-Spectrum Communications

Approved by:

Professor Gordon L. Stüber, Advisor

Professor Faramarz Fekri

Professor Nikil S. Jayant

Professor Alfred D. Andrew
School of Mathematics

Professor Ye (Geoffrey) Li

Date Approved: September 16, 2004

*To my parents, Sungkoo Kim and Dukhwa Jung, and my wife, Youngwon Kim, without who I would not be at this point in my life.*

# ACKNOWLEDGEMENTS

I would like to express my deep appreciation to my advisor, Dr. Gordon Stüber. His guidance and expertise was invaluable to me during my graduate study. I would also like to thank the remaining members of my thesis committee, Dr. Nikil Jayant, Dr. Ye (Geoffrey) Li, Dr. Faramarz Fekri, and Dr. Alfred Andrew for their interest and input into my reseach. Their thoughtful advice and encouragement was greatly treasured.

I would like to thank current and previous labmates of Wireless Systems Laboratory including Wajih Abu-Al-Saud, Galib Asadullah, Jinsoup Jung, Heewon Kang, Dukhyun Kim, Joonbeom Kim, Kihong Kim, John Kim, Apurva Mody, Krishna Narayanan, Jun Tan, and Qing Zhao, and colleagues of Telecom group including who discussed with me about research and provided a fun and enjoyable environment to work.

Finally, I am especially grateful to my beloved wife, Youngwon Kim, and my parents, Sungkoo Kim and Dukhwa Jung, for providing me with enduring love, unselfish sacrifice, and heartful encouragement throughout my life and opportunity to fulfill all of my academic endeavors.

# TABLE OF CONTENTS

# LIST OF TABLES

# LIST OF FIGURES

# LIST OF ABBREVIATIONS

| | |
|---|---|
| 3GPP | 3rd generation partnership project |
| AEC | Adaptive error control |
| AJ | Anti-jam |
| AMC | Adaptive modulation and coding |
| APP | *a posteriori* probability |
| ARQ | Automatic repeat request |
| AWGN | Additive white Gaussian noise |
| BER | Bit error rate |
| BICM | Bit-interleaved coded modulation |
| BPSK | Binary phase-shift keying |
| CC | Convolutional code |
| CDMA | Code division multiple access |
| COWEF | Conditional output weight enumerating function |
| CPE | Continuous phase encoder |
| CPFSK | Continuous phase frequency-shift keying |
| CPM | Continuous phase modulation |
| CRC | Cyclic redundancy check |
| CSI | Channel side information |
| DE | Density evolution |
| DPSK | Differential phase-shift keying |
| DS | Direct-sequence |
| DSL | Digital subscriber line |
| DVB | Digital video broadcasting |
| FEC | Forward error correction |
| FER | Frame error rate |

| | |
|---|---|
| FH | Frequency-hopping |
| FSK | Frequency-shift keying |
| HARQ | Hybrid-ARQ |
| HSDPA | High speed downlink packet access |
| ID | Iterative decoding |
| IDD | Iterative demodulation and decoding |
| IGE | Interleaving gain exponent |
| IOWEF | Input-output weight enumerating function |
| IP | Internet protocol |
| JSI | Jammer state information |
| LDPC | Low-density parity-check |
| LLR | Log-likelihood ratio |
| LPD | Low-probability of detection |
| LPI | Low-probability of intercept |
| MAI | Multiple access interference |
| MAP | Maximum *a posteriori* |
| MCC | Mixed concatenated code |
| MHCPM | Multi-h CPM |
| MIMO | Multiple-input multiple-output |
| MIS | Modulation index set |
| ML | Maximum-likelihood |
| MM | Memoryless modulator |
| MNSED | Minimum normalized squared Euclidean distance |
| MSK | Minimum-shift keying |
| OFDM | Orthogonal frequency division multiplexing |
| PBNJ | Partial-band noise jamming |
| PCCC | Parallel concatenated convolutional code |
| PDF | Probability density function |
| PEP | Pairwise error probability |

| | |
|---|---|
| PN | Pseudo-noise |
| PNJ | Pulse-noise jamming |
| QoS | Quality of service |
| QPSK | Quadrature phase-shift keying |
| RA | Repeat-accumulate |
| RCPC | Rate compatible punctured convolutional |
| RCPS | Rate compatible punctured SCCC |
| RCPT | Rate compatible punctured turbo |
| RS | Reed-Solomon |
| RSC | Recursive systematic convolutional |
| SCBC | Serially concatenated block code |
| SCCC | Serially concatenated convolutional code |
| SISO | Soft-input soft-output |
| SNR | Signal-to-noise ratio |
| SOVA | Soft-output Viterbi algorithm |
| SS | Spread-spectrum |
| TLC | Turbo-like code |
| TLCM | Turbo-like coded modulation |
| TPC | Turbo product code |
| UWB | Ultra-wideband |
| W-CDMA | Wideband-CDMA |
| WEF | Weight enumerating function |
| WLAN | Wireless local-area-network |

# SUMMARY

This thesis studies advanced error control schemes using turbo-like codes, turbo-like coded modulations, turbo hybrid-ARQ (Automatic Repeat reQuest) schemes, and rate compatible puncturing techniques for reliable and adaptive commercial and tactical spread-spectrum communications, especially for code-division multiple access (CDMA) cellular systems and direct-sequence (DS) and frequency-hopping (FH) anti-jam systems. Furthermore, we utilize both the maximum-likelihood (ML) bounding techniques and convergence analysis to design and analyze various turbo-like coding schemes that show different behaviors in error performance from conventional trellis coding schemes.

In the area of DS-CPM, we propose a DS concatenated coded CPM system for pulse-noise jamming channels and an anti-jam iterative receiver utilizing jammer state information. We also design a mixed concatenated CPM system that mixes CPM schemes with different convergence characteristics. In addition, we present the ML bound and convergence analysis for the jamming channel.

In the area of FH-CPM, we propose anti-jam serially concatenated slow FH-CPM systems, whose phase is continuous during each hop interval, along with coherent and non-coherent iterative receivers. We also propose an iterative jamming estimation technique for the iterative receiver.

In the area of multi-h CPM, we propose a power- and bandwidth-efficient serially concatenated multi-h CPM along with an appropriate iterative receiver structure. Serially concatenated multi-h CPM is shown to outperform single-h CPM.

To design adaptive and versatile error control schemes using turbo-like codes for packet-data networks, we propose turbo hybrid-ARQ (HARQ) and rate compatible puncturing techniques for retransmission.

In the area of turbo hybrid-ARQ, we propose a Type-I turbo HARQ scheme using a

concatenated RS-turbo code and a packet combining technique for W-CDMA system to improve the performance of error and decoding latency. The W-CDMA system including the fast power control and coherent Rake receiver with a channel estimation technique for multipath fading channels is considered.

Finally, in the area of rate compatible punctured turbo-like codes, we propose rate compatible punctured turbo (RCPT) codes and rate compatible punctured serially concatenated convolutional (RCPS) codes along with their puncturing methods. In addition, we propose Type-II RCPT-HARQ and RCPS-HARQ schemes to perform an efficient incremental redundancy retransmission.

# CHAPTER I

# INTRODUCTION

## *1.1 Motivations*

In recent years, the demands for new wireless services such as mobile Internet/broadcasting, multimedia messaging/streaming, all-IP mobile network, broadband ad-hoc/ubiquitous and home networking, and high-speed packet-data transmission have grown very rapidly. Therefore, there has been increasing design challenges for efficient and reliable communication systems, especially coding and modulation of the physical layer, on time-varying wireless channels. Spread-spectrum (SS) techniques have also been broadly adopted for digital cellular [125], wireless local-area network (WLAN) [46], ultra-wideband (UWB) [132], and military communication [115] systems because they offer interference-resilient transmission as well as large capacity.

Ever since Shannon proved his noisy coding theorem [113], the construction of practical capacity-achieving coding schemes that can be decoded in a limited time has been the primary goal of coding research. The field was revolutionized by the introduction of capacity-approaching turbo codes [17, 18] of which power comes not only from the code concatenation through interleaver, but also from the low-complexity soft-input soft-output (SISO) iterative decoding algorithm used. In general, the error performance is mainly dependent on the characteristics of constituent encoders, concatenation structure, iterative decoding algorithm, interleaver design, number of iterations, and block length. However, there is still a gap between theory and practice due to encoding/decoding complexity and constructional/implemental difficulty. Motivated by the successful turbo codes, various forms of iteratively decodable codes have been proposed and have yielded graphical codes [128] such as low-density parity-check (LDPC) codes [88, 105]. Various families of powerful, yet low-complexity, turbo-like codes that can be iteratively decoded have been widely applied to deep-space communications [30], cellular systems [70], digital video broadcasting

(DVB) [73], data storage systems [90], optical networks [68], digital subscriber line (DSL) [24], multicarrier systems [85], satellite systems [78], and tactical radio systems [59].

Communication systems, especially wireless systems, have to be designed so that the required error protection levels are met. The design of forward error correction (FEC) codes usually consists of selecting a fixed code with a certain code rate, encoding/decoding complexity, and error-correcting capability [129]. However, since different types of data have different requirements in the error protection and latency and wireless channel is time-varying or unknown in many practical cases, adaptive error control coding schemes are usually required with a smart automatic repeat request (ARQ) scheme. In addition, the coding rate or amount of redundancy of turbo-like codes can be adjusted using the same encoder with a puncturing technique, achieving the versatility of coding and communication systems.

In this thesis, the main objective is to devise powerful, yet low-complexity, turbo-like coding and coded modulation schemes, and turbo hybrid-ARQ and rate compatible puncturing techniques for the design of reliable and adaptive commercial and military spread-spectrum communication systems, especially for code-division multiple access (CDMA) cellular systems and direct-sequence (DS) and frequency-hopping (FH) systems.

For the design of power- and bandwidth-efficient DS signals, we propose DS concatenated coded continuous phase modulation (DS-CPM) schemes. We also propose serially concatenated slow FH-CPM system to achieve excellent anti-jamming performance in the presence of partial-band jamming. Further, we propose a power- and bandwidth-efficient serially concatenated multi-$h$ CPM that outperforms single-$h$ CPM.

For reliable and high-throughput packet retransmission in wideband-CDMA (W-CDMA) systems, we propose turbo hybrid-ARQ schemes by efficiently combining turbo codes with ARQ schemes. Finally, to support adaptive code rate and incremental redundancy retransmission of turbo-like codes in packet data networks, we propose rate compatible punctured turbo codes and serially concatenated convolutional codes and their Type-II hybrid-ARQ schemes.

## 1.2 Outline of the Thesis

The remainder of this thesis is organized as follows.

Chapter II presents some brief background on turbo-like codes and iterative decoding, adaptive turbo-like coding schemes including the hybrid-ARQ and rate compatible punctured coding schemes, analysis frameworks of turbo-like codes, and spread-spectrum communications.

In Chapter III, we propose a DS concatenated coded CPM system. The error performance of an anti-jam iterative receiver is evaluated through union bound analysis and simulations in the presence of pulse noise jamming. We also design a mixed concatenated coded CPM scheme with a proper mixture ratio to further enhance anti-jam performance through the convergence analysis.

In Chapter IV, we propose an anti-jam slow FH system with serially concatenated CPM in the presence of partial-band noise jamming and investigate issues regarding the outer code and the inner CPM as well as FH parameters. Coherent and non-coherent iterative demodulation and decoding schemes utilizing jammer state information are proposed. Furthermore, we propose an iterative jamming estimation technique.

In Chapter V, we propose a serially concatenated multi-$h$ CPM along with appropriate iterative receiver by extending conventional CPM. We derive Chernoff upper bounds on the error probability using the transfer functions. Convergence analysis based on the extrinsic information is also used to evaluate the error performance in the water-fall region.

In Chapter VI, we propose a turbo hybrid-ARQ scheme using a concatenated RS-turbo code for reliable and adaptive packet data retransmission in power-controlled coherent W-CDMA system for multipath fading channels.

In Chapter VII, we propose rate compatible punctured turbo (RCPT) codes and rate compatible punctured serially concatenated convolutional (RCPS) codes along with appropriate puncturing methods. In addition, we propose Type-II RCPT-HARQ and RCPS-HARQ schemes, which are classes of the incremental redundancy retransmission schemes, to provide excellent error rate and throughput performances.

Finally, Chapter VIII will conclude this thesis and give suggestions for future research.

# CHAPTER II

# BACKGROUND

## *2.1 Turbo-Like Codes and Iterative Decoding*

### 2.1.1 Turbo-Like Codes

The concept of concatenated coding was first introduced by Forney [37]. The basic idea behind concatenated codes is to build a powerful code, whose error probability exponentially decreases at rates less than capacity, by concatenating more than two less powerful constituent codes with less complex decoding algorithms and shorter decoding delay. However, a soft-output decoder and a concatenation interleaver for achieving near-Shannon-limit performance are not utilized. With the introduction of the capacity-approaching turbo code in 1993 [18], which is a recent paradigm shift in coding field, iterative decoding algorithm (or *turbo principle*) [49] becomes a practical suboptimal decoding scheme for various concatenated codes.

The general classes of powerful concatenated codes that can be iteratively decoded are referred to as *turbo-like codes (TLCs)* [28, 26, 55, 111]. They show exceptionally good error performance, particularly at the region of low-to-moderate signal-to-noise ratio (SNR) and for a very long block-length[1]. Except for the class of parity-check codes, turbo-like codes can be generally composed of two or more simple constituent codes, arranged in a variation of a parallel or serial concatenation scheme, along with the concatenation of (random) interleavers, as shown in Fig. 1. For example, a systematic recursive convolutional code and a single parity-check code correspond to constituent codes of a parallel turbo code and low-density parity-check (LDPC) code, respectively.

[1]However, the large delay due to long block length diminishes the advantage of turbo-like codes over conventional codes for real-time wireless applications.

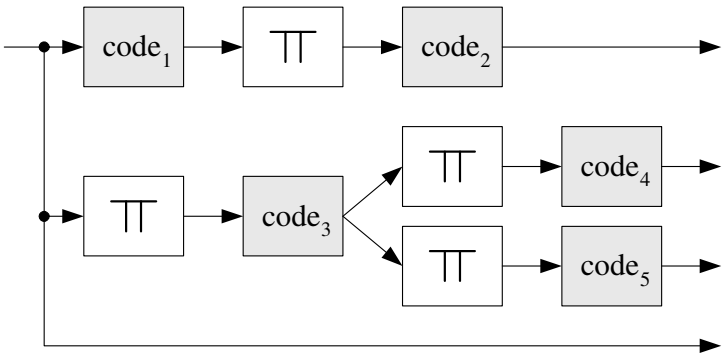


**Figure 1:** The general structure of a turbo-like code. Π represents a concatenation interleaver.

The turbo-like codes include classical turbo codes (or parallel concatenated convolutional codes (PCCCs) [14]), serially concatenated convolutional codes (SCCCs) [13], serially concatenated block codes (SCBCs) or turbo product codes (TPCs) [49, 86], the simplest repeat-accumulate (RA) codes [56, 101], product accumulate codes [77], power- and bandwidth-efficient coded modulation [108, 79, 97], hybrid concatenated codes [27], regular/irregular LDPC codes[2] [105], and concatenated tree codes[3] [102]. The main idea of the turbo-like coding is to match low-weight encoding of one permutation with high-weight encodings of the other(s). The overall encoder generates total weights that are significantly greater than the low weights that are possible from each of the component codes taken individually [31]. Especially, the iterative decoding performance of RA codes is surprisingly good in spite of the simplicity of the component codes[4].

Furthermore, a proper mixture of constituent codes whose individual advantages and disadvantages complement each other can improve the error performance over that of the constituent codes taken alone. *Mixed concatenated codes (MCCs)* where the outer and/or inner codes can be constructed by using multiple constituent codes are considered as a family of turbo-like codes. Fig. 2 shows an example of the MCCs having multiple outer and

[2]In terms of codes on graphs, the time-axis of the trellis can be represented by an arbitrary bipartite factor (or Tanner) graph [120].

[3]comprise $M$ two-state trellis codes interconnected by interleavers.

[4]The RA codes can achieve the Shannon limit $\log 2$ = -1.592 dB as the code rate goes to zero on an AWGN channel [55].

inner codes. The output bits from the constituent codes are demultiplexed according to a mixture ratio and then passed to the next encoding stage. The design and finding of an optimal mixture ratio of the MCCs can be aided by using a decoding convergence analysis, since it helps us to know advantages and disadvantages of constituent codes.

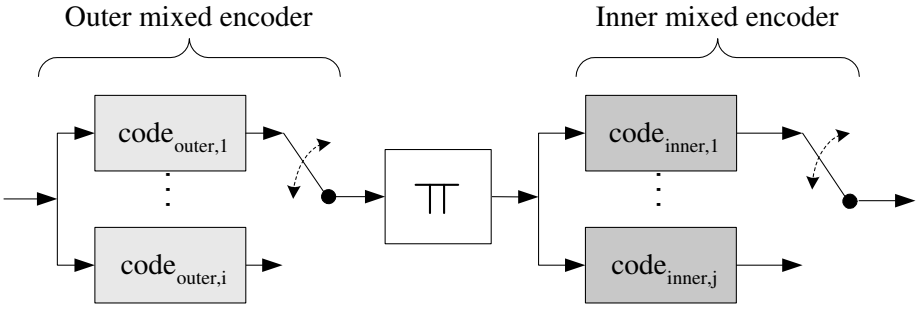


**Figure 2:** A mixed concatenated code. Π represents a concatenation interleaver.

### 2.1.2 Turbo-Like Coded Modulations

By replacing the inner recursive encoder in SCCC with a recursive modulator, iterative decoding algorithm can be applied to coded modulation schemes, such as bit-interleaved coded modulation (BICM) [79], serially concatenated differential phase-shift keying (SC-DPSK) [96, 98], and serially concatenated continuous phase modulation (SC-CPM) [97]. In general, *turbo-like coded modulations (TLCMs)* are composed of two or more simple constituent encoders and modulators, arranged in a variation of the concatenation scheme, along with interleaver(s). The constituent outer encoders can be trellis or block encoders, such as a repetition code, convolutional code, turbo code, single parity-check (SPC) code, or LDPC code.

DPSK modulation has been used for non-coherent detection where an accurate carrier phase is difficult to establish [118]. In particular, binary DPSK can be viewed as a rate-1 differential encoder with the generator polynomial of $1/(1+D)$ (or an accumulator) followed by a memoryless mapper. This inner rate-1 *recursive* trellis encoder plays an important role

in SC-DPSK[5] [96, 98], similar to the recursive inner code in an SCCC scheme, such that it provides a coding gain without adding redundancy because the weight-1 input-sequence generates an infinite weight outout-sequence[6]. The differentially encoded output $y_k \in \{0, 1\}$ at epoch $k$ is

$$y_k = y_{k-1} \oplus x_k, \tag{1}$$

where $x_k$ is the convolutionally encoded output and $\oplus$ denotes the binary sum. The carrier phase $\theta_k \in \{0, \pi\}$ is calculated as

$$\theta_k = \theta_{k-1} + \pi x_k. \tag{2}$$

Some important observations regarding the SC-DPSK are as follows: 1) the interleaving gain is dependent only on the interleaver size and minimum free-distance of the outer code, and is independent of the inner DPSK parameters for large interleaver size, and 2) codewords with *small* output-weight dominate bit error rate (BER) at high SNR.

Another popular and important modulation scheme is CPM [4, 106], which is a spectrally efficient constant envelope non-linear digital modulation scheme and has inherent trellis coding features created by the phase continuity. The CPM signals not only offer a compact spectral main lobe and rapidly decaying side lobes, but also make it possible to use low-cost and power-efficient non-linear amplifiers.

Consider SC-CPM consisting of an outer convolutional code, a random interleaver, and an inner CPM [45, 97]. The transmitted CPM signal provides phase memory, and can be decomposed into a time-invariant continuous-phase encoder (CPE) and a memoryless modulator (MM) [106]. Therefore, CPM can be also viewed as an inner recursive trellis encoder and it is well suited for a turbo-like coded modulation scheme.

Minimum-shift keying (MSK) is the simplest and most popular binary CPM scheme with a rectangular frequency shaping pulse. In particular, binary Gaussian MSK (GMSK) has been widely used in GSM, Bluetooth, DECT, CDPD, and Mobitex. The MSK is decomposed into a rate-1/2 two-state recursive convolutional CPE with the generator polynomial

[5]Sometimes, it is called trellis-coded and interleaved DPSK.
[6]However, the output weight is kept finite due to the trellis termination.

of $(1, D/1+D)$[7] followed by a MM, as shown in Fig. 3. Note that the only requirement for the CPE is to keep phase continuity.

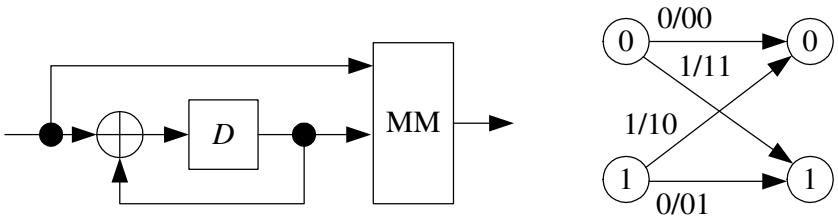


**Figure 3:** The recursive CPE with $(1, D/1+D)$ and the input/output trellis for MSK.

Since the transmission of all-zero information codewords cannot be assumed for the decoding error probability analysis of CPM, we must consider all pairs of transmitted and information codewords. However, error events[8] for CPM are dependent on the *difference* sequence between transmitted and information codewords, not on the specific transmitted sequence [114, 138].

### 2.1.3 SISO Iterative Decoding

For decoding of turbo-like codes, suboptimal iterative decoding [15, 49] is performed by employing low-complexity SISO decoders for each constituent code in an iterative fashion, in which the soft output values[9] of one decoder are passed to the other and vice versa until the final decoding estimate is obtained.

The function of the *a posteriori* probability (APP) algorithm is to compute *a posteriori* probabilities on the information bits or the encoded symbols. For turbo-like codes, iterative decoding schemes with a soft-decision decoder require these APPs. Maximizing the *a posteriori* probabilities by themselves leads to only minor improvements in terms of BER compared to the Viterbi algorithm. The algorithm was originally invented by Bahl, Cocke, Jelinek, and Raviv (BCJR) [9] in 1972 maximizes the probability of each symbol

[7] Different representations of the CPE having different generator polynomials, such as $(1, 1/1+D)$, are possible.

[8] An error event occurs whenever a nonzero path in trellis diverge and remerge to the reference path.

[9] These are represented by log-likelihood ratio (LLR) or probability.

being correct, and is referred to as the maximum *a posteriori* probability (MAP) algorithm. The MAP algorithm was not widely used until the invention of the turbo code, since it provided no significant improvement over the maximum-likelihood (ML) decoder that is implemented by the Viterbi algorithm [126] in spite of its increase in complexity. Various implementation of decoding algorithms have been proposed, such as the Log-MAP [15], Max-Log-MAP [107], soft-output Viterbi algorithm (SOVA) [49], sliding-window MAP [12]. They have a trade-off relationship between performance and complexity.

Finally, one of the weak points of iterative decoding is the latency due to iterative calculations. This also results in more power consumption at the receiver.

From the viewpoint of graphical codes [128], the MAP and the Viterbi algorithms are special cases of generic sum-product and min-sum algorithms [69], respectively. Therefore, the iterative decoding occurs when the graph has *cycles* and, thus, is suboptimal with lower-complexity compared to cycle-free optimal cases.

## *2.2 Adaptive Turbo-Like Coding and Hybrid-ARQ*

### 2.2.1 Adaptive Error Control Systems

The *adaptive error control system (AECS)*[10] can adaptively change the modules in transmitter to diversify retransmissions according to estimated or unknown channel information. Examples of the useful channel information include the SNR, data rate, received power, bit/frame errors, fading parameters (fade duration, Doppler frequency, and other channel parameters), path loss, interference level, ARQ status messages, throughput, and round trip delay. According to the estimated channel information, the AECS can adaptively change code rates, packet size, forward error correction (FEC) code, modulation scheme, ARQ protocol, and so on. In particular, since data needs different error protection and channel is time-varying or unknown in many cases, *adaptive error control coding (AECC)* scheme is an important design issue. Therefore, it is promising to design adaptive turbo-like coding schemes by utilizing both the powerful error-correcting capability of turbo-like codes and

[10]In a nutshell, it includes adaptive coding, adaptive modulation [104], and adaptive antenna schemes. However, our primary concern is about the AECC system.

adaptability of the AECC scheme. The general structure of the AECC system is shown in Fig. 4.

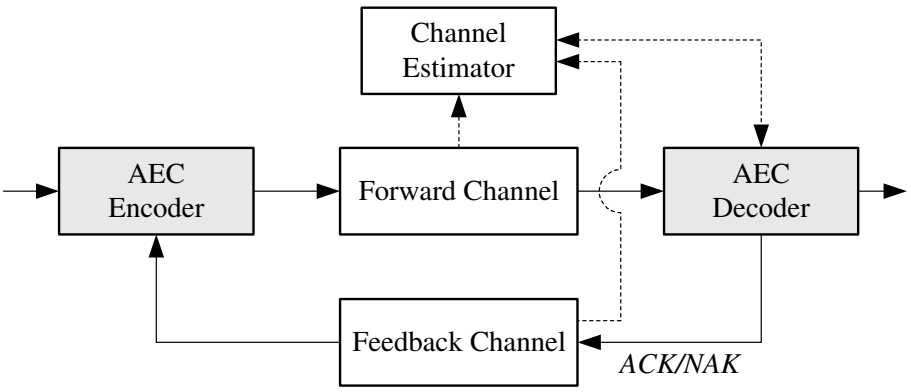


**Figure 4:** General structure of the AECC system with a channel estimator. Forward and feedback channels exist.

The change of modules (or their possible combinations) in the AECS system and their examples for AECS systems are summarized in Table 1.

**Table 1:** Change of modules for the adaptive error control system.

| Change | Example |
|---|---|
| Code rates | $1/2 \rightarrow 1/3$ |
| FEC coding schemes | convolutional code $\rightarrow$ turbo code |
| HARQ schemes | Type-II $\rightarrow$ Type-I (adaptive HARQ) |
| Puncturing patterns | $\mathbf{P}(\mathbf{k}) \rightarrow \mathbf{P}'(\mathbf{k})$ |
| Packet sizes (formats) | 640 $\rightarrow$ 2 $\times$ 320 bits/packet |
| Transmit power | 0.05 dB $\rightarrow$ 0.1 dB |
| Frequency subchannels | subchannel assignment switching (multi-carrier) |
| Modulation | QPSK $\rightarrow$ 16-QAM (adaptive modulation) |
| Interleaver | switching of interleaver pattern |
| Antenna diversity | antenna numbers (MIMO),<br>switching of TX antenna and beam pattern |

### 2.2.2 Hybrid-ARQ Schemes

There are two basic categories of error control schemes for data communications: FEC schemes and ARQ schemes. Drawbacks of the ARQ and FEC schemes can be overcome if they are properly incorporated. Such a combination of the two basic error control schemes

is referred to as hybrid-ARQ (HARQ)[11] [80], [82]. The HARQ techniques have been extensively used for packet data networks where retransmission is allowed. The main function of the FEC system is to reduce the number of retransmissions by correcting the error patterns that occur most frequently, usually at low SNR. This increases the system throughput performance. However, when a less-frequent error pattern occurs and is detected, the receiver requests a retransmission rather than passing the unreliably decoded message to the user. This increases the system reliability. As a result, a proper combination of FEC and ARQ provides higher reliability than an FEC system alone and higher throughput than a system with ARQ alone.

HARQ schemes can be classified into two categories: Type-I and Type-II HARQ schemes. Briefly, the Type-I and Type-II HARQ schemes can be viewed as a full retransmission ARQ and a partial retransmission ARQ strategies, respectively. Fig. 5 illustrates the examples of the pure ARQ scheme and three types of HARQ schemes for comparison purpose.

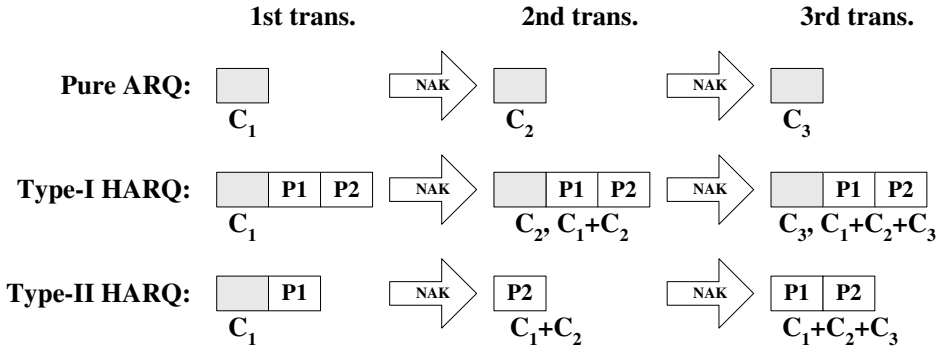


**Figure 5:** Pure ARQ and hybrid-ARQ schemes. Three transmissions are shown. $C_i$ denotes a codeword for the $i$-th transmission, and $P$ denotes the parity-check bits.

A straightforward Type-I HARQ scheme uses codes that are designed for error detection and correction. When a received codeword is detected in error, the receiver first attempts to correct the errors. If the number of errors is within the designed error correcting capability of the code, the errors will be corrected and the decoded message will be delivered to the user or saved in the buffer until it is ready to be passed to the user. It an uncorrectable error

[11]The hybrid-ARQ is sometimes called as the FEC/ARQ.

pattern is detected, the receiver rejects the received codeword and requests a retransmission. The same codeword is retransmitted. When the retransmitted codeword is received, the receiver again attempts to correct the errors (if any). If the decoding is not successful, the receiver again rejects the received codeword and requests another retransmission. This continues until the codeword is either successfully received or successfully decoded. Since a code is used for both error correction and detection in a Type-I HARQ system, it requires more parity-check bits than a code used only for error detection in a pure ARQ system. As a result, the overhead for each transmission is increased. When the channel error rate is low, a Type-I HARQ system has lower throughput than its corresponding ARQ system. However, when the channel error rate is high, a Type-I hybrid ARQ system provides higher throughput than its corresponding ARQ system, because its error-correction capability reduces the retransmission frequency, as shown in Fig. 6 [82].

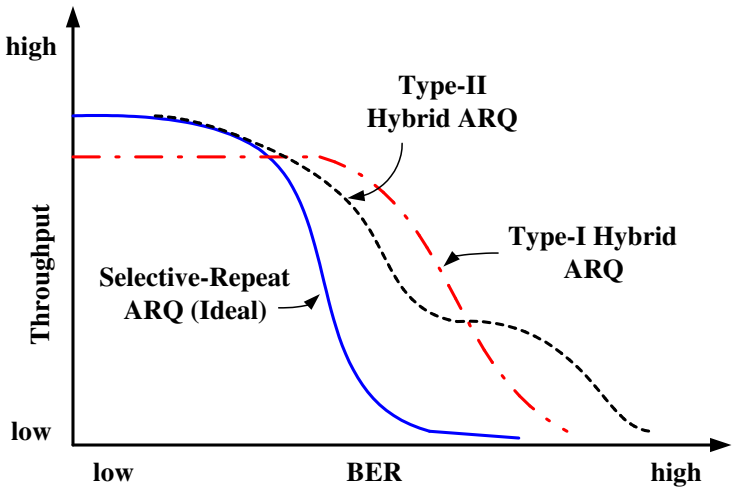


**Figure 6:** Typical throughput behavior of ARQ and hybrid-ARQ schemes.

Type-I HARQ schemes are best suited for communications systems in which a fairly constant level of noise and interference is anticipated on the channel like AWGN channel. In this case, enough error correction can be designed into the system to correct the vast majority of received codewords, thereby greatly reducing the number of retransmissions and enhancing the system performance. However, for a non-stationary channel where the bit

error rate changes, a Type-I HARQ scheme may have some drawbacks. When the BER of channel is low, the transmission is smooth and no (or little) error correction is needed. As a result, the extra parity-check bits for error correction included in each transmission represent a waste. When the channel is very noisy, the designed error correcting capability may become inadequate. As a result, the frequency of retransmission increases and hence reduces the throughput. Several Type-I HARQ schemes using either block or convolutional codes have been proposed and analyzed [136], [32]. For a channel with a non-stationary error rate, one would like to design an adaptive HARQ system. When the channel is quiet, the system behaves just like a pure ARQ system. However, when the channel becomes noisy, extra bits are needed. This concept forms the basis of the Type-II HARQ schemes. A message in its first transmission is coded with parity-check bits for error detection only. When the receiver detects any error in a received codeword, it saves the erroneous codeword in a buffer and at the same time requests a retransmission. The retransmission is not the original codeword but a block of parity-check bits and an error correction code. When this block of extra bits is received, it is used to correct the errors in the erroneous codeword stored in the receiver buffer. The detailed algorithm depends on the retransmission strategy and the type of error correcting code to be used. The concept of parity retransmission for error correction and the first Type-II HARQ using a parity retransmission strategy were first introduced by Mandelbaum [89] and by Metzner [92], respectively. Metzner's scheme was later extended and modified [82].

### 2.2.3 Rate Compatible Punctured Codes

Mandelbaum [89] was the first to propose punctured codes for transmitting redundancy incrementally by using RS codes. However, Cain *et al.* [20] first introduced punctured convolutional codes (PCC) as a method for obtaining higher codes rates of 2/3 and 3/4 from a rate 1/2 code, while using a same Viterbi decoder. Later, Hagenauer [48] proposed rate compatible punctured convolutional (RCPC) codes and Type-II RCPC-HARQ scheme. RCPC codes are constructed by puncturing a single rate-$1/n$ convolutional code rate-compatibly to produce a family of higher rate codes. Erasures are inserted to mark the location of the

punctured bits at the decoder. The puncturing pattern should be generated such that the rate compatible puncturing rules are satisfied. The rate compatible puncturing rule limits the puncturing pattern such that all of the code symbols of a high rate punctured code must be included in the lower rate codes (i.e., the higher rate codes should be used in the lower rate codes). Instead of transmitting all the bits of a completely different low rate code, the lower rate code must reuse the bits already transmitted. Therefore, only additional incremental redundancy bits are transmitted.

The RCPC codes are briefly explained by taking an example shown in Fig. 7. RCPC encoder consists of convolutional encoder of mother code rate $R = 1/N = 1/2$ and memory $M = 3$, puncturing (or perforation) tables with puncturing period $P = 4$, and multiplexer. A '0' in the puncturing table means that the code symbol is not to be transmitted (i.e., puncturing). Each puncturing table is described by $N \times P$ matrix denoted as $\mathbf{P}(\mathbf{k})$ and puncturing period $P$ determines the range of code rates ($R_k$) between $P/(P+k)$ and $1/N$.

$$\mathbf{P}(\mathbf{1}) = \begin{bmatrix} 1 & 1 & 1 & 0 \\ 1 & 0 & 0 & 1 \end{bmatrix}, \ \mathbf{P}(\mathbf{2}) = \begin{bmatrix} 1 & 1 & 1 & 0 \\ 1 & 1 & 0 & 1 \end{bmatrix},$$

$$\mathbf{P}(\mathbf{3}) = \begin{bmatrix} 1 & 1 & 1 & 1 \\ 1 & 1 & 0 & 1 \end{bmatrix}, \ \mathbf{P}(\mathbf{4}) = \begin{bmatrix} 1 & 1 & 1 & 1 \\ 1 & 1 & 1 & 1 \end{bmatrix}.$$

$$R_k = \frac{P}{P+k} \qquad k = 1, 2, \cdots, (N-1)P \tag{3}$$

Instead of transmitting all the bits of a completely different low rate code, the lower rate code must reuse the bits already transmitted. Thus, we just transmit only additional incremental redundancy bits (e.g., $\mathbf{P}(\mathbf{1}) \rightarrow \mathbf{P}(\mathbf{2}) \rightarrow \mathbf{P}(\mathbf{3}) \rightarrow \mathbf{P}(\mathbf{4})$). The applied rate-compatibility rule can be defined as following:

$$\text{if } p_{ij}(l) = 1 \text{ then } p_{ij}(k) = 1 \text{ for all } k \geq l \geq 1 \tag{4}$$

where $p_{ij}(l) \in (0,\ 1)$ represents the entry of $i$-th column and $j$-th row of $\mathbf{P}(\mathbf{l})$. Fig. 7 illustrates a RCPC encoder[12] structure with $R = 1/2$ and $P = 4$.

[12]Generator polynomials are of $g^{(0)} = (1011)$ and $g^{(1)} = (1101)$.

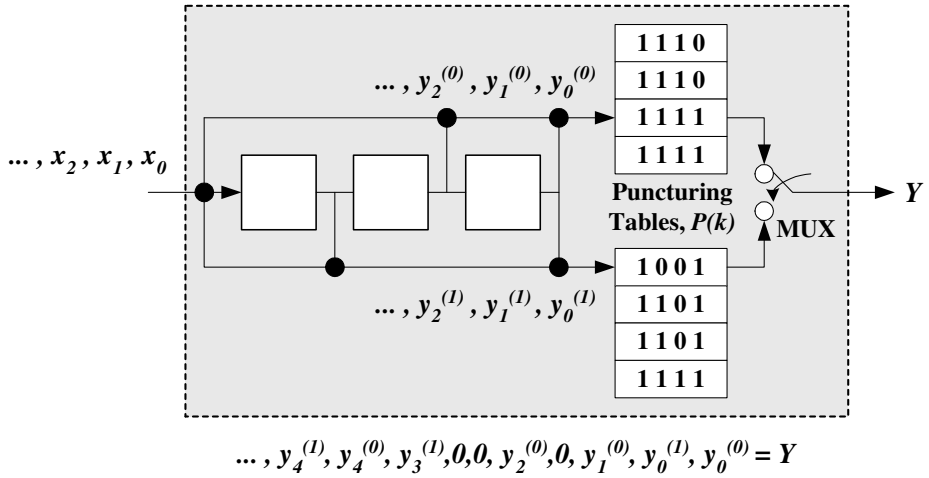


**Figure 7:** The structure of an RCPC encoder (puncturing period = 4).

## *2.3 Analysis of Turbo-Like Codes*

Two successful analysis/design techniques for turbo-like codes have been proposed. One is ML bounding technique that is purely analytical one using a transfer function and works nicely for moderate-to-high SNR region (error-floor region) [15, 111]. The other is based on density evolution technique that is semi-analytical one and works well for low-to-moderate SNR region (water-fall region) [43, 27, 122]. Interestingly, the two techniques have something in common and are mutually counterbalancing, but sometimes they lead to different result. Therefore, the choice of designed code depends on the error requirements of target service.

### 2.3.1 ML Decoding Bounds and Distance Spectrum

For very long codes, suboptimal and more practical decoding schemes are required since ML decoding becomes prohibitively complex. A nice approach for analyzing iterative decoding is to minimize or disregard the influence of the cycles of turbo-like codes. Therefore, we can still use the ML bound as an invaluable practical tool for the design and analysis, and as a benchmark for the comparison of the suboptimal decoding methods.

The most commonly used upper bound on the error probability of a digital communication system is union bound. For the calculation of the union bound for a binary block

code, one only needs to have the input-output weight enumerating function (or distance spectrum) of the code. For turbo-like codes, the modified *ensemble* distance spectrum that is calculated from a *uniform interleaver* assumption has been often used, because it is quite difficult to evaluate the performance for a specific interleaver [13]. The probabilistic uniform interleaving is devised to map a given input-sequence of length $N$ and weight $l$ into its $\binom{N}{l}$ distinct permutations with equal probability of $1/\binom{N}{l}$. The premise is that there exists at least one interleaver, which performs better than the average.

However, the union bound diverges in the low SNR region and, in particular, it is useless at rates above the channel cutoff-rate. Recently, several new geometrical bounds that estimate the BER performance more accurately at SNRs smaller than the cutoff-rate threshold have been proposed [33, 34, 127, 110]. Most geometrical bounds are essentially derived from the general Gallager's *first* bound (GFB) in 1963 [41, 25]. The GFB is particularly suited for fixed (particular) codes rather than random codes. The tangential-sphere bound (TSB) proposed by Herzberg and Poltyrev [103] is always tighter than the conventional union bound and the Berlekamp's tangential bound (TB) [16], especially for the low-to-moderate SNR region. This is achieved by separating the radial and tangential components of the Gaussian noise with a half-space as the underlying Gallager region. Recently, improved bounds by Duman and Salehi [33, 34] and Sason and Shamai [110, 111, 112] have also been proposed. The Duman-Salehi bound (DSB) based on the Gallager's *second* bound (GSB) technique in 1965 [42] requires a two-parameter optimization without integration. The DSB is tight for a wide range of SNR where the union bound is already very loose.

The error probability is divided into joint probability of error and noise residing in a Gallager region and joint probability of error and noise residing in the complement of $\Re$, where $\Re$ is a volume around the transmitted codeword. The choice of region $\Re$ is of importance in the GFB-based bounding techniques. Different choices of the region result in different bounds in different ranges of SNR. Therefore, the word error probability (WEP), $P_w(E)$, is

$$P_w(E) \quad = \quad P(E, \mathbf{r} \in \Re) + P(E, \mathbf{r} \notin \Re) \tag{5}$$

$$= \quad P(E|\mathbf{r} \in \Re)P(\mathbf{r} \in \Re) + P(E|\mathbf{r} \notin \Re)P(\mathbf{r} \notin \Re), \tag{6}$$

where $\mathbf{r}$ is the $n$-dimensional received vector. Having $P(E|\mathbf{r} \notin \Re) \leq 1$, $P_w(E)$ is upper-bounded by[13]

$$P_w(E) \leq P(E, \mathbf{r} \in \Re) + P(\mathbf{r} \notin \Re), \tag{7}$$

The ML bounds for fading channels can be obtained with some modifications for the the case of an AWGN channel. There have been efforts to derive bounds for fully interleaved (independent) fading channels [51] and correlated (or partially interleaved) fading channels [40, 60, 75].

The excellent performance of turbo-like codes using iterative decoding can also be attributed to the *spectrum thinning* phenomena [99]. The multiplicity, which is the number of codewords with the same Hamming weight, of the near neighbors is significantly decreased, especially, at the region of low-to-moderate output-weights. The error performance of turbo-like codes is governed by a whole region of low-weight distances, not only by the minimum distance [110]. This is in contrast to ensembles of random codes [23] where typical weights associated with typical sequences dominate. The weight spectra for RA codes and SC-DPSK are closer to the binomial distribution of the random codes than those of component codes and, thus, these codes provide excellent error performance.

The ensemble distance spectra of SCCCs and random codes are well matched for weights larger than twice the Gilbert-Varshamov (GV) distance[14], although the former is significantly larger than the latter for relatively low weights. As an example, Fig. 8 shows the output-weight spectra for RA codes and random codes with different code rates. Notice that RA codes have lower weights than random codes at the region of low output-weights.

The beneficial *interleaving gain* [15] of turbo-like codes, which means that a longer block length always improve error performance, is possible only for a *recursive*[15] inner convolutional encoder such as differential encoders, and differential modulators such as

[13] In other words, instead of calculating the total error probability, the region of many errors is entirely treated as erroneous and the region of few errors is only calculated.

[14] For normalized Hamming weight, the GV distance is $2H_2^{-1}(1-R)$, where $H_2^{-1}(\cdot)$ denotes the inverse of binary entropy function and $R$ is code rate.

[15] For a recursive code, a single-weight input sequence does not cause an error event.

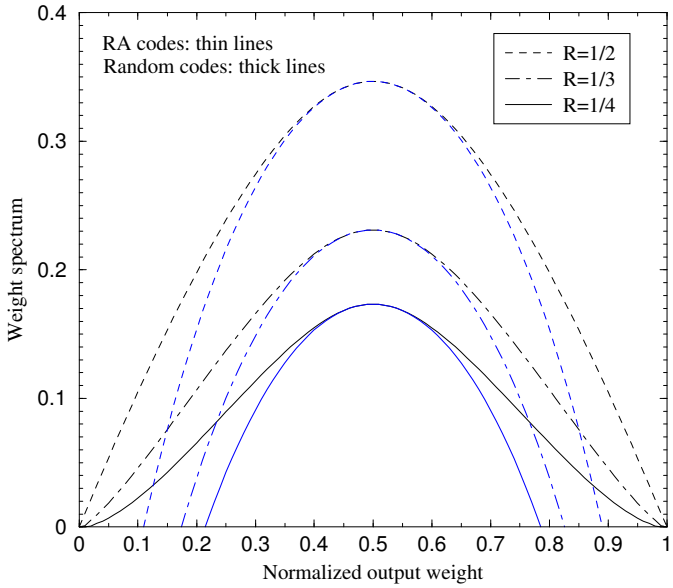


**Figure 8:** Weight spectra for RA codes and random codes.

DPSK, DQPSK, and CPM. The interleaving gain depends on the interleaver length rather than on the constraint length of the constituent convolutional code.

The interleaver gain exponent (IGE) considers the ensemble growth rate of $\bar{A}_d(N)$, for fixed output-weight $d$, for an ensemble sequence as the interleaver length $N$ goes to infinity. The IGE and the maximum IGE are defined as [56]

$$\alpha(d) = \limsup_{N\to\infty} \log_N \bar{A}_d(N), \tag{8}$$

and

$$\beta_M = \max_{d\geq 1} \alpha(d), \tag{9}$$

respectively. Let $l$, $n^o$, and $n^i$ be input-weight, the number of error events of outer and inner codes, respectively. Then, there exists a threshold $z$ such that, for any $z < z^*$, the probabilities of bit and word errors are $P_b = O(N^{\beta_M - 1})$ and $P_w = O(N^{\beta_M})$, respectively, where the maximum IGE is given by $\beta_M = n^o + n^i - l$ [15]. For $\beta_M - 1 = n^o + n^i - l - 1 < 0$, increasing $N$ decreases $P_b$ exponentially and thus provides the interleaving gain. For the case of SCCC, the maximum IGE is $\beta_M = 1 - d_f^o$, where $d_f^o$ denotes the free distance of the outer code. Therefore, if the free distance of the outer code satisfies $d_f^o > 2$, the

exponent of $N$ is always negative. For a non-recursive inner code, $\beta_M = n^o - 1 \geq 0$ and an interleaving gain is not obtained. However, for a recursive inner code, $P_b$ decreases with $N$ as $N^{-\lfloor (d_f^o+1)/2 \rfloor}$ and is mainly dependent on the minimum weight of the codewords for the input sequences of weight-2 and -3.

### 2.3.2 Density Evolution and Convergence Analysis

For turbo-like codes, the traditional ML bounding techniques based on distance spectrum usually do not exactly explain the error performance at low-to-moderate SNR region or the water-fall region where the excellent performance is achieved [13]. However, the performance of the iterative systems can be investigated by convergence analysis, as proposed in [43, 27, 122]. The iterative decoder can be viewed as a nonlinear dynamical feedback system. The density of extrinsic information in iterative decoders can be tracked by actual density evolution (DE) and by Gaussian density functions to analyze the performance of the turbo-like codes [27, 26] and graphical codes [128]. By doing so, we can gain many insights into the performance at the water-fall region and we can design more powerful turbo-like codes by using the characteristics of constituent codes (e.g., recursiveness and state-complexity). This asymptotic semi-analysis requires very long block lengths (i.e., $N \rightarrow \infty$) and an infinite number of iterations (i.e., $m \rightarrow \infty$). The accurate analysis for short-to-moderate block lengths (or finite interleaver lengths) remains unsolved. In this case, adjacent extrinsic information will be correlated, thus causing performance degradation.

The density evolution method tracks the probability density function (pdf)[16], $p(\lambda)$, of the input and output extrinsic information messages, $\lambda$, in the iterative decoders as the iterations proceed, and computes the decoding threshold. In Fig. 9, the density evolution phenomenon of the rate-1/3 parallel turbo code is simulated. In case of $E_b/N_0 = 1.5$ dB, the Gaussian-shaped density evolves with wider distribution and with both increasing mean and variance as the iterations proceed.

The decoding *threshold* represents some $E_b/N_0$ point where the two input-output extrinsic information curves intersect. If the decoder operates an $E_b/N_0$ greater than the

[16]The pdf can be calculated from the histogram of $\lambda$.

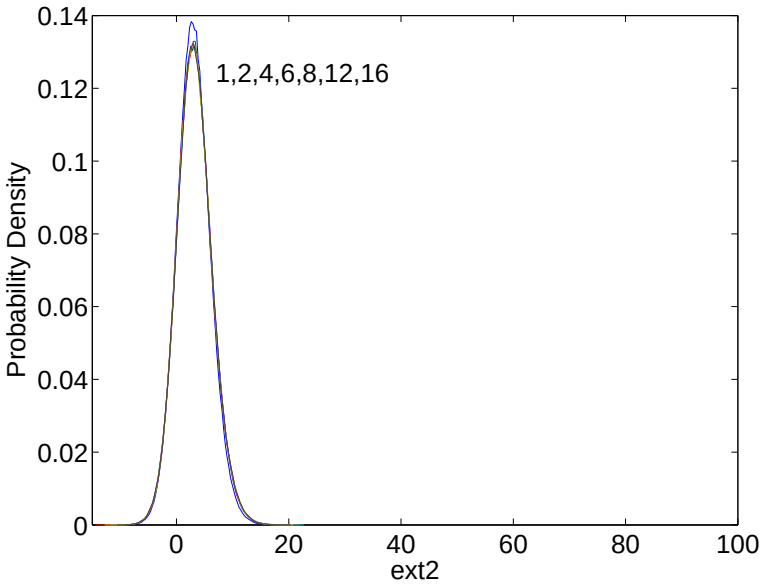


(a) $E_b/N_0 = 0.5$ dB.

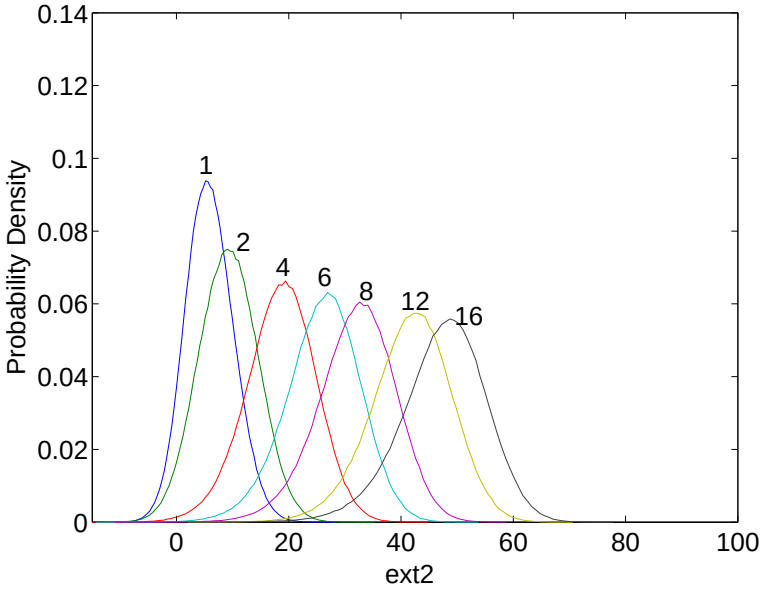


(b) $E_b/N_0 = 1.5$ dB.

**Figure 9:** Density evolution for the parallel turbo code with the increase in $E_b/N_0$ and decoding iterations. The number of iterations is marked on each curve.

threshold, the iterative decoder converges and thus the BER goes to zero ($P_b \to 0$) as the iterations increase ($m \to \infty$). The threshold is found to correspond to the sharp water-fall region on BER curve.

Furthermore, the exchange of extrinsic information can be visualized as a decoding trajectory in the extrinsic information transfer chart (EXIT chart) [121, 122]. This measure is found to be more robust for clipping since no Gaussian assumption is imposed on the extrinsic output distributions $p(\lambda)$. However, for short-to-moderate block lengths, the averaged trajectory dies out after some iterations (i.e., fail to reach the right-upper corner) due to the increasing correlations of extrinsic information. If the mutual information is zero, the extrinsic information has no information about transmitted codewords. On the contrary, if it approaches one, the transmitted codewords are known and, thus, error-free decoding is possible.

For a BER curve for turbo-like codes, three different regions can generally be classified as depicted in Fig. 10. Firstly, the *pinch-off* region – the low SNR region where negligible BER reduction through iterations is observed. The decoder transfer characteristics intersect at the low value of mutual information (corresponding to high BER) and the trajectory gets stuck. Secondly, the *water-fall* region – the bottleneck region where the trajectory just manages to sneak through a narrow tunnel. Convergence is slow, but is possible, since both curves do not intersect anymore. Finally, the *error-floor* region – the wide-open tunnel region with fast convergence. The BER improvement is relatively small.

As an example, Fig. 11 shows the convergence behavior of the SC-CPM having inner MSK and 4-state outer code for different $E_b/N_0$. For $E_b/N_0 = 1.0$ dB, the decoder transfer characteristics inevitably intersect at around $(I_{I,in}, I_{I,out}) = (0.25,\ 0.4)$ after some iterations. The trajectory just sneaks through the curves in case of $E_b/N_0 = 1.2$ dB.

## *2.4 Spread-Spectrum Communications*

### 2.4.1 W-CDMA System

CDMA [74, 125] has successfully been adopted for IS-95 digital cellular systems [54] to provide high user-capacity and high data rate. Later, W-CDMA technology has been chosen as

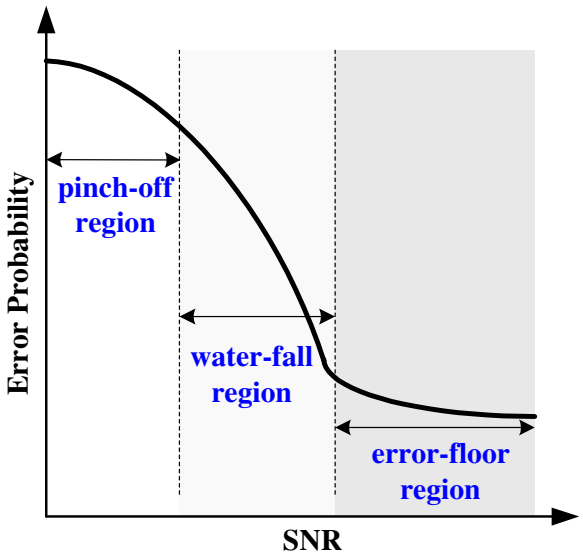


**Figure 10:** Three different error regions of turbo-like codes.

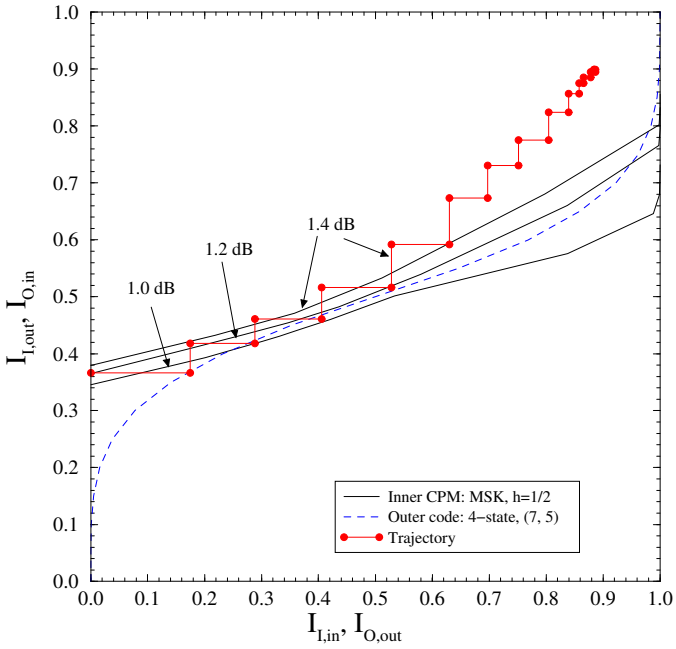


**Figure 11:** Convergence behavior of the SC-CPM for different SNR. The mutual information transfer characteristics and the corresponding trajectory are shown.

the basic radio access technology for 3G IMT-2000 systems such as UMTS and cdma2000[17] [21].

The key features of W-CDMA are as follows: 1) improved coverage and capacity owing to a higher bandwidth and coherent uplink detection; 2) the possibility to transport multiple parallel services with different quality requirements on one connection; 3) different coding and interleaving schemes depending on the specific requirements; 4) support of rate matching to match the bit rate of the traffic channel to one of the limited sets of bit rates of physical channels; 5) use of fast closed-loop power control and variable power control step in both the uplink and downlink; 6) support of inter-frequency handover necessary for high-capacity hierarchical cell structures; 7) support for capacity-improving technologies such as adaptive antennas, multiple antennas, and multiuser detection; 8) support of a fast and efficient packet-access protocol; and 9) support for mutually asynchronous base stations (i.e., there is no universal time reference known to all base stations).

### 2.4.2 DS and FH Systems for Anti-Jamming

Spread-spectrum systems use a bandwidth that is much greater than the information rate. They use either DS or FH spreading are effective for combating hostile jamming and unintentional interference [115]. The combinations of DS and FH as well as multi-carrier (MC) SS have also been used. In FH systems, the available channel bandwidth is subdivided into a large number of contiguous frequency slots. Spread-spectrum techniques have extensively been used for combat radio systems [93, 47] due to the favorable low-probability of intercept (LPI) and low-probability of detection (LPD) capabilities [100, Ch. 10]. Channel coding, interleaving, diversity, and their combinations effectively counter the severe degradation due to a jamming and, thus, reduce the detectability of signals by an intercept receiver.

Jammers are usually defined as the group of hostile communicators or intentional interferers that attempt to disrupt the communications of targeted users by transmitting an interfering signal over the same communication range [115]. The pulse noise jammer (PNJ), which is one of the most detrimental jammers against DS signals, transmits pulses

[17] 3GPP UMTS (W-CDMA) and 3GPP2 cdma2000 are 3G evolutions of 2G GSM and CDMA systems, respectively.

of band-limited white Gaussian noise having power $J_{peak} = J/\rho$ where $J$ is the time-averaged jamming power. The PNJ turns ON with enough power to degrade significantly the performance of a target communication system. The jammer determines its pulse duty factor, $\rho$ $(0 < \rho \leq 1)$, which is a fraction of time during the jammer is ON, to maximize the system degradation while keeping the constant average transmitted power $J$ that is averaged over total spread-spectrum bandwidth. The communicator must guarantee performance in worst case jamming.

Jammer state information (JSI) yields the knowledge of jamming state (i.e., jammed or unjammed) of the symbols where JSI is available at the receiver and it serves a variety of purposes ranging from soft decoding metrics to jamming detection. The jammer state random variable $z$ is defined such that $P(z = 1) = \rho$ if jammer is ON and $P(z = 0) = 1 - \rho$ if jammer is OFF. The use of JSI is essential for coded spread-spectrum systems employing soft-decision decoding, since a smart jammer can completely destroy the communications links not utilizing JSI even with minimal jammer power [115].

Partial-band noise jamming (PBNJ) is one of the most effective jamming strategies against FH systems. A PBNJ spreads noise of total power of $J$ evenly over a frequency range of bandwidth $W_J$, which is a subset of the full spread bandwidth $W_{ss}$. The jammer determines its duty factor, $\rho \stackrel{\triangle}{=} W_J/W_{ss} \in (0, 1]$, to maximize the system degradation. During a FH dwell time of $T_h$, let us define the jammer state random variable, $z$. A hop is jammed with probability of $P(z = 1) = \rho$, and unjammed with probability of $P(z = 0) = 1 - \rho$. It is usually assumed that the JSI yields the knowledge regarding the jamming state of the modulated symbols.

# CHAPTER III

# DIRECT-SEQUENCE CONCATENATED CODED CPM

Spread-spectrum (SS) techniques using either DS or FH spreading with channel coding, interleaving, diversity, and their combinations are effective for anti-jam and low probability-of-intercept low probability-of-detection (LPI/LPD) communications [115]. CPM is a class of constant envelope modulation schemes [4] having excellent spectral efficiency. Therefore, coded DS-CPM signals promise good low LPI/LPD features.

Previous studies of *uncoded* DS multi-$h$ CPM have demonstrated a 3-4 dB reduction in detectability over conventional DS-BPSK modulation [72]. DS-MSK was also shown to outperform DS-BPSK for an equivalent overall bandwidth [7]. Trellis-coded DS-CPM with a *non-iterative* Viterbi receiver was proposed in [84]. A DS system employing coded and interleaved CPM and Viterbi decoder was proposed in [137]. However, since the spreading was performed after the CPM modulator, the phase continuity of CPM carrier was not maintained.

In this chapter, we propose a DS concatenated coded CPM system, such that the carrier phase continuity is maintained with DS spreading. Coherent detection of CPM signaling on fading channels is possible by using joint data detection and estimation [83] or pilot symbol aided modulation [53]. Our receiver uses coherent iterative demodulation and decoding as described in [45], [97]. DS spreading effectively yields a very low rate repetition code with a code rate equal to the processing gain. We show that chip-wise interleaving degrades the BER performance with iterative demodulation and decoding due to the non-optimality of the iterative decoder. To remedy this artifact, we use a block-wise random interleaver [66]. Motivated by better BER performance due to improved iterative decoder convergence characteristics at low-to-medium $E_b/N_J$, we propose a mixed concatenated coded system consisting of a mixture of recursive and non-recursive CPM modulators with an optimized mixture ratio. Such mixing can also improve LPI performance because an intercept receiver

must know the mixture ratio for correct detection. Finally, since jammer state information (JSI) is crucial with soft-decision decoding [115], the soft-decision metrics in our iterative receiver employ JSI.

The main contributions can be summarized as follows: i) phase-continuous DS concatenated coded CPM transmitter and an iterative receiver that incorporates JSI; ii) anti-jamming performance of coded DS-CPM signaling with iterative demodulation/decoding is investigated through simulation and union bound analysis; iii) code mixing for the enhancement of BER performance by improving iterative decoder convergence.

## *3.1 System Model*

### 3.1.1 Transmitter Structure

Fig. 12 shows the transmitter of the block-random interleaved concatenated coded DS-CPM system. A length-$N$ binary input sequence $\mathbf{u}$ is encoded by a rate-$N/N'$ outer convolutional encoder. The length-$N'$ binary output sequence $\mathbf{d}$ from the outer encoder is multiplexed, and each code bit is repeated $G$ times to yield the sequence $\mathbf{b}$, where $G$ is the processing gain. The sequence $\mathbf{b}$ is input to a buffer of size $G \times N'$, such that the $G$ rows repeat the length-$N'$ sequence. Block-wise interleaving is performed, where the columns of the $G \times N'$ matrix are randomly interleaved. Such block-wise random interleaving is used rather than chip-wise random interleaving to overcome the BER degradation that will result from non-maximum likelihood iterative decoding at a very low chip energy-to-noise ratios. The interleaver output is converted into a length-$GN'$ serial sequence $\tilde{\mathbf{b}}$ that is scrambled with a user-specific binary PN sequence $\mathbf{c}$. The binary sequence $\tilde{\mathbf{b}}$ is mapped onto the $M$-ary symbol sequence $\boldsymbol{\alpha}$, $\alpha \in \{\pm 1, \pm 3, \ldots, \pm(M-1)\}$, which is input to the $M$-ary recursive CPM modulator. Note that the dotted-line block is used in the case of the mixed recursive (R) and non-recursive (NR) CPM modulator as will be described later. Let $s(t, \boldsymbol{\alpha})$ denote the coded and spread CPM modulated complex baseband signal, given by

$$s(t, \boldsymbol{\alpha}) = \sqrt{\frac{2E_s}{T_s}} \exp[\phi(t, \boldsymbol{\alpha}) + \phi_0], \; nT_s \leq t < (n+1)T_s \tag{10}$$

where $\boldsymbol{\alpha}$ is the symbol sequence, $E_s$ is the modulated symbol energy, $T_s$ is the transmitted symbol duration, $\phi_0$ is an initial phase assumed to be zero. The information carrying phase

$\phi(t, \boldsymbol{\alpha})$ is given by $\phi(t, \boldsymbol{\alpha}) = \phi_n + 2\pi h \sum_{i=n-L+1}^{n} \alpha_i q(t - iT_s),\ nT_s \leq t < (n+1)T_s$, where $q(t) = \int_{-\infty}^{t} g(t)dt$ is the phase shaping function such that $q(t) = 0$ for $t < 0$ and $q(t) = 1/2$ for $t > LT_s$, $\phi_n = \pi h \sum_{i=0}^{n-L} \alpha_i$ is the accumulated phase, and $h$ is the modulation index.

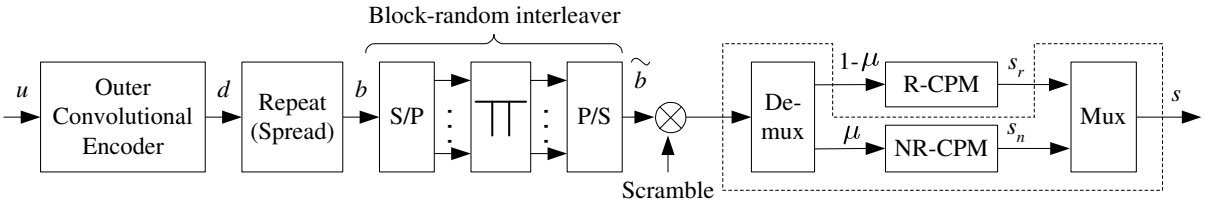


**Figure 12:** Transmitter structure for the DS concatenated coded CPM communication system with the block-random interleaver which is denoted as Π, and the decomposed inner CPE and the memoryless modulator.

### 3.1.2 Anti-Jam Iterative Receiver

The received signal is down-converted to complex baseband signal $r(t) = r_I(t) + jr_Q(t) = s(t, \boldsymbol{\alpha}) + n(t)$ and then passed through an ideal anti-aliasing filter. The bandwidth of the filter is wide enough that for practical purposes all of the signal energy is passed [83], [53]. The filter output is then sampled at a rate of $1/T_s$ to provide discrete-time sequence with a set of sufficient statistic. The $k$-th sample of $r(t)$ is given by $r_k = r(kT_s) = s_k + n_k$, where $n_k \sim \mathcal{N}(0, N_0 + z_k N_J/\rho)$ is a zero-mean complex Gaussian random noise sample representing the sum of the additive white Gaussian noise (AWGN) and pulse noise jamming noise where the jammer state variable $z$ is defined as $P(z = 1) = \rho$ if jammer is ON and $P(z = 0) = 1 - \rho$ if jammer is OFF and the duty factor $\rho$ $(0 < \rho \leq 1)$ is the probability that a symbol is jammed, forming a discrete chip sequence $\mathbf{r} = [r_1, \ldots, r_{GN'}]$ where $r_k = r_{Ik} + jr_{Q_k}$. Note that perfect bit synchronization and timing recovery, and perfect coherent carrier phase reference are assumed.

The symbol-by-symbol inner demodulator for the DS concatenated coded CPM system generates log-likelihood ratios (LLRs) based on the channel output. The chip sequence $\mathbf{r}$ is

descrambled and despread using the known PN sequence $\mathbf{c}$ as

$$y_j = \sum_{k=1}^{G} c_{j+(k-1)N'} \cdot r_{j+(k-1)N'},\ j = 1, \ldots, N'. \tag{11}$$

Given the despread sequence $\mathbf{y}$, the inner demodulator generates LLRs for each element in the sequence $\tilde{\mathbf{d}}$ that represents the randomly interleaved code bit sequence of $\mathbf{d}$. The composite LLRs for the $j$-th code bit at the output of the demodulator are given by

$$L_i^m(\tilde{d}_j) = \log\left[\frac{P(\mathbf{y}|\tilde{d}_j = 1, z_j = z)}{P(\mathbf{y}|\tilde{d}_j = 0, z_j = z)}\right] + \log\left[\frac{P(\tilde{d}_j = 1)}{P(\tilde{d}_j = 0)}\right], \tag{12}$$

where subscript $i$ and superscript $m$ denote the inner demodulator and the $m$-th iteration, respectively, and the branch transition probability in the MAP decoder for channel use $j$ in the presence of pulse noise jamming is $p(y_j|\tilde{d}_j, z_j = z) = \exp\left[-|y_j - \tilde{d}_j|^2/2\sigma_z^2\right]/\sqrt{2\pi\sigma_z^2}$, where $y_j$, $z_j$, $\tilde{d}_j$, and $\sigma_z^2$ represent the demodulator output, the jammer state, the channel input, and noise variance, respectively. Then, (12) can be decomposed as

$$L_i^m(\tilde{d}_j) = L_{i,e}^m(\tilde{d}_j) + L_{i,a}^m(\tilde{d}_j) = L_{i,e}^m(\tilde{d}_j) + L_{o,e}^{m-1}(\tilde{d}_j), \tag{13}$$

where the subscripts $o$, $a$, and $e$ denote the outer decoder, the *a priori* information, and the extrinsic information, respectively. The extrinsic LLRs $L_{i,e}^m(\tilde{d}_j)$ in (13) are deinterleaved and forwarded to the outer decoder. The *a posteriori* LLRs $L_o^m(\tilde{d}_j)$ for the outer decoder is calculated using the trellis structure and $L_{i,e}^m(\tilde{d}_j)$ as $L_o^m(\tilde{d}_j) = L_{o,e}^m(\tilde{d}_j) + L_{o,a}^m(\tilde{d}_j) = L_{o,e}^m(\tilde{d}_j) + L_{i,e}^m(\tilde{d}_j),\ m \geq 1$. Finally, only the bit extrinsic information $L_{o,e}^m(\tilde{d}_j)$ is fed back to the inner demodulator after interleaving as the *a priori* LLRs for $\tilde{d}_j$, $L_{o,e}^{m-1}(\tilde{d}_j)$, as shown in (13).

### 3.1.3 Chip-by-Chip Random Interleaved System

In this section, the iterative receiver for the chip-wise random interleaved DS concatenated coded CPM system is described for purposes of comparison with block-wise random interleaving. In contrast to block-wise random interleaving, the spread sequence $\mathbf{b}$ is randomly permuted chip-by-chip and then scrambled using the PN sequence $\mathbf{c}$. Finally, the scrambled sequence $\boldsymbol{\alpha}$ is input to the CPM modulator. Note that the length of the random interleaver is $G \cdot N'$. In the presence of pulse jamming, the jammer will stay on for the entire duration

of a chip when jammed. At the receiver, the inner demodulator generates LLRs for each bit in the sequence $\tilde{\mathbf{b}}$ given the received sequence $\mathbf{r}$. The composite LLRs of the inner demodulator at the $j$-th bit and $k$-th chip intervals can be calculated by replacing $\tilde{d_j}$ and $\mathbf{y}$ in (12) with $\tilde{b}_{j,k}$ and $\mathbf{r}$, respectively. The generated extrinsic LLRs $L^m_{i,e}(\tilde{b}_{j,k})$ that are used as inputs to the outer decoder are descrambled and then deinterleaved chip-by-chip. Then the deinterleaved extrinsic LLRs $\tilde{L}^m_{i,e}(\tilde{b}_{j,k})$ are combined such that constituent probabilities are weighted according to the JSI, i.e.,

$$\begin{aligned}\tilde{L}^m_{i,e}(\tilde{b}_j) &= \sum_{k=1}^{G} \tilde{L}^m_{i,e}(\tilde{b}_{j,k}) \\ &= \sum_{k=1}^{G} \log\left[\frac{\sum_m \sum_{m'} \alpha_{j-1}(m')\beta_j(m)\gamma_1(r_{j,k}, z_{j,k}, m', m)}{\sum_m \sum_{m'} \alpha_{j-1}(m')\beta_j(m)\gamma_0(r_{j,k}, z_{j,k}, m', m)}\right], \end{aligned} \tag{14}$$

where $s_j = m$ and $s_{j-1} = m'$ represent the trellis state transition, $\alpha_j(m)$ and $\beta_j(m)$ represent the forward and backward recursion probability functions, respectively, and the branch transition probability is $\gamma_i(r_{j,k}, z_{j,k}, m', m) = p(r_{j,k}|\tilde{b}_{j,k} = i, z_{j,k} = z, s_{j-1} = m', s_j = m)p(z_{j,k} = z)P(s_j = m|\tilde{b}_{j,k} = i, s_{j-1} = m')$. The combined LLRs in (14) are forwarded to the outer decoder, and the *a posteriori* LLRs $L^m_o(\tilde{b}_j)$ from the outer decoder can be calculated in a similar way. To pass the chip extrinsic LLRs to the inner demodulator, the extrinsic LLRs are spread and then scrambled.

## *3.2 Bound Analysis of the Anti-Jamming Performance*

The upper bound on BER for the block-wise random interleaved DS concatenated coded CPM system is calculated by applying the serially concatenated code approach based on the ensemble uniform interleaver in [13]. We briefly describe this modification by considering a system with overall rate $R = m/p$, wherein the outer convolutional code with rate $R^o = m/n$ and the inner CPM with rate $R^i = n/p = 1$ are joined by an interleaver of length $N'$. The pairwise error probability $P_{pw}(d)$ in the presence of pulse noise jamming is calculated by conditioning on the event that $k$ of $d$ CPM symbols are jammed. Therefore, we can obtain a closed-form upper bound on the bit error probability assuming ML soft-decision decoder

and uniformity of CPM sequence[1] as

$$P_b \leq \sum_{d=d_m}^{N'} \sum_{w=w_m^o}^{N'R^o} \frac{w}{NR^o} A_{w,d} P_{pw}(d) \tag{15}$$

$$= \sum_{d=d_m}^{N'} \sum_{w=w_m^o}^{N'R^o} \sum_{k=0}^{d} \frac{w}{NR^o} A_{w,d} P_{pw}(d|z_k^d) P(z_k^d), \tag{16}$$

where $d_m$ of a length-$N'$ compound error event is the minimum weight of the codewords for the concatenated coded CPM that is calculated by $\min_{\boldsymbol{\alpha},\hat{\boldsymbol{\alpha}}} \int_0^{N'T_s} |s(t,\boldsymbol{\alpha}) - s(t,\hat{\boldsymbol{\alpha}})|^2 dt/2E_s$ $= \min_{\boldsymbol{\alpha},\hat{\boldsymbol{\alpha}}} \int_0^{N'T_s} [1 - \cos\Delta\phi(t)] dt/T_s$ [115], $w_m^o$ is the minimum weight of an input sequence generating an error event of the outer code, $A_{w,d}$ represents the average number of codewords with weight $d$ associated with an information words of weight $w$, the upper bound of $P_{pw}(d|z_k^d)$ assuming known JSI can be calculated as

$$P_{pw}(d|z_k^d) \leq Q\left(\sqrt{E_b R\left[k/\sigma_1^2 + (d-k)/\sigma_0^2\right]}\right) < \frac{1}{2}\exp\left(-\frac{E_b R}{2}\left[k/\sigma_1^2 + (d-k)/\sigma_0^2\right]\right), \tag{17}$$

and $P(z_k^d)$ denotes the probability that $k$ of $d$ CPM symbols are jammed and is given by

$$P(z_k^d) = \binom{d}{k} P(z=1)^k P(z=0)^{d-k} = \frac{d!}{k!(d-k)!}\rho^k(1-\rho)^{d-k}, \tag{18}$$

where $k = 0, 1, \ldots, d$.

## *3.3 Mixed Concatenated Coded CPM and Convergence Analysis*

Mixed concatenated codes (MCCs) where outer and/or inner codes can be constructed using multiple constituent codes are a family of turbo-like codes. The output bits from the constituent codes are demultiplexed according to their mixture ratios and then passed to the next stage. Part of the MCC design is to find the optimal mixture ratio. The design of MCCs can be undertaken by using a decoding convergence analysis based on density evolution [122], [43], [27] since such analysis exposes the advantages and disadvantages of candidate constituent codes.

[1]The error probability is independent of the reference sequence that corresponds to all-zero input sequence and depends only on the input error sequence [97].

Having the known transmitted inner information bits, the *a priori* input $L1, in$ can be modelled as $L1, in = \nu_{L1,in} \cdot x + n_{L1,in} = 2(x + n_J)/\sigma_z^2$ where $\sigma_z^2 = N_0 + zN_J/\rho$, and the mean $\nu_{L1,in} = 2/\sigma_z^2$ and variance $\sigma_{L1,in}^2 = 4/\sigma_z^2$. The derivation of the transfer characteristics are described in the Appendix B. Input extrinsic information $I_{L1,in} = I(X; L1, in)$ between transmitted inner information bits $X$ and the LLR-values $L1, in$ is calculated as

$$\begin{aligned} I_{L1,in} &= \frac{1}{2} \sum_{x=\pm 1} \int_{-\infty}^{+\infty} p_{L1,in}(\lambda|X=x) \log_2 \left[ \frac{2p_{L1,in}(\lambda|X=x)}{p_{L1,in}(\lambda|X=-1) + p_{L1,in}(\lambda|X=+1)} \right] d\lambda \\ &= \int_{-\infty}^{+\infty} p_{L1,in}(\lambda|X=x) \left[ 1 - \log_2(1+e^{-\lambda}) \right] d\lambda \\ &= E\left[ \log_2(2/(1+e^{-\lambda}) \right], \end{aligned} \tag{19}$$

where the conditional probability density function $p_{L1,in}(\lambda|X=x)$ is represented as $p(\lambda|X = x) = \frac{1}{\sqrt{2\pi\sigma_{L1,in}^2}} \exp\left\{ -\frac{(\lambda - \nu_{L1,in} \cdot x)^2}{2\sigma_{L1,in}^2} \right\}$. It is monotonically increasing and thus reversible. The output extrinsic information $I_{L1,out}$ for the inner CPM demodulator can be obtained as $I_{L1,out} = I(X; L1, out) = f_{L1}(I_{L1,in}, E_b/N_J)$ where $0 \leq I_{L1,in},\ I_{L1,out} \leq 1$. Similarly, the input and output extrinsic information $I_{L2,in}$ and $I_{L1,out}$ for the outer decoder are calculated.

In our work, we focus on the use of the code mixing to the inner code, i.e., inner CPM, where recursive and non-recursive forms replace the conventional recursive CPM modules, as illustrated in Fig. 13. For MSK, the generator polynomials for the recursive and non-recursive continuous phase encoders are $(1, 1/1 + D)$ and $(1 + D, D)$, respectively. The interleaved sequence is demultiplexed into two sub-sequences according to a predefined mixture ratio $\mu$. One is modulated using recursive CPM and the other is modulated using non-recursive CPM. Two modulated CPM symbol sequences, $s_r(t, \boldsymbol{\alpha})$ and $s_n(t, \boldsymbol{\alpha})$, are transmitted one after another in a serial fashion to keep phase continuity. To accommodate the mixed CPM at the receiver, mixed MAP demodulators for the recursive and non-recursive CPMs are used instead of the single recursive MAP demodulator. The combined sequence is demultiplexed into two sub-sequences according to the mixture ratio. One is demodulated through the recursive MAP and the other is demodulated through the non-recursive MAP. Then two sub-sequences are multiplexed and passed to the next stage.

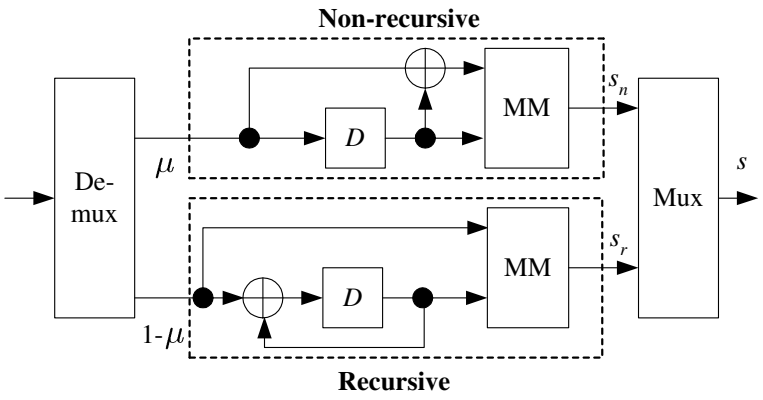


**Figure 13:** Mixed CPM consisting of recursive and non-recursive MSKs. The generator polynomials for the recursive and non-recursive CPEs are $(1, 1/1 + D)$ and $(1 + D, D)$, respectively.

## *3.4 Numerical Results and Discussions*

In this section, we present the simulation and analytical anti-jamming performance results for the proposed DS concatenated coded CPM system. An outer rate-1/2 non-recursive convolutional code with memory of 2 and octal generator polynomials $(7, 5)$ is used. Binary MSK with and $L = 1$ and $h = 1/2$ is used for CPM, unless stated otherwise. The information block size is 1000 bits and the maximum number of decoding iteration is set to 15. The background AWGN in case of the existence of jamming is set to 20 dB since the jamming is dominant.

### 3.4.1 Chip- vs. Block-wise Random Interleaving

Comparing the block-random interleaved system to the chip-by-chip random interleaved system is investigated. Fig. 14 shows the BER performance of the chip-by-chip random interleaved DS concatenated coded CPM of varying the processing gain $G$. Note that a single recursive form of MSK, which corresponds to $\mu = 0$, is used for the simulation. As the processing gain increases, the BER degrades. The reason for this result is that the sum of the chip extrinsic information from the inner demodulator gets less reliable as the processing gain increases. Thus, this system is not suitable for the spread-spectrum application on an AWGN channel. To remedy this significant degradation without the

destruction of the phase continuity of the CPM signal, the random-block interleaved system has been designed. Fig. 15 shows the BER performance of the random-block interleaved DS concatenated coded CPM of varying the processing gain $G$ and decoding iterations. In contrast to the performance of the chip-by-chip random interleaved system, same BER performance regardless of the processing gain can be achieved and, thus, it is suitable for the transmission of the SS CPM signal.

Furthermore, it is shown in Fig. 15 that the case of binary MSK with $h = 1/2$ outperforms the case of full-response 4-ary CPFSK with $h = 1/4$ by about 0.3 dB.

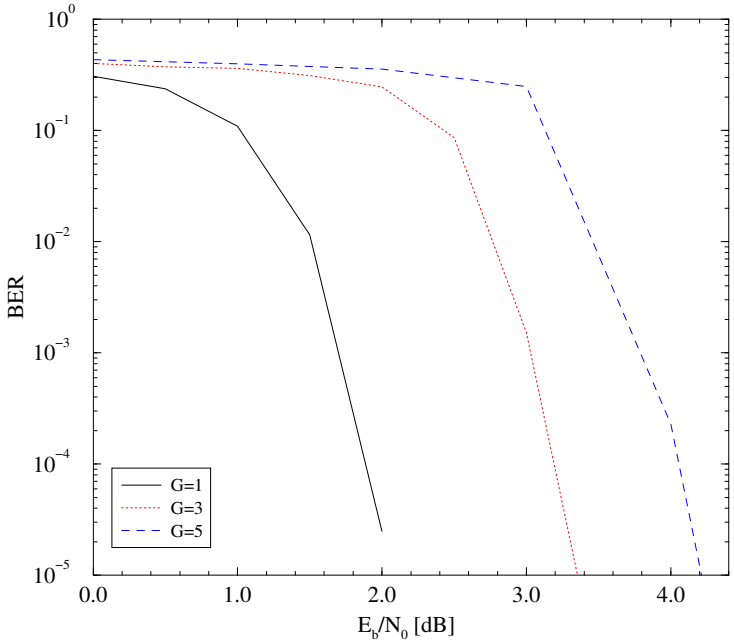


**Figure 14:** BER performance of chipwise random interleaved system as a function of processing gain $G$ on an AWGN channel.

### 3.4.2 Effect of the Jamming Duty Factor under Pulse Jamming

Fig. 16 exhibits the anti-jamming performance of the block-random interleaved DS concatenated coded CPM for different duty factors $\rho$ and decoding iterations. It is assumed that the JSI is known to the receiver. The plots demonstrate how the anti-jamming performance for the proposed iterative receiver depends on the duty factor. The $y$-axis represents a required $E_b/N_J$ needed to achieve the target BER=$10^{-4}$. The worst-case pulse noise jammer adjusts

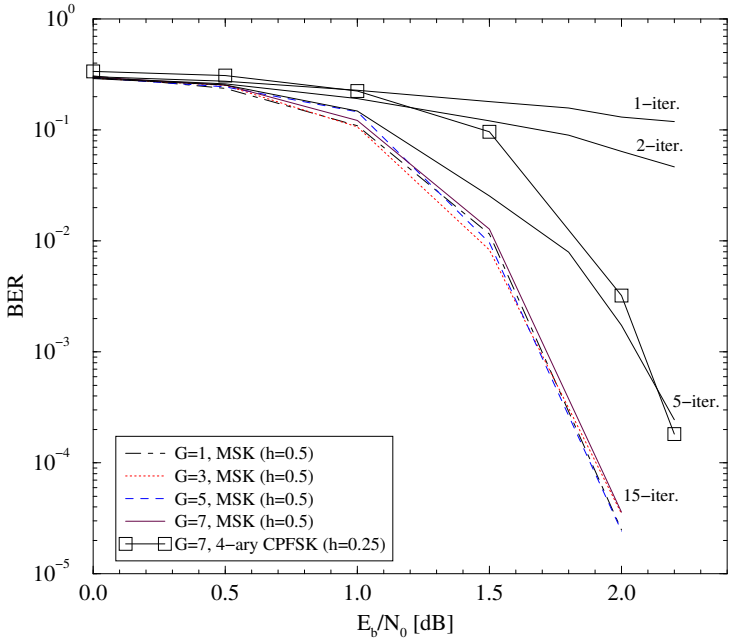


**Figure 15:** BER performance of block-random interleaved system (MSK and 4-ary CPFSK) as a function of processing gain $G$ on an AWGN channel. Curves for 1, 2, 5, and 15-iteration are also plotted.

$\rho$ to maximize the bit error probability $P_b$ for a given $E_b/N_J$. For the target BER of $10^{-4}$, the worst-case jamming occurs when the continual jamming (i.e., $\rho = 1.0$) exists except the case with a single decoding iteration. As the iteration in the IDD receiver increases, the required $E_b/N_J$ decreases and thus better anti-jamming capability can be achieved. For the worst-case jamming, a significant anti-jamming gain as much as 5 dB is achieved. It is also observed that the improvement through iterations increases when the duty factor is smaller than around 0.3.

### 3.4.3 Analytical Anti-Jamming Performance

Upper bound analysis on the error probability for the iterative receivers can be performed at very low BER region where the error floor effect is usually observed. The analytical anti-jamming performance using the upper bound, which has been derived in Section III, and simulation results for the random-block interleaved DS concatenated coded CPM system are plotted in Fig. 17 for various duty factors $\rho$. The BER upper bound at relatively high

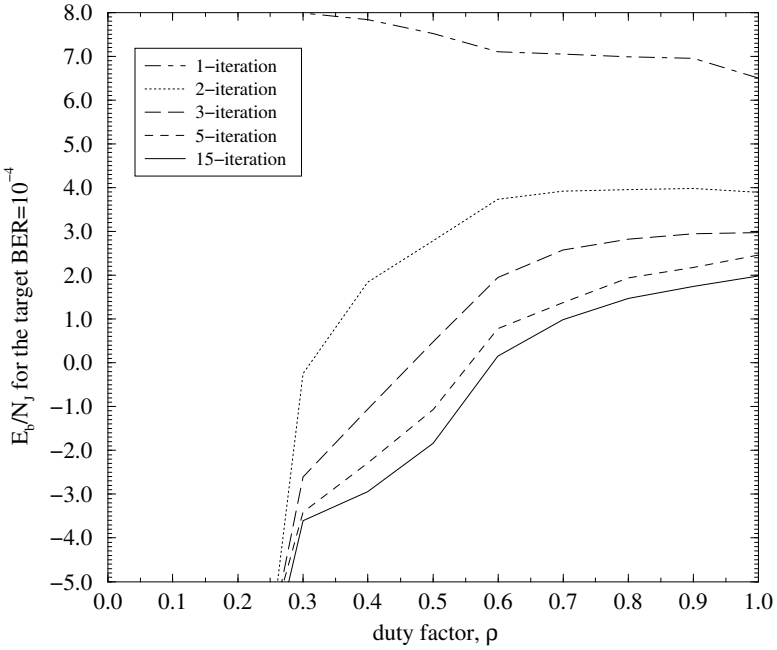


**Figure 16:** Anti-jamming performance for varying duty factor $\rho$ and decoding iterations. Curves for 1, 2, 3, 5, and 15 decoding iterations are plotted.

$E_b/N_J$ reduces as the duty factor of the pulse jamming decreases and the peak jamming power increases.

The anti-jamming performance for the worst-case duty factor $\rho^{wc}$ can be expressed as $P_b^{wc} = P_b(\rho)|_{\rho=\rho^{wc}}$ where $0 < \rho^{wc} \leq 1$. The obtained analytical bound results are used for finding the worst-case duty factor $\rho^{wc}$ since the mathematical manipulation of $dP_b(\rho)/d\rho = 0$ is very difficult for the proposed iterative anti-jam system. The worst-case jamming occurs when the pulse jamming with $\rho^{wc}$ as shown in Fig. 18 is applied. It is evident from the bound analysis that the optimal duty factor for the jammer when the worst-case jamming occurs is different depending on a target BER. From the upper bound results, it is clear that the anti-jamming performance of the case with low duty factor yields significant error floor at very low BER. Although small portion of sequence is jammed, it cannot be demodulated and decoded correctly due to a relatively strong jamming power.

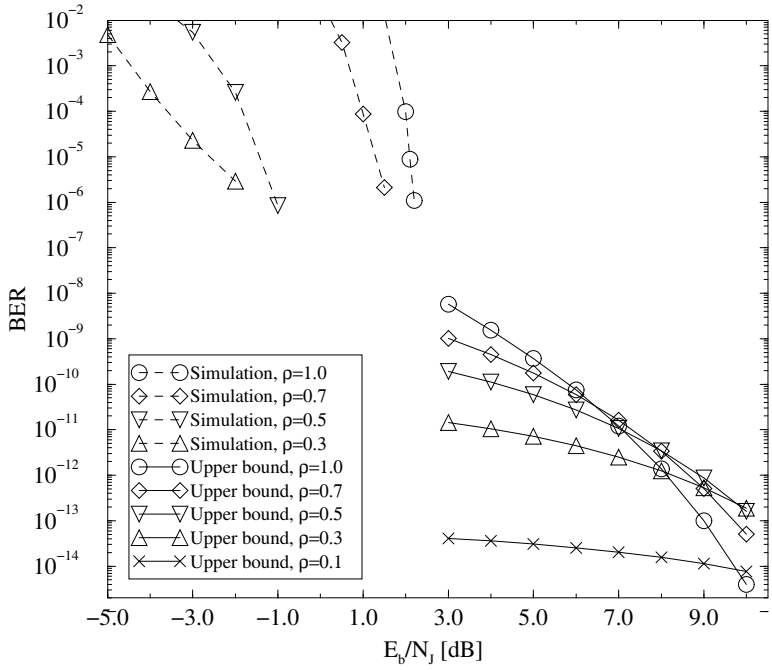


**Figure 17:** Analytical anti-jamming performance using the upper bound analysis and simulation results.

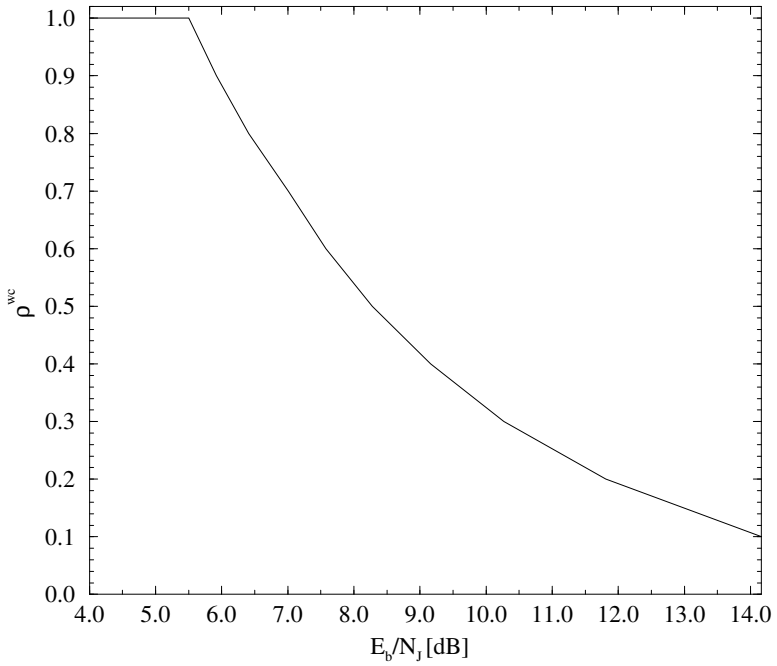


**Figure 18:** The worst-case duty factor $\rho^{wc}$ as a function of $E_b/N_J$ in the presence of pulse jamming.

### 3.4.4 Effect of the Mixture Ratio on the Iterative Receiver

Fig. 20 (a) and (b) show the decoding convergence chart for the recursive and non-recursive MSK forms and the effect on the anti-jamming performance of the block-random interleaved DS mixed concatenated coded CPM as a function of mixture ratio $\mu$ under the continual jamming (i.e., $\rho = 1$), respectively. The recursive MSK has a good convergence capability that is represented by a high slope, but low initial value $I_{L1,out}$ of about 0.42. On the contrary, the non-recursive MSK has relatively high initial value $I_{L1,out}$ of about 0.65, but little convergence capability that is represented by almost zero slope. For the non-recursive MSK, this explains the fact that little convergence is achieved as iteration continues although it offers better BER performance than the counterpart at low-to-medium SNR region. Thus, it is desirable to exploit the advantages of both the recursive and the non-recursive CPM forms to improve performance further.

As more bits are assigned to the non-recursive modulator (i.e., the case with large $\mu$), error floor effect is more significant at higher $E_b/N_J$. Also, $E_b/N_J$ where the error floor appears gets lower as the mixture ratio increases due to poor convergence capability of the non-recursive part. However, at relatively low $E_b/N_J$, as more bits are assigned to the non-recursive modulator, more BER reduction is achieved owing to the higher initial value $I_{Li1,out}$ as shown on Fig. 19. Therefore, an optimal mixture ratio can be selected according to a target BER range that is of interest to the communicators. For example, if the target BER ranges from on the order of $10^{-3}$ to $10^{-5}$, the optimal mixture ratio for the communicators will be 0.3 as shown in Fig. 20.

### 3.4.5 Effect of the Duty Factor and the Mixture Ratio on the Anti-Jamming Performance

Fig. 21 shows the effect of duty factor and mixture ratio on the anti-jamming performance at a target BER=$10^{-4}$. As the duty factor decreases from 1.0 down to 0.55, lower $E_b/N_J$ is required for achieving the target BER. In contrast to this tendency, higher $E_b/N_J$ is required when $\rho \leq 0.55$. For the worst-case jamming with $\mu = 0.3$, smaller $E_b/N_J$ as much as 0.5 dB is required although more dominant error floor is shown. Therefore, the MCCs

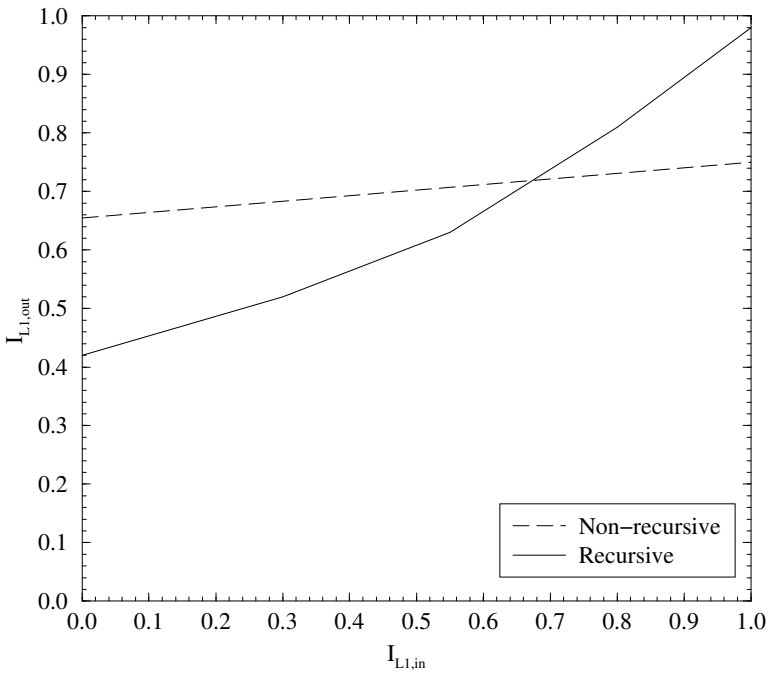


**Figure 19:** Convergence chart for MSK at $E_b/N_J = 2$ dB.

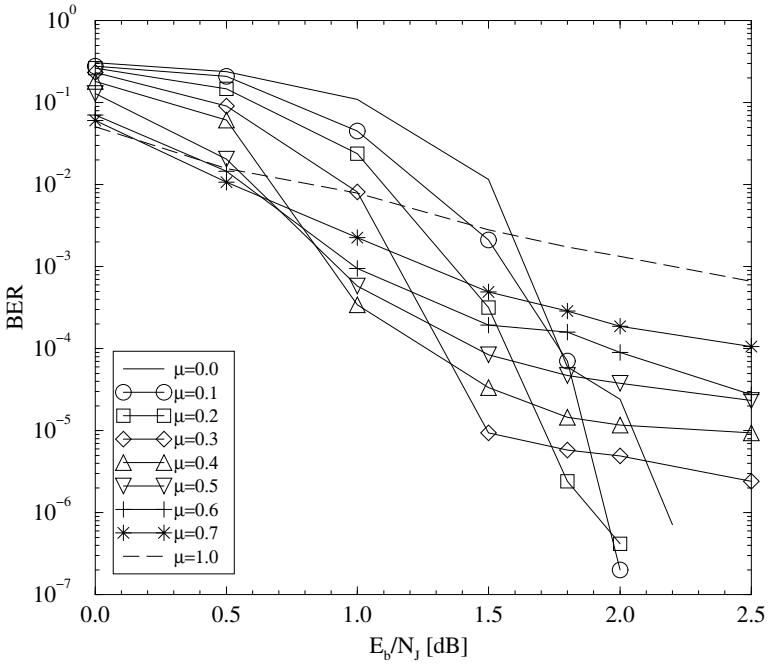


**Figure 20:** BER performance as a function of the mixture ratio $\mu$ under continual jamming. Note that $\mu = 0.0$ and $\mu = 1.0$ mean the recursive and non-recursive MSKs, respectively.

with a proper mixture ratio has a beneficial effect on the anti-jamming performance. In addition, it is worthy noting that the communicators employing code mixing can benefit better LPD/LPI since a surveillance receiver should know the used mixture ratio to detect signals correctly.

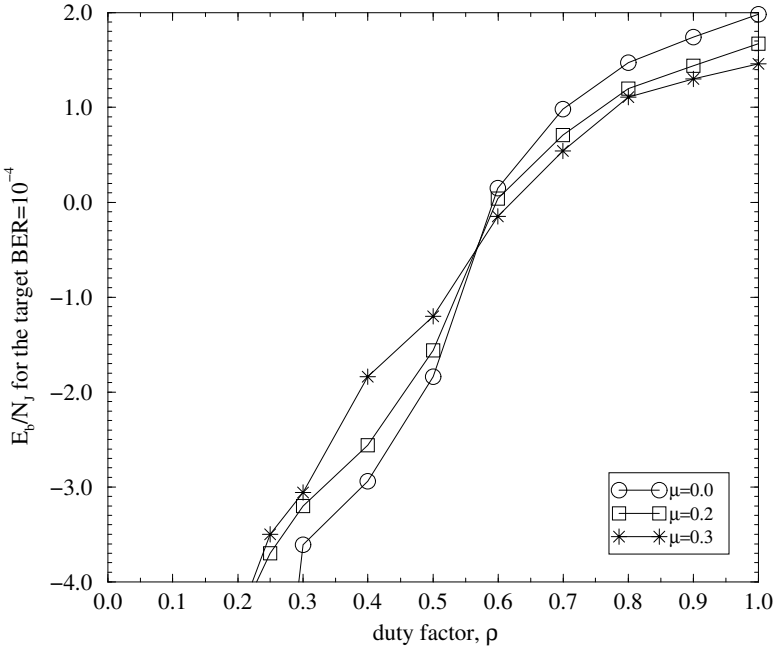


**Figure 21:** Effect of duty factor $\rho$ and mixture ratio $\mu$ on the anti-jamming performance.

### 3.4.6 Convergence Analysis on Anti-Jamming Performance

Further investigation using the convergence analysis that is described in Section IV is needed to assess the effect of the CPM mixing in the iterative anti-jam receiver on the anti-jamming performance. Fig. 22 visualizes the decoding trajectory of the block-random interleaved DS mixed concatenated coded CPM system for different duty factors and mixture ratios. It is noted that we pick the case with continual jamming and the case with a relatively small duty factor to compare the density evolution. At $E_b/N_0$=1.5 dB, the trajectory has managed to sneak through because both inner and outer decoders characteristics does not intersect below $I_{L1,in} < 0.9$ as shown in Fig. 22 (a). However, two trajectory curves get stuck when $E_b/N_0 < 1.5$ dB. It is noted that this point approximately corresponds to the BER waterfall

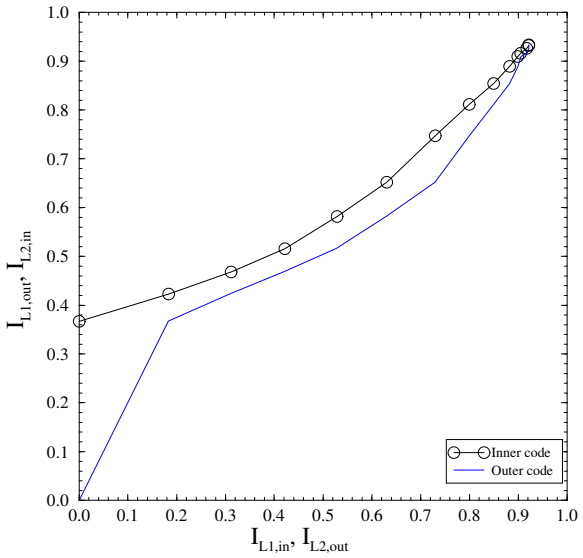


(a) $\mu = 0$ and $\rho = 1.0$ at $E_b/N_J = 1.5$ dB.

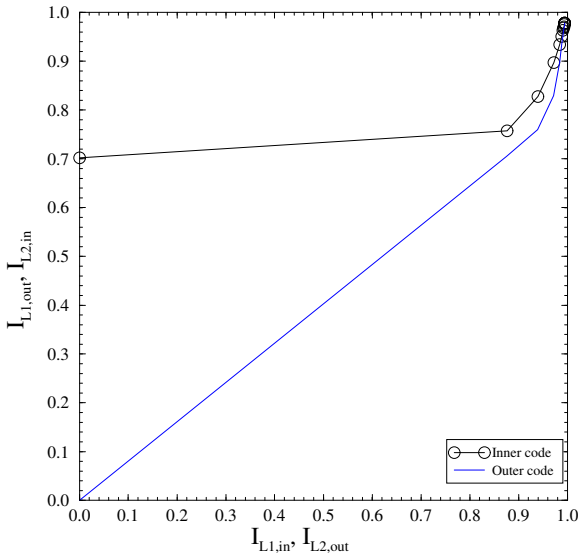


(b) $\mu = 0$ and $\rho = 0.3$ at $E_b/N_J = -3.5$ dB.

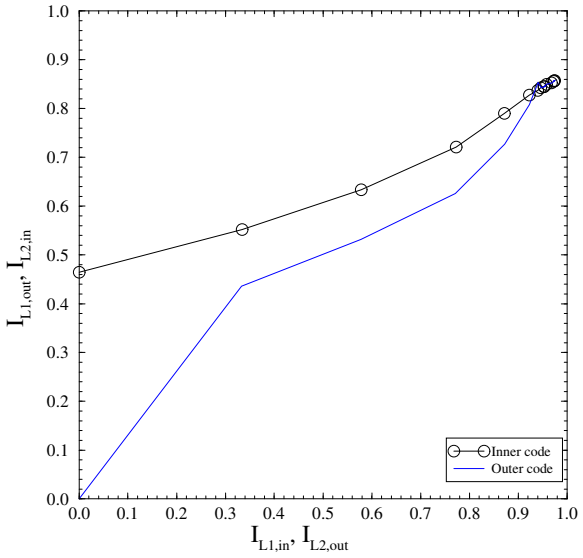


(c) $\mu = 0.3$ and $\rho = 1.0$ at $E_b/N_J = 1.5$ dB.

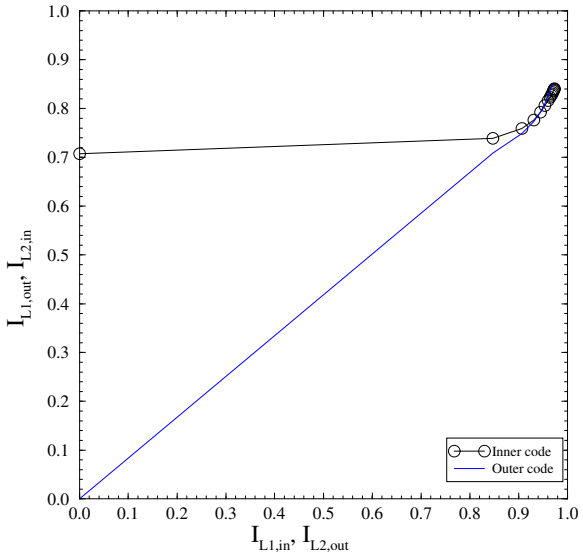


(d) $\mu = 0.3$ and $\rho = 0.3$ at $E_b/N_J = -3.5$ dB.

**Figure 22:** Convergence behavior for the anti-jamming performance in the presence of pulse jamming. CPM and convolutional code are used as the inner and outer codes, respectively. $\mu$ and $\rho$ denote the mixture ratio and the jamming duty factor, respectively.

region where low BER can be achieved through many iterations. Having compared Fig. 22 (a) with (c) to investigate the effect of mixture ratio $\mu$ on the performance for the worst-case jamming, (a) yields better convergence than (c) although the initial value of $I_{L1,out}$ of (a) is smaller than that of (c). Similar behavior is observed for the case with small duty factor as shown in Fig. 22 (b) and (d). It is observed that the initial values of $I_{L1,out}$ for (b) and (d) are larger than that of (a) and (c) since the jamming duty factor $\rho$ of (b) and (d) is smaller thanin (a) and (c). Furthermore, better decoding convergence is observed for (a) and (b) where $\mu = 0$ than for (c) and (d) where $\mu = 0.3$. This is confirmed by the curves in Fig. 17 that the error floor can be attributed to poor convergence capability.

## *3.5 Conclusions*

We have proposed a power- and bandwidth-efficient DS concatenated coded CPM system to provide anti-jamming and LPD/LPI performance as well as to keep phase continuity. Coherent iterative demodulator and decoder utilizing the JSI has been utilized in the presence of pulse noise jamming. Block-wise interleaving has been shown to outperform chip-wise interleaving. It has been shown that as the iteration in the receiver increases, the required $E_b/N_J$ decreases and thus better anti-jamming capability can be achieved. A mixed concatenated coded CPM system with a proper mixture ratio has been shown to improve the anti-jamming performance. Finally, we have explained the error-floor phenomenon in the case of a large mixture ratio by the poor decoding convergence through the convergence analysis.

# CHAPTER IV

# SERIALLY CONCATENATED SLOW FH-CPM

A coded frequency-hopping spread-spectrum technique is effective in combating hostile jamming and unintentional interference [115], reducing the signal detectability by an intercept receiver for tactical SS systems [19]. In particular, spectrally efficient CPM signals with high processing gain are desirable because the transmission of multiple symbols per hop enables high-speed data transmission.

FH-CPM and FH-FSK signals have been used as the basic waveforms of FH combat radio systems. It was reported in [124] that FH continuous-phase FSK (FH-CPFSK) outperforms FH-MFSK as much as 4 dB in terms of BER when limiter-discriminator detection is employed. Slow FH-BFSK signals with a concatenated coding on a partial-band noise jamming (PBNJ) channel were studied in [39]. Lam and Wittke proposed a *uncoded* slow FH-CPM system that is phase-continuous during each hop, which offers improved spectrum utilization [71]. Recently, a turbo-coded FH-BFSK waveform on a PBNJ channel has been investigated and compared with an RS coded system [59]. However, the approach in [59] does not utilize an iterative coded modulation scheme and requires a block-interleaved FH pattern that is specific to the turbo code. Convolutional- and turbo-coded FH-BPSK system and pilot symbol-aided coherent iterative decoding have been studied in [44]. In this scheme, a block channel interleaver followed by a frequency hopper is used to distribute the modulated sequence across different frequency bands. However, there has been little work done on the design and analysis of anti-jam slow FH-CPM signals combined with concatenated coding.

In this chapter, we propose a serially concatenated slow FH-CPM system in the presence of PBNJ. Slow FH (i.e., multiple data symbols per hop) must be used with CPM because the phase-continuity of the transmitted signals within each hop interval must be preserved.

Coherent and non-coherent, suboptimal SISO MAP-based iterative receivers having a reasonable complexity have been proposed in [45], [97]. Such receivers can well approximate joint optimal demodulation and decoding of concatenated codes. The slow FH-CPM signal suffers from channel memory because channel interleaving preceded by CPM cannot be used unlike PSK and FSK modulation schemes [67]. The resulting degradation on anti-jamming performance is investigated. We also address the effect of the choice of outer convolutional code and modulation index on performance.

JSI is critical for trellis-coded FH/SS systems, and the iterative soft-decoding metric should account for JSI. However, it is not realistic to assume that jamming parameters such as the jammer state, duty factor, and noise variances of jamming and AWGN are known to the receiver. Therefore, we propose a *blind* iterative jamming estimation technique to estimate jamming parameters for an anti-jam serially concatenated slow FH-CPM system in the presence of PBNJ. In addition, since iterative system shows different performance from non-iterative system, we investigate the effects of them on the anti-jamming performance and jamming estimation.

The main contributions can be summarized as follows: i) proposal of a slow FH-CPM system combined with a concatenated coding along with coherent and non-coherent anti-jam iterative demodulation and decoding, ii) investigation of the iterative anti-jamming performance as well as the worst-case jamming performance against PBNJ through simulation and ML bound analysis, and iii) proposal of an iterative jamming estimation technique in the presence of PBNJ.

## *4.1 System Model*

### 4.1.1 Transmitter Structure

Fig. 23 shows the serially concatenated slow FH-CPM communication system, consisting of the transmitter and the iterative receiver in conjunction with a JSI estimator. The transmitter includes an outer convolutional encoder, a random interleaver, an inner CPM modulator [106], and a frequency hopper.

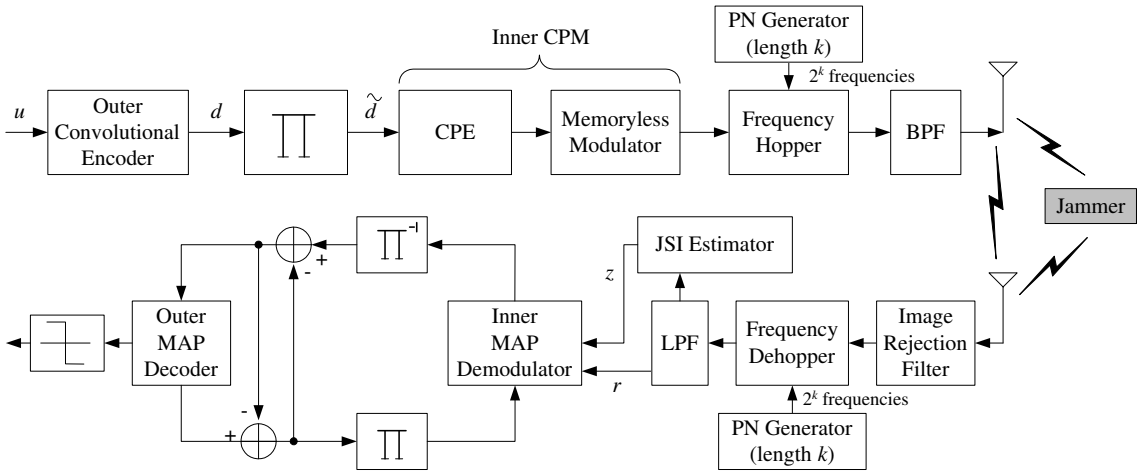


**Figure 23:** Transmitter and iterative receiver including a jamming estimator for the serially concatenated slow FH-CPM communication system. $\Pi$ and $\Pi^{-1}$ represent the concatenation interleaver and the corresponding deinterleaver, respectively.

An independent binary information sequence $\mathbf{u}$ of length $N_u$ bits is encoded by a rate-$N_u/N$ outer convolutional encoder. The binary coded sequence $\mathbf{d}$ of length $N$ from the outer encoder is multiplexed and then randomly interleaved. The permuted coded sequence $\tilde{\mathbf{d}}$ is then mapped on to the symbol sequence, $\boldsymbol{\alpha}$, $\alpha \in \{\pm 1, \pm 3, \ldots, \pm(M-1)\}$, that is input into the $M$-ary CPM module. The time-invariant CPE is linear over a finite field and acts as an inner recursive convolutional encoder. Note that the recursive nature of the CPE plays an important role in the convergence of the iterative decoder. A binary pseudo-noise (PN) sequence of length $k$ drives a frequency synthesizer which hops the carrier over $2^k$ frequencies. Because slow FH-CPM is used without additional channel interleaving, jammed frequency bands affect multiple consecutive symbols of the transmitted signals.

The serially concatenated FH-CPM signal is phase continuous during each hop interval but has a phase discontinuity at the start of a new hop, and is represented by

$$s(t, \boldsymbol{\alpha}) = \sqrt{\frac{2E_s}{T_s}} \sum_{i=-\infty}^{\infty} p(t - iN_hT_s) \cos[2\pi f_i t + \phi(t, \boldsymbol{\alpha})], \; nT_s < t \leq (n+1)T_s, \tag{20}$$

where $\boldsymbol{\alpha}$ is the CPM symbol sequence, $E_s$ is the energy per CPM symbol, $T_s$ is the CPM symbol interval, $p(t)$ is a unit amplitude rectangular pulse of duration $N_hT_s$ seconds, $f_i$ is the carrier frequency during the $i$-th hop, and $\phi(t, \boldsymbol{\alpha})$ is the information carrying phase.

Note that hop dwell interval is $T_h = N_h T_s = 1/R_h$.

### 4.1.2 Anti-Jam Coherent and Non-Coherent Iterative Receivers

PBNJ is one of the most effective jamming strategies against FH systems. A PBNJ spreads noise of total power of $J$ evenly over a frequency range of bandwidth $W_J$, which is a subset of the full spread bandwidth $W_{ss}$. The jammer determines its duty factor, $\rho \triangleq W_J/W_{ss} \in (0, 1]$, to maximize the system degradation. Because the pseudo-random FH is assumed to be used to produce uniform FH slot usage, the PBNJ can be modeled as a two state model and is independent from hop to hop. During a FH dwell time of $T_h$, let us define the jammer state random variable, $z$, where the hop is jammed with probability of $P(z = 1) = \rho$, and unjammed with probability of $P(z = 0) = 1 - \rho$. It is also assumed that the JSI yields the knowledge regarding the jamming state of the CPM symbols except of FH pattern and phase. JSI plays an important role in the SISO IDD process since a smart jammer can completely destroy a link even with minimal jammer power if JSI is not utilized.

The received FH-CPM signal is passed through a wideband image rejection filter. Afterwards, it is dehopped synchronously with a locally generated reference signal, which is given by $f_R(t) = 2\sum_{i=-\infty}^{\infty} p(t - iN_hT_s)\cos[2\pi(f_i + f_{\text{IF}})t]$ where $f_{\text{IF}}$ represents an intermediate carrier frequency. Therefore, the received dehopped complex CPM signal during the $i$-th hop in the presence of the PBNJ is

$$r^i(t) = \sqrt{\frac{2E_s}{T_s}}\cos[2\pi f_{\text{IF}}t + \phi_i(t, \boldsymbol{\alpha}) + \theta_i] + n_i(t),\ iN_hT_s < t \le (i+1)N_hT_s, \tag{21}$$

where $n_i \sim \mathcal{N}(0, N_0/2 + z_i N_J/2\rho)$ is the sum of double-sided AWGN and jamming noise and the random phase $\theta_i$ is assumed to be constant during the $i$-th hop interval but independent from hop to hop.

The MAP-based IDD is a SISO process that utilizes *a priori* symbol probabilities at its input and produces soft information at its output. The refined input symbol probabilities are fed back to the decoder as *a priori* information [45], [97]. Coherent and non-coherent reception schemes are applied to the proposed FH-CPM system. In practice, a pilot symbol-aided detection technique can be used for coherent reception [53]. Given the dehopped discrete complex sequence $\mathbf{r} = [\mathbf{r}^0, \ldots, \mathbf{r}^{N_f-1}]$, where $\mathbf{r}^i = [r_0^i, \ldots, r_{N_h-1}^i]$ and $N_f$ denotes

the number of total frequency bands, the inner MAP demodulator generates log-likelihood ratios (LLRs) for each bit in the interleaved sequence $\tilde{\mathbf{d}}$. The composite LLRs of the inner coherent demodulator for the $l$-th bit interval in the presence of the PBNJ is

$$L_I^m(\tilde{d}_l) = \log\left[\frac{P(\mathbf{r}|\tilde{d}_l = 1, z_l = z)}{P(\mathbf{r}|\tilde{d}_l = 0, z_l = z)}\right] + \log\left[\frac{P(\tilde{d}_l = 1)}{P(\tilde{d}_l = 0)}\right], \tag{22}$$

where subscript $I$ and superscript $m$ denote the inner demodulator and the $m$-th iteration, respectively. Assuming known JSI, the branch transition probability for channel use $l$ in the presence of the PBNJ is

$$P(r_l|\tilde{d}_l, z_l = z) = \frac{1}{\sqrt{2\pi\sigma_z^2}} \exp\left\{\frac{-|r_l - \tilde{d}_l|^2}{2\sigma_z^2}\right\}, \tag{23}$$

where $\sigma_z^2 = N_0/2 + zN_J/2\rho$ is the noise variance.

In the following, let us consider non-coherent iterative detection where the random phase $\theta_i$ of the dehopped signal is unknown to the receiver but is assumed to be constant during a hop duration. Non-coherent reception does not require any known symbol to estimate the random phase. Therefore, the conventional BCJR algorithm assuming the coherent detection has to be modified for the non-coherent reception of FH-CPM signals. Non-coherent iterative demodulation and decoding scheme using multiple symbol differential detection (MSDD) in [97], [138], [114] can be applied to our system. It is noted that the channel memory can be utilized in the proposed non-coherent iterative receiver.

To generate the LLRs for coded sequence $\tilde{\mathbf{d}}$, the non-coherent MAP demodulator observes the received dehopped signal over the $i$-th hop interval. The JSI is incorporated into the LLR calculations of the MAP demodulator and decoder. Since the number of distinct data sequences during a given hop is $M^{N_h}$, we have $M^{N_h}$ possible sequences of length $N_h$, represented by $\tilde{\mathbf{d}}_k^i = [\tilde{d}_{k,j}^i, \ldots, \tilde{d}_{k,l}^i, \ldots, \tilde{d}_{k,j+N_h-1}^i],\ k = 0, \ldots, M^{N_h} - 1$. Let $\mathbf{s}_k^i$ be the CPM signal corresponding to the sequence $s(t, \tilde{\mathbf{d}}_k^i)$ for simplicity of notation. The composite LLR of the inner non-coherent demodulator at time $j \le l \le j + N_h - 1$ for the PBNJ channel is

$$L_I^m(\tilde{d}_l) = \log\left[\sum_{k:\tilde{d}_{k,j}^i=1} P(\mathbf{r}^i, z^i|\mathbf{s}_k^i) \prod_{j=0}^{N_h-1} P(\tilde{d}_{k,j}^i)\right] - \log\left[\sum_{k:\tilde{d}_{k,j}^i=0} P(\mathbf{r}^i, z^i|\mathbf{s}_k^i) \prod_{j=0}^{N_h-1} P(\tilde{d}_{k,j}^i)\right]. \tag{24}$$

The *a priori* probability is calculated as

$$\prod_{j=0}^{N_h-1} P(\tilde{d}_{k,j}^i) = \prod_{j=0}^{N_h-1} \frac{e^{L_{O,e}^{m-1}(\tilde{d}_{k,j}^i)\tilde{d}_{k,j}^i}}{1+e^{L_{O,e}^{m-1}(\tilde{d}_{k,j}^i)}}. \tag{25}$$

Then, $P(\mathbf{r}^i, z^i|\mathbf{s}_k^i)$ in (24) is

$$\begin{aligned} P(\mathbf{r}^i, z^i|\mathbf{s}_k^i) &= P(\mathbf{r}^i|z^i=z, \mathbf{s}_k^i)P(z^i=z) \\ &= \int_0^{2\pi} P(\mathbf{r}^i|z^i=z, \mathbf{s}_k^i, \theta_i)p(\theta_i)d\theta_i \cdot P(z^i=z), \end{aligned} \tag{26}$$

where the phase $\theta_i$ is uniformly distributed random variable on the interval $[0, 2\pi)$. After some manipulation, (26) can be rewritten as

$$P(\mathbf{r}^i, z^i|\mathbf{s}_k^i) = K \cdot I_0\left(\frac{1}{\sigma_z^2}\left|\int_0^{N_hT_s} r^{i*}(t)\mathbf{s}_k^i dt\right|\right), \tag{27}$$

where $K$ is a constant and $I_0(\cdot)$ is the zeroth-order modified Bessel function of the first kind. The method for calculating $\int_0^{N_hT_s} r^{i*}(t)\mathbf{s}_k^i dt$ can be found in [97] and [138].

The composite LLR in (24) can be decomposed as $L_I^m(\tilde{d}_l) = L_{I,e}^m(\tilde{d}_l) + L_{O,e}^{m-1}(\tilde{d}_l)$, where the subscripts $O$ and $e$ denote the outer MAP decoder and the extrinsic LLRs, respectively. The extrinsic LLR $L_{I,e}^m(\tilde{d}_l)$ is calculated by excluding the contribution of $P(\tilde{d}_{k,l})$ as

$$\begin{aligned} L_{I,e}^m(\tilde{d}_l) = &\log\left[\sum_{k:\tilde{d}_{k,j}^i=1} P(\mathbf{r}^i, z^i|\mathbf{s}_k^i)\prod_{j=0,j\neq l}^{N_h-1} P(\tilde{d}_{k,j}^i)\right] \\ &- \log\left[\sum_{k:\tilde{d}_{k,j}^i=0} P(\mathbf{r}^i, z^i|\mathbf{s}_k^i)\prod_{j=0,j\neq l}^{N_h-1} P(\tilde{d}_{k,j}^i)\right], \end{aligned} \tag{28}$$

and the $L_{I,e}^m(\tilde{d}_l)$ are deinterleaved and forwarded to the outer decoder. The bit extrinsic LLR $L_{O,e}^m(\tilde{d}_l)$ is then passed to the inner demodulator. Note that only the extrinsic LLRs are fed back to the inner demodulator as the *a priori* LLRs for $\tilde{d}_l$ after bit interleaving. In case JSI is not available to the receiver, the decoder makes decisions on average transition probabilities over all jamming states.

## *4.2 Bound Analysis of the Anti-Jamming Performance*

Assuming ML decoding, an asymptotic union bound on anti-jamming bit error probability (BEP) performance of FH-CPM signals in the presence of the PBNJ is derived. It is

quite difficult to analyze exactly the error performance of an iterative system for a specific interleaver at low-to-moderate SNR. For large $N_h$, the performance of the non-coherent receiver performs to within a half dB that of the coherent receiver, as will be shown in Fig. 27. Therefore, a framework similar to the analysis for a serially concatenated convolutional code using the *ensemble* input-output transfer function (IOWEF) bounding technique and a hypothetical averaging uniform interleaver [97], [126], [13] is used.

Given the outer code with the code rate of $R^o = m/n$, the union bound for the BEP assuming the ML soft-decision decoder is

$$P_b \leq \sum_{d=d_m}^{N} \sum_{w=w_m^o}^{NR^o} \frac{w}{NR^o} A_{w,d} P_{pw}(d), \tag{29}$$

where $d_m$ is the minimum weight of all codewords, $w_m^o$ is the minimum weight of an input sequence generating an error event of the outer code, $P_{pw}(d)$ represents the pairwise error probability (PEP), and $A_{w,d}$ represents the overall IOWEF that is based on the use of the uniform interleaver[1] of length $N$. The detailed calculation of the IOWEF can be found in Appendix A, and the value of the minimum weight $d_m$ of a length-$N$ compound error event is calculated from

$$\begin{aligned} d_m &= \min_{\boldsymbol{\alpha},\hat{\boldsymbol{\alpha}}} \left\{ \frac{1}{2E_b} \int_0^{NT_s} |s(t,\boldsymbol{\alpha}) - s(t,\hat{\boldsymbol{\alpha}})|^2 dt \right\} \\ &= \min_{\boldsymbol{\alpha},\hat{\boldsymbol{\alpha}}} \left\{ \frac{\log_2 M}{T_s} \int_0^{NT_s} [1 - \cos \Delta\phi(t)] dt \right\}, \end{aligned} \tag{30}$$

where $\Delta\phi(t)$ denotes the phase difference between the coded FH-CPM signals. Finally, the PEP $P_{pw}(d)$ in (29) in the presence of the PBNJ is calculated by conditioning on the event that $k$ of $d$ symbols are jammed as

$$P_{pw}(d) = \sum_{k=0}^{d} \binom{d}{k} \rho^k (1-\rho)^{d-k} \cdot Q\left( \sqrt{E_b R \left[ \frac{k}{\sigma_1^2} + \frac{d-k}{\sigma_0^2} \right]} \right), \tag{31}$$

where $R$ is the overall code rate and $Q(\cdot)$ denotes the Q-function. For a receiver operating without JSI, the receiver makes bit decisions by summing the channel outputs. The corresponding PEP is

$$P_{pw}(d) = \sum_{k=0}^{d} \binom{d}{k} \rho^k (1-\rho)^{d-k} \cdot Q\left( \sqrt{\frac{E_b R d}{\frac{k}{d}\sigma_1^2 + \frac{d-k}{d}\sigma_0^2}} \right). \tag{32}$$

[1]The uniform interleaving is devised in [13] to map a given input sequence of length $N$ and weight $l$ into its all distinct $\binom{N}{l}$ permutations with equal probability of $1/\binom{N}{l} = l!(N-l)!/N!$.

## 4.3 An Iterative Jamming Estimation Technique

An important issue in the design of a FH system is the generation of jammer information such as the jammer state, duty factor, and noise variances of jamming and AWGN. A jamming estimation technique is required to generate jammer state estimates that are used to weight the branch metrics in an iterative receiver. It is promising that the anti-jamming performance can be further improved by incorporating the jammer information with iterative processing. Since random FH pattern is known to the coherent receiver, we need to estimate jamming states $\hat{\mathbf{z}}$, duty factor $\hat{\rho}$, and the noise variances of jamming noise and AWGN $\hat{\sigma}_z^2$ $(z = 0, 1)$ for the jamming estimation.

Given the dehopped discrete complex sequence $\mathbf{r} = [\mathbf{r}^0, \ldots, \mathbf{r}^{N_f'-1}]$, where $\mathbf{r}^i = [r_0^i, \ldots, r_{N_h-1}^i]$ and $N_f'$ denotes the number of total frequency bands, we first calculate the ratio of jammer state estimates $P(\hat{z}^i = 1|\mathbf{r}^i)/P(\hat{z}^i = 0|\mathbf{r}^i)$ from the received signal and pass this along with data bit estimates between demodulator and decoder. As decoding iterations proceed, we obtain more refined jammer state estimates as well as more refined data bit estimates. Let us define a log-probability ratio $L^m(\hat{z}^i)$ for the $i$-th hop during $m$-th iteration as

$$L^m(\hat{z}^i) = \log\left[\frac{P(\hat{z}^i = 1|\mathbf{r}^i)}{P(\hat{z}^i = 0|\mathbf{r}^i)}\right], \tag{33}$$

$$= \log\left[\frac{P(\mathbf{r}^i|\hat{z}^i = 1)P(\hat{z}^i = 1)}{P(\mathbf{r}^i|\hat{z}^i = 0)P(\hat{z}^i = 0)}\right], \tag{34}$$

where

$$P(\mathbf{r}^i|\hat{z}^i = z) = \prod_{l=0}^{N_h-1} \frac{1}{\sqrt{2\pi\hat{\sigma}_z^2}} \exp\left\{-\frac{1}{2\hat{\sigma}_z^2}|r_l^i - \mathrm{sign}(r_l^i)|^2\right\}, \tag{35}$$

$$= \frac{1}{(2\pi\hat{\sigma}_z^2)^{N_h/2}} \exp\left\{-\frac{1}{2\hat{\sigma}_z^2}\sum_{l=0}^{N_h-1}|r_l^i - \mathrm{sign}(r_l^i)|^2\right\}, \tag{36}$$

where $i = 0, \ldots, N_f' - 1$ and $\sigma_z^2 = N_0/2 + zN_J/2\rho$ is the noise variance. At the first iteration, initial duty factor of 0.5 and $E_b/N_0$ and $E_b/N_J$ offsets relative to the true $E_b/N_0$ and $E_b/N_J$ are used since they are unknown. Further, defining $V^i = \sum_{l=0}^{N_h-1}|r_l^i - \mathrm{sign}(r_l^i)|^2/2N_h$, we can rewrite (34) as

$$L^m(\hat{z}^i) = \log\left\{\frac{\hat{\rho}}{1-\hat{\rho}} \cdot \frac{\hat{\sigma}_0^{N_h}}{\hat{\sigma}_1^{N_h}} \cdot \exp\left[(\hat{\sigma}_0^{-2} - \hat{\sigma}_1^{-2})N_h V^i\right]\right\}. \tag{37}$$

This yields a log-likelihood threshold test for the jammer state estimate, where the $i$-th hop jammed is deemed to be jammed if $V^i > \epsilon$, or unjammed otherwise. The threshold $\epsilon$ can be obtained by equating (37) to zero, such that

$$\epsilon = K_\sigma \cdot \left\{ \frac{1}{2} \log \left( \frac{\hat{\sigma}_1^2}{\hat{\sigma}_0^2} \right) + \frac{1}{N_h} \log \left( \frac{1-\hat{\rho}}{\hat{\rho}} \right) \right\}, \tag{38}$$

where $K_\sigma = \hat{\sigma}_1^2 \hat{\sigma}_0^2 / (\hat{\sigma}_1^2 - \hat{\sigma}_0^2)$. Note that the threshold, *epsilon*, is updated every iteration. As a result, duty factor $\hat{\rho}$ is updated by counting the estimated $\hat{\mathbf{z}}$ such that

$$\hat{\rho} = \frac{N_1'}{N_f'}, \quad N_0' + N_1' = N_f', \tag{39}$$

where $N_1'$ and $N_0'$ denote the numbers of jammed hops and unjammed hops, respectively.

Having the JSI and duty factor, we can estimate the noise variances of jamming and AWGN, $\hat{\sigma}_1^2$ and $\hat{\sigma}_0^2$, in case that the noise variances are unknown to the receiver, i.e.,

$$\hat{\sigma}_1^2 = \frac{1}{N_1'} \sum_{i \in Z_J} \sum_{l=iN_h}^{(i+1)N_h - 1} |r_l^i - \text{sign}(r_l^i)|^2 / 2N_h, \tag{40}$$

and

$$\hat{\sigma}_0^2 = \frac{1}{N_0'} \sum_{i \notin Z_J} \sum_{l=iN_h}^{(i+1)N_h - 1} |r_l^i - \text{sign}(r_l^i)|^2 / 2N_h, \tag{41}$$

where $Z_J$ denotes a set of jammed hops. Once the jamming state and jamming noise variance have been estimated, they are used in the soft-input soft-output (SISO) maximum *a posteriori* (MAP)-based IDD process that utilizes *a priori* symbol probabilities at its input and produces soft information at its output. The flowchart for the jamming estimation is illustrated in Fig. 24.

## *4.4 Numerical Results and Discussions*

In this section, we present the simulation and analysis results of the anti-jamming performance. For the purpose of comparison with other systems, a rate-1/2 non-recursive and non-systematic convolutional code with octal generator polynomials of $(7, 5)$ and full-response binary CPFSK with modulation index $h = 1/2$ are used for the reference outer code and inner CPM, respectively. Although we limit ourselves to binary CPFSK, results can be extended to $M$-ary CPM schemes. The information block length is 1000 bits and the

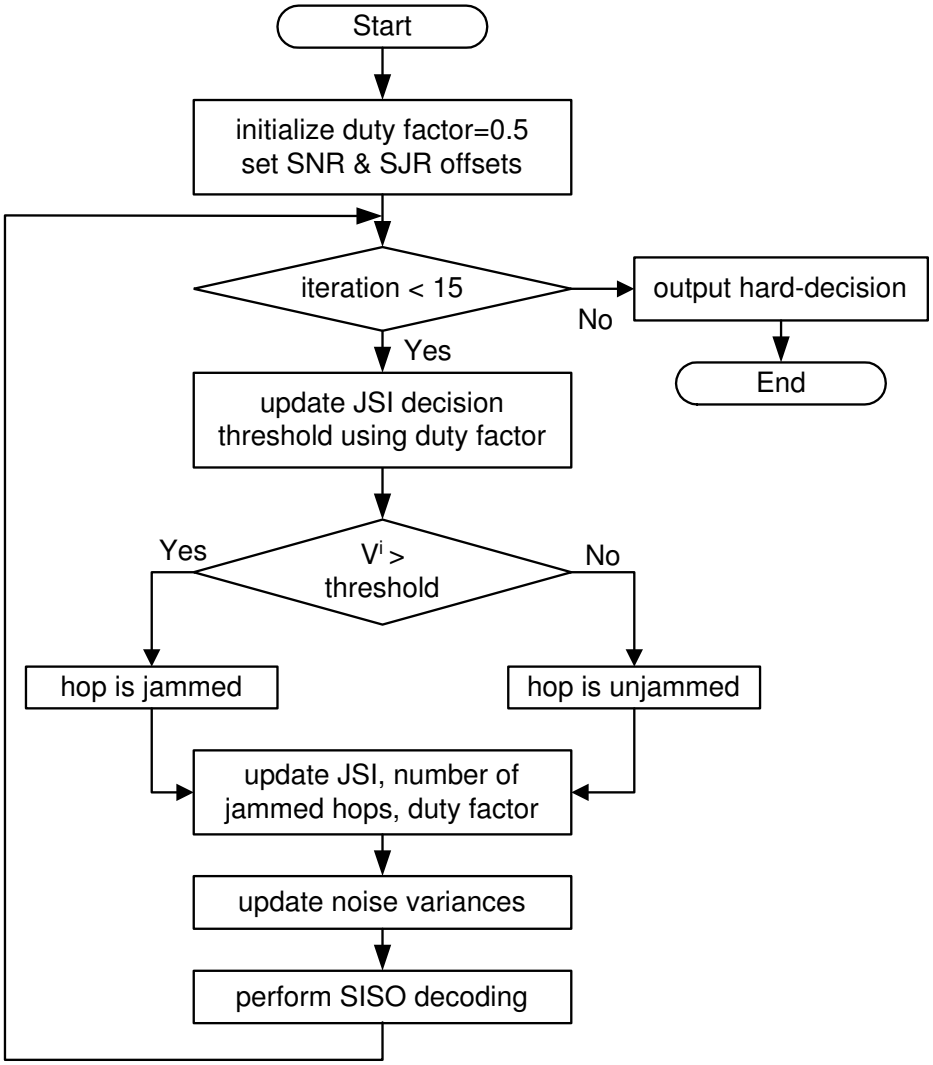


**Figure 24:** Flowchart for iterative jamming estimation.

maximum number of iterations at the receiver is set to 15. It is also assumed that perfect JSI is available at the receiver, unless stated otherwise. The background thermal noise in the presence of the PBNJ is set to 20 dB since the jamming noise is dominant. In addition, perfect symbol and carrier synchronization and timing recovery are assumed.

### 4.4.1 Effect of the Slow FH Channel on the Anti-Jamming Performance

The proposed system will experience performance degradation due to slow FH memory channel unlike the case of the usual memoryless channel. The degradation of the anti-jamming performance induced by the slow FH block interference is investigated. Fig. 25 shows how the anti-jamming performance for the coherent iterative receiver depends on the the number of symbols per hop $N_h$ $(= 1 \sim 20)$[2] and the duty factor $\rho$. The $y$-axis represents a required $E_b/N_J$ needed to achieve the target BER=$10^{-3}$. The optimal jamming corresponds to $\rho = 1.0$ regardless of $N_h$. It means that the worst-case error performance occurs when all symbols are jammed. The reduced number of hops per transmitted codeword, denoted by $N_c$, leads to decrease of the benefit by independent hopping and the degradation of the MAP algorithm due to the memory channel. However, little additional degradation is observed for the case of $N_h \geq 10$. It was shown by spectral analysis in [71] that, for the slow FH-CPM waveforms, a more compact dehopped power density spectrum can be obtained as the number of symbols per hop $N_h$ increases. The 99%-power bandwidth of a frequency-hopped MSK signal for $N_h$ =20, 10, and 5 is greater than 1.5, 2, and 4 times, respectively, greater that of an MSK signal without FH. In the following, we set $N_h$ to 20 to provide a good trade-off between bandwidth-efficiency and power-efficiency of FH waveforms, unless stated otherwise.

### 4.4.2 Anti-Jamming Performance of the Iterative Receivers

The worst-case jamming performance of the coherent iterative receiver, represented as $P_b^{wc} = P_b(\rho)|_{\rho=\rho^{wc}}$, is shown in Fig. 26. As the iteration in the receiver increases, the required $E_b/N_J$ decreases and thus a good anti-jamming capability can be achieved.

[2]The corresponding numbers of hops per codeword, denoted by $N_c$, for $N_h$ =1, 5, 10, and 20 are 2000, 400, 200, and 100 hops, respectively.

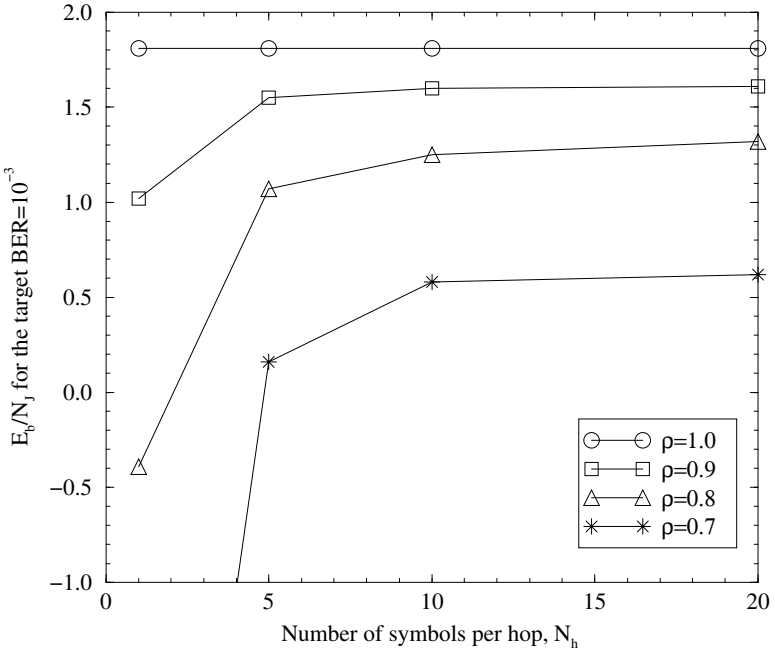


**Figure 25:** Effect of the slow FH channel on the anti-jamming performance in terms of the number of symbols per hop $N_h$ under the PBNJ.

The anti-jamming performance for the MSDD non-coherent iterative receiver described in Section 4.1.2 is shown in Fig. 27. It is observed that the performance gap between the non-coherent reception employing the MSDD with $N_h$ =20 and ideal coherent detection is less than 0.5 dB. Therefore, the non-coherent iterative receiver can perform close to that of the ideal coherent receiver as the number of observation symbols $N_h$ increases.

### 4.4.3 The Worst-Case Jamming Performance for Different Modulation Indexes and Outer Codes

The overall BER is significantly affected by the choice of different modulation index of the inner CPM and the free distance of the outer codes. Modulation indices of $h = 3/4$ and $h = 1$ show the best and the worst cases in terms of power-efficiency, respectively, as shown in Fig. 28. Non-coherent reception ($N_h = 20$) with 2, 4, and 8-state outer codes and four different modulation indexes $h$ =1/4, 1/2, 3/4, and 1 is considered. Since CPM with $h = 3/4$ has the largest minimum squared Euclidean distance (MSED)[3] among them,

[3]The upper bounds on the MSED for $h$ =1/4, 1/2, 3/4, and 1 are 0.72, 2.0, 2.42, and 1.68, respectively.

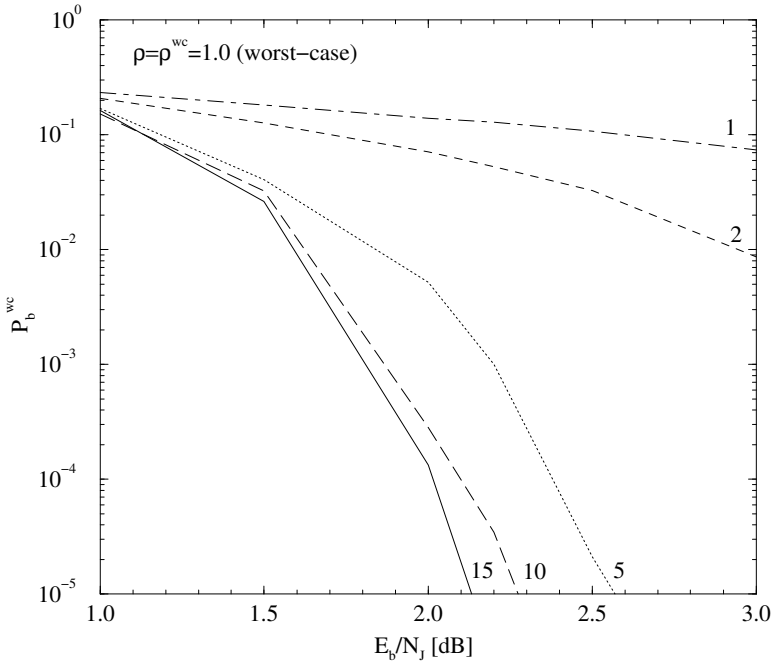


**Figure 26:** The worst-case jamming performance for different iteration. $\rho^{wc}$ and $P_b^{wc}$ denote the worst-case duty factor and the corresponding BER, respectively. The number of iterations is marked on each curve.

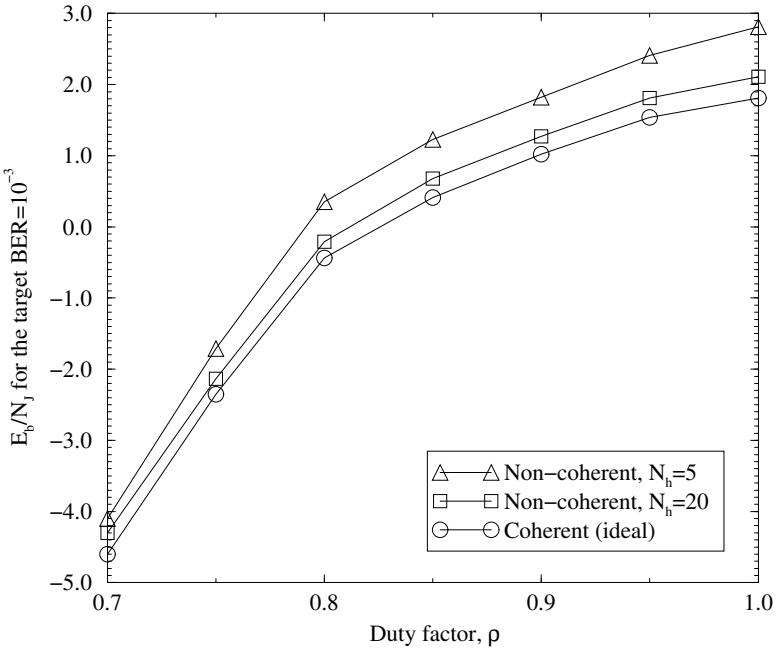


**Figure 27:** Anti-jamming performance of the MSDD-based non-coherent iterative receiver for different numbers of symbols per hop $N_h$ under the PBNJ.

the worst-case jamming performance is the best as expected. However, the degradation in case of integer $h = 1$ can be attributed to the first inevitable trellis merge at the time of $T_s$ unlike $2T_s$ for the cases of $h$ =1/4, 1/2, and 3/4. In addition, 4-state outer coded system shows a sharper slope than 2-state outer code and, thus, gives a lower BER in the high $E_b/N_J$ region. In terms of complexity, the number of phase states for $h = 1/2$ is four, corresponding to a half of that for $h = 1/4$ and 3/4.

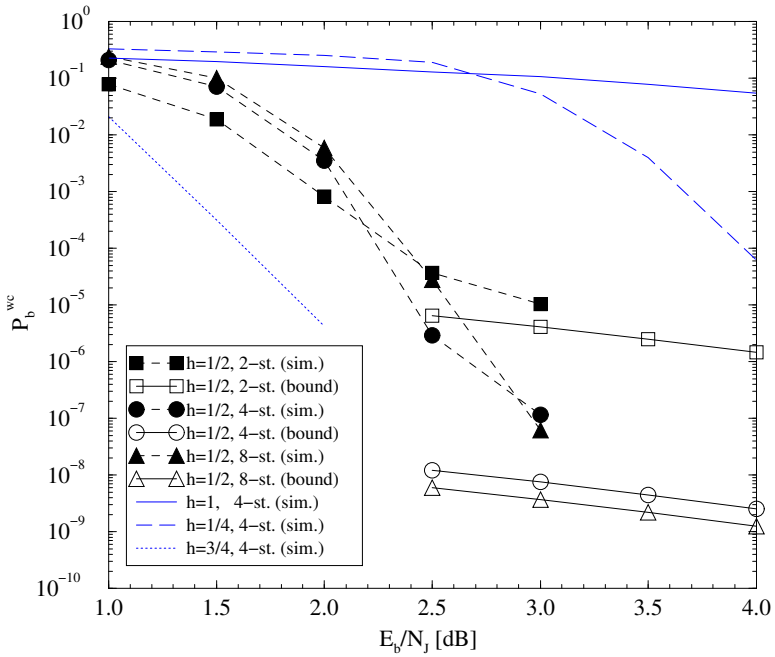


**Figure 28:** The worst-case jamming performance for different outer codes and modulation indexes of the inner CPM. The simulation and bound curves are shown.

Different outer convolutional codes with 2, 4, and 8-states are also compared along with analytical bound results. Each outer code is non-recursive and non-systematic and has the generator polynomials of $(2, 3)$, $(5, 7)$, and $(15, 17)$, respectively. The free distance $d_f^o$ of the outer codes are 3, 5, and 6, respectively[4]. The calculated ML union bound results are similar to the simulation results at moderate-to-high $E_b/N_J$ (e.g., at 3 dB), as shown in Fig. 28. In particular, it is disadvantageous to use the 2-state outer code because the error floor starts to occur early and thus poor BER performance is observed at moderate-to-high

[4]Large interleaving gain can be achieved when the free distance of an outer code $d_f^o$ is greater than 2 [13].

$E_b/N_J$. However, as we can see the simulation results for low-to-moderate $E_b/N_J$ region, an outer code with larger state (or larger free distance) does not necessary provide better anti-jamming performance. This result below $E_b/N_J$ corresponding to the waterfall region is shown to be rather different from the bound analysis. The error performance of turbo-like code is not only determined by *whole* distance spectrum[5], but also by the convergence characteristics of component codes. For low-to-moderate SNR, an outer code with larger memory is more likely to stuck early during iterations [27]. Therefore, it results in the degradation of iterative anti-jamming performance.

### 4.4.4 Anti-Jamming Performance of Jamming Estimation

Fig. 29 shows the anti-jamming performance for the cases with different jamming parameters. The $y$-axis represents a required $E_b/N_J$ needed to achieve the target BER=$10^{-3}$. The proposed jamming estimation technique is used to estimate jamming states as well as the noise variances of jamming and AWGN. The cases with perfect JSI and noise variances can be regarded as the lower bounds on the anti-jamming performance since both the JSI and noise variances are completely known to the receiver. Since the anti-jamming performance for the jamming estimation degrades with the increase in the offset, we plot curves for different offsets (i.e., 0, 2, and 4 dB). The offset of 0 dB means that the noise variances are known. The JSI estimation case with 4 dB offset only looses less than 1 dB relative to the case with the perfect JSI for $\rho \leq 0.7$. In addition, for the cases with the JSI estimation, the required $E_b/N_J$ decreases as $\rho$ decreases in contrast to the case without the JSI estimation. For no JSI cases, two cases with known and unknown duty factor are here considered. They show almost same performance regardless of the duty factor information. The result confirms that the proposed jamming estimation technique assists the iterative decoding process and thus improves the anti-jamming performance as the iteration increases. Therefore, the anti-jamming performance of iterative soft-decision decoding is highly dependent of the availability of the JSI.

[5]Turbo-like codes have usually a different spectrum shape from random codes, especially for low-to-moderate weight (see [110] and references therein).

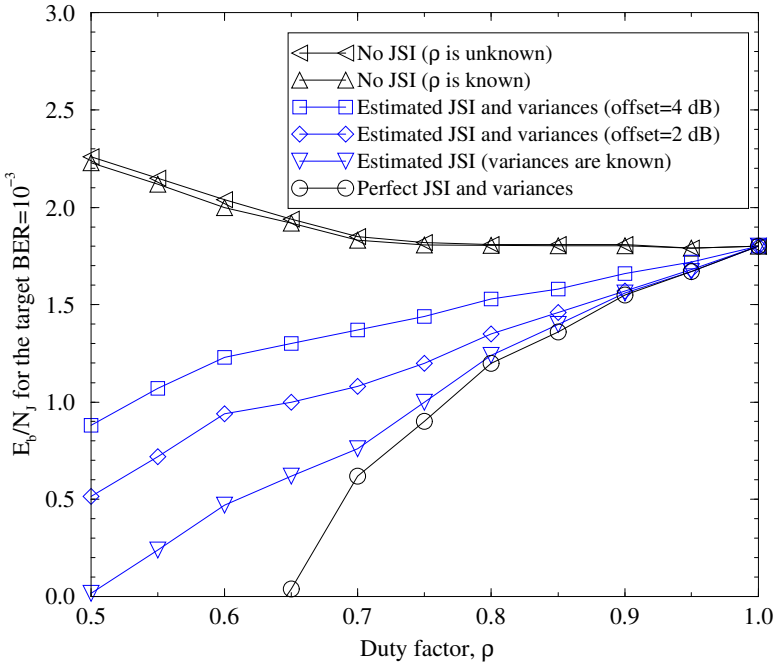


**Figure 29:** Effect of the jamming estimation on the anti-jamming performance ($N_h = 20$). The cases with perfect JSI, estimated JSI, and no JSI are compared.

### 4.4.5 Jamming Estimation for Different Slow FH Parameters

Because the proposed system results in slow FH channel unlike the case of the usual memoryless channel, different number of symbols per hop $N_h$ affects the anti-jamming performance. The reduced number of hops per transmitted codeword, denoted by $N_c$, leads to decrease in the benefit by independent hopping and the degradation of the MAP algorithm that assumes the memoryless channel. Note that the corresponding numbers of hops per codeword, denoted by $N_c$, for $N_h$ =5 and 20 are 400 and 100 hops, respectively. However, it was shown by spectral analysis in [71] that, for the slow FH-CPM waveforms, a more compact dehopped power density spectrum can be obtained as the number of symbols per hop $N_h$ increases. The 99%-power bandwidth of a frequency-hopped MSK signal for $N_h$ =20 and 5 is greater than 1.5 and 4 times, respectively, greater that of an MSK signal without FH. As a result, the case with $N_h = 5$ outperforms the case with $N_h = 20$ in the perfect JSI case, as shown in Fig. 30.

In contrast to the perfect JSI cases, since the observation interval for estimating noise

variances increases with the increase in $N_h$, we can achieve more reliable estimation and improved performance. Therefore, the case with $N_h = 20$ outperforms the case with $N_h = 5$ in the jamming estimation case, as shown in Fig. 30.

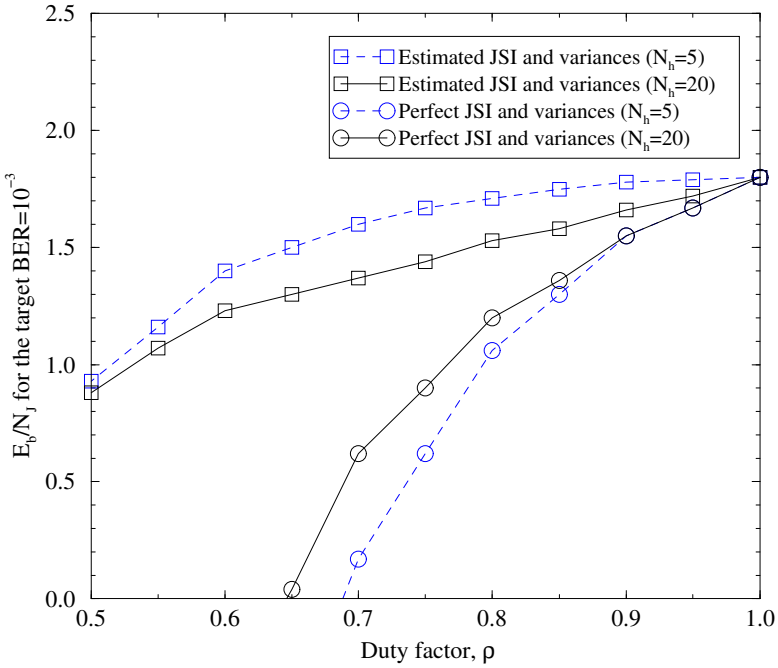


**Figure 30:** Effect of the jamming estimation for different slow FH channels in terms of $N_h$. $E_b/N_0$ and $E_b/N_J$ offsets of 4 dB are used for the jamming estimation.

### 4.4.6 Effect of Outer Channel Codes on Anti-Jamming Performance

Fig. 31 shows the effect of outer codes on anti-jamming performance in case of the jamming estimation. The outer convolutional codes with different number of states (i.e., 2, 4, and 8-state) and duty factor are compared.

Let us consider the target BER=$10^{-3}$ to see the required $E_b/N_J$. The worst-case jamming for the 2-state code occurs at $\rho = 0.8$ in contrast to $\rho = 1.0$ for the 4- and 8-state codes. As a result, the 2-state code provides the best jamming protection in the presence of the worst-case jamming. However, the 2-state code provides worse anti-jamming performance for $\rho < 0.9$ and $\rho < 0.83$ compared to 4-state and 8-state codes, respectively. Finally, it should be kept in mind that the results of the worst-case jamming depend on the target

BER due to the decoding convergence characteristics of the iterative system.

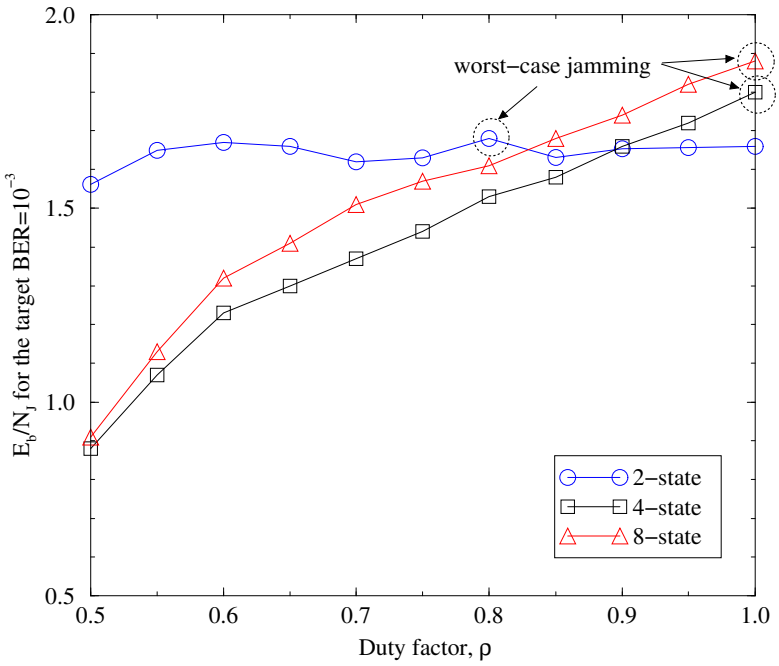


**Figure 31:** Anti-jamming performance of the jamming estimation for different outer codes. $E_b/N_0$ and $E_b/N_J$ offsets of 4 dB are used for the jamming estimation.

## *4.5 Conclusions*

We have proposed the coherent and non-coherent serially concatenated slow FH-CPM systems. We have also proposed an iterative jamming state estimation technique combined with the anti-jam iterative receiver. We have showed the anti-jamming performance in the presence of the PBNJ through simulation and ML bound analysis. Consequently, some important design considerations with regard to the outer convolutional codes and the inner CPMs as well as FH parameters have been drawn. The MSDD-based non-coherent iterative receiver exploiting channel memory performs close to the coherent one with increase in the observation interval. Furthermore, it has been shown that an outer code with larger state does not necessary provide better anti-jamming performance at low $E_b/N_J$ as opposed to the bound analysis at high $E_b/N_J$.

# CHAPTER V

# TURBO-LIKE CODED MULTI-H CPM

Multi-$h$ CPM [5], [8] is a generalization of single-$h$ CPM, wherein the modulation index is cyclically changed for successive symbol intervals. A properly chosen cyclic set of modulation indexes results in delayed merging of neighboring phase trellis paths and, therefore, provides a larger minimum Euclidean distance than conventional single-$h$ CPM. The error performance for uncoded multi-$h$ CPM schemes on AWGN and flat fading channels were presented in [130] and [135], respectively. Convolutionally coded multi-$h$ CPM schemes using a Viterbi decoder were considered in [36].

Serial concatenated interleaved convolutional codes and their variants have been developed that concatenate and outer convolutional code, an interleaver, and a recursive inner code [13], [26]. With iterative decoding, serial turbo codes exhibit exceptionally good error performance, particularly at low-to-moderate SNR and for very large interleaver sizes. The serial turbo coding concept has been extended to iterative demodulation and decoding by replacing the recursive inner code of a serial turbo code with a recursive modulator, such as a CPM modulator (e.g., [45]-[94]). Existing serially concatenated CPM schemes use a single-$h$ CPM modulator. We extends serially concatenated single-$h$ CPM schemes to multi-$h$ CPM [64].

The ML upper bounds on error probability [13] and convergence analysis [27] are two widely used analytical techniques for turbo-like codes. The former is useful for characterizing the error-floor region, while the latter is useful for characterizing the water-fall region. We utilizes both of these analytical approaches to better understand serially concatenated multi-$h$ CPM schemes with iterative demodulation and decoding, presenting new observations and results.

## 5.1 Turbo-Like Coded Modulation

Turbo-like coded modulation schemes consist of one or more constituent channel encoders and one or more modulators, arranged in a variation of a parallel or serial concatenation scheme and separated by interleavers, as shown in Fig. 32. The constituent channel sub-encoders can be any channel encoder, such as a trellis, block, or turbo encoder. The constituent sub-modulators can be any recursive $M$-ary modulator such as CPM, DPSK, and others.

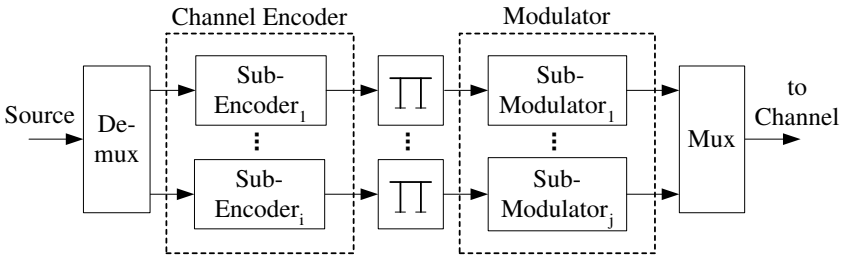


**Figure 32:** General structure of a turbo-like coded modulation scheme. Π represents a concatenation interleaver.

## 5.2 Serially Concatenated Multi-$h$ CPM

Multi-$h$ CPM has a finite state description, and can be decomposed into a recursive multi-$h$ phase encoder (MHPE) and a memoryless multi-$h$ modulator (MHM), similar to single-$h$ CPM [106]. Unlike single-$h$ CPM, the multi-$h$ CPM trellis is *time-varying* due to the cyclic variation of the modulation indices. We considers a serially concatenated multi-$h$ CPM scheme that includes a convolutional channel encoder, random interleaver, demultiplexer and multiplexer, mapper, and $K$ phase encoders and $K$ memoryless modulators, as shown in Fig. 33. For simplicity, we use of a single channel encoder while focusing on the impact of the multi-$h$ CPM modulator.

A length-$N_u$ binary information sequence $\mathbf{u}$ is encoded by a rate-$N_u/N$ convolutional encoder. The binary output sequence $\mathbf{d}$ from the convolutional encoder is multiplexed and randomly permuted through a bit-wise interleaver of length $N$. The interleaver output $\tilde{\mathbf{d}}$ is mapped onto a length-$L$ symbol sequence $\boldsymbol{\alpha} = \{\alpha_k\}$, $\alpha_k \in \{\pm 1, \pm 3, \ldots, \pm(M-1)\}$, that is

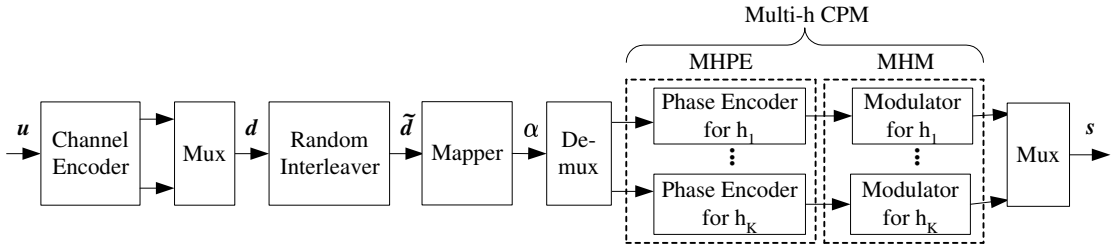


**Figure 33:** Transmitter structure of serially concatenated multi-$h$ CPM. The multi-$h$ modulator consists of $K$ multi-$h$ phase encoders and $K$ memoryless modulators.

input to the $M$-ary multi-$h$ CPM modulator. The modulation index set (MIS) consists of a set of rational fractions

$$H_K = (h_1, h_2, \ldots, h_K) = (P_1/Q, P_2/Q, \ldots, P_K/Q), \tag{42}$$

where $K$ is the number of different modulation indexes, $P_i < Q, 1 \leq i \leq K$, and $P_i$ and $Q$ are integers. During transmission the modulation indices are used in a cyclic fashion such that $h_{nK+j} = h_j, n = 0, 1, \ldots$. The mean and variance of the MIS are defined by $\bar{h} = \sum_{i=1}^{K} h_i/K$ and $\sigma_h^2 = \sum_{i=1}^{K}(h_i - \bar{h})^2/K$, respectively.

The multi-$h$ CPM modulator has $Q$ phase states and the state transition from epoch $n$ to $n+1$ is

$$\phi_{n+1} = [\phi_n + \pi h_n \alpha_n] \mod 2\pi \ . \tag{43}$$

The phase-difference states for a pair of sequences are defined by

$$\Delta\phi_n = \left[\pi \sum_{i=1}^{n-L} h_i \gamma_i\right] \mod 2\pi, \tag{44}$$

where $\gamma_i = \alpha_i - \hat{\alpha}_i \in \{0, \pm 2, \ldots, \pm M\}$. There are $2M-1$ branches entering and exiting each node of the phase-difference state trellis. Generally, a long delay of the first inevitable merge in the phase difference trellis yields good power-efficiency, and there exists a multi-$h$ CPM scheme that can achieve an unmerged span of $K+1$ steps provided that $Q \geq M^K$. The constraint length, $\eta$, of a multi-$h$ CPM scheme with $K$ different modulation indexes is at most $K+1$. As an example, Fig. 34(a) shows the phase difference trellis of a 2-$h$ CPM

scheme with $H_2 = (2/4,\ 3/4)$[1]. Note that the first merge occurs at $K+1 = 3$ steps for this case.

The iterative receiver for serially concatenated multi-$h$ CPM consists of *multiple* Log-MAP sub-demodulators that operate with their corresponding modulation indices and a single Log-MAP channel decoder. The Euclidean distance between the received and candidate transmitted signals is used to calculate the branch metrics. Given the received complex low-pass sequence $\mathbf{y}$, the multi-$h$ CPM demodulator generates the log-likelihood ratios (LLR) for each bit in the sequence $\tilde{\mathbf{d}}$. For a coherent Log-MAP demodulator, the LLRs for the $l$-th bit interval with modulation index $h_i$ are

$$L_M^m(\tilde{d}_l)|_{h_i} \quad = \quad \log\left\{\frac{P(\mathbf{y}|\tilde{d}_l = 1)}{P(\mathbf{y}|\tilde{d}_l = 0)}\right\} + \log\left\{\frac{P(\tilde{d}_l = 1)}{P(\tilde{d}_l = 0)}\right\}, \tag{45}$$

where subscript $M$ and superscript $m$ denote the multi-$h$ CPM demodulator and the $m$-th iteration, respectively, and $i = l \bmod K$. The LLRs in (45) can be decomposed as $L_M^m(\tilde{d}_l)|_{h_i} = L_{M,e}^m(\tilde{d}_l)|_{h_i} + L_{O,e}^{m-1}(\tilde{d}_l)|_{h_i}$, where the subscripts $C$ and $e$ denote the convolutional decoder and the extrinsic LLRs, respectively. The extrinsic LLR sequences $L_{M,e}^m(\tilde{d}_l)|_{h_i}$ are cyclically multiplexed, and the multiplexed sequence is deinterleaved and forwarded to the convolutional decoder. The *a posteriori* LLRs $L_C^m(\tilde{d}_l)$ for the convolutional decoder are $L_C^m(\tilde{d}_l) = L_{C,e}^m(\tilde{d}_l) + L_{M,e}^m(\tilde{d}_l)|_{h_i},\ m \geq 1$. The bit extrinsic LLRs $L_{C,e}^m(\tilde{d}_l)$ are passed to the multi-$h$ CPM demodulators after bit interleaving and demultiplexing. Only the extrinsic LLRs are fed back to the demodulators as the *a priori* LLRs for $\tilde{d}_l$, $L_{C,e}^{m-1}(\tilde{d}_l)$. Afterward, the above described process is repeated iteratively.

## *5.3 Performance Analysis*

### 5.3.1 Union-Chernoff Bound

Since the serially concatenated coded multi-$h$ CPM scheme can be viewed as a rate-$R$ block code consisting of a convolutional code with rate $R^C = m/n$ and a multi-$h$ CPM modulator with rate $R^M = n/p$, joined by an interleaver of length $N$, the transfer function bounding

[1]Although modulation indices such as $h = 2/4$ are used in the description of multi-$h$ CPM, the actual modulation indices used are rational fractions of integers having no common factors. For example, $h = 2/4$ corresponds to a modulation index $h = 1/2$.

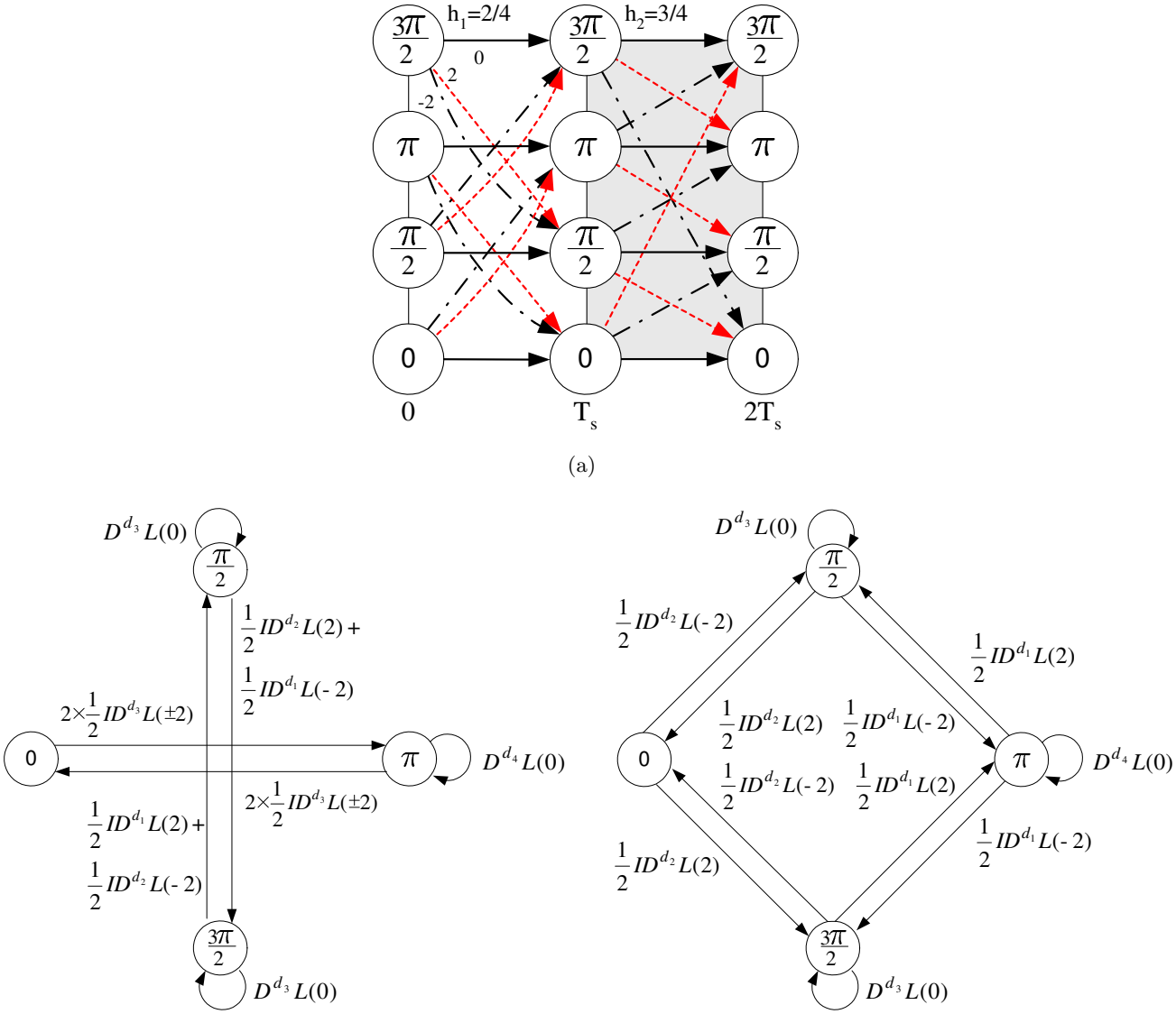


**Figure 34:** Trellis and state transition representations of the binary multi-$h$ CPM with $H_2 = (2/4, 3/4)$. (a) Trellis for the phase-difference states $\Delta\phi_n$. — $\gamma_n = 0$, ... $\gamma_n = 2$, and $- \cdot - \gamma_n = -2$. (b) Transition diagram for the phase-difference states of $h_1 = 2/4$. The exponents of $D$ are $d_1 = 1-\pi/2$, $d_2 = 1+\pi/2$, $d_3 = 1$, and $d_4 = 2$. (c) Transition diagram for the phase-difference states of $h_2 = 3/4$. The exponents of $D$ are $d_1 = 1 - \sin(3\pi/2)/(3\pi/2)$, $d_2 = 1 + \sin(3\pi/2)/(3\pi/2)$, $d_3 = 1$, and $d_4 = 2$.

approach in [13] based on *uniform interleaving* can be used. In addition, since the multi-$h$ CPM phase difference trellis is *time-varying*, the error probability must be averaged over the ensemble of modulation indices. When the coded multi-$h$ CPM signals are transmitted over *correlated fading* channels, the received signals are affected by *fading correlation*. Let $\boldsymbol{\tau} = [t_1, t_2, \ldots, t_\kappa]$ be a vector of $\kappa$ symbol positions for which $\phi_k(t) = \phi(t, \boldsymbol{\alpha})$ differs from $\hat{\phi}_k(t) = \hat{\phi}(t, \hat{\boldsymbol{\alpha}})$. Further, let $\mathbf{D}$ be a diagonal matrix of NSEDs, where the $(i, i)$ entry is $d_i$. Then, in case that the correlated Rayleigh fading vector $\mathbf{a} = [a_{t_1}, a_{t_2}, \ldots, a_{t_\kappa}]$ corresponds to the $\kappa$ time instants for which $\mathbf{s}(t, \boldsymbol{\alpha})$ and $\hat{\mathbf{s}}(t, \hat{\boldsymbol{\alpha}})$ differ, the NSED between $\mathbf{a} \cdot \mathbf{s}(t, \boldsymbol{\alpha})$ and $\mathbf{a} \cdot \hat{\mathbf{s}}(t, \hat{\boldsymbol{\alpha}})$ is $d = RE_b\Lambda$ where $\Lambda = \mathbf{a}\mathbf{D}\mathbf{a}^T$. Therefore, the bit error probability with $K$ modulation indices is

$$P_b = \frac{1}{K}\sum_{i=1}^{K} P_b|_{h_i}, \tag{46}$$

where $P_b|_{h_i}$ represents the bit error probability conditioned on $h_i$ being the initial deviation. The union bound on $P_b|_{h_i}$ is

$$P_b|_{h_i} \leq \sum_{w}\sum_{\kappa} \frac{w}{N_u} A_{w,\kappa}|_{h_i} P(\mathbf{s} \to \hat{\mathbf{s}}), \tag{47}$$

where $A_{w,\kappa}|_{h_i}$ is the number of input error sequences with input weight $w$, such that the multi-$h$ CPM signal has a time diversity of $\kappa$ from the transmitted signal, and $P(\mathbf{s} \to \hat{\mathbf{s}})$[2] can be bounded by the pairwise error probability between two sequences that differ in $\kappa$ time instants, such that $P(\mathbf{s} \to \hat{\mathbf{s}}) \leq P(\kappa, \boldsymbol{\tau}, \mathbf{D})|_{\boldsymbol{\tau}=\boldsymbol{\tau}_w, \mathbf{D}=\mathbf{D}_m}$, where $\boldsymbol{\tau}_w$ corresponds to the worst-case $\boldsymbol{\tau}$, and $\mathbf{D}_m$ is the approximation of $\mathbf{D}$ where the entries are given by $\min_i \min_{\phi_{t_i}(t), \hat{\phi}_{t_i}(t)} d$. Details of the calculation method can be found in [4, Appendix-A]). Finally, assuming the uniform interleaving enables us to calculate the ensemble $A_{w,\kappa}|_{h_i}$ conditioned on $h_i$ being the initial deviation as [13]

$$A_{w,\kappa}|_{h_i} \leq \sum_{l=d_f}^{N}\sum_{n_c=1}^{n^C}\sum_{n_m=1}^{n^M} \frac{\binom{N/n}{n_c}\binom{N/n}{n_m}}{\binom{N}{l}} A^C_{w,l,n_c} \cdot A^{h_i}_{l,\kappa,n_m}, \tag{48}$$

where $A_{i,j,k}$ represents the number of sequences having input weight $i$, output weight $j$, and consisting of $k$ concatenated error events $k$; $d_f$ is the free distance of the channel code, and

[2]Note that for an AWGN channel the pairwise error probability $P(\mathbf{s} \to \hat{\mathbf{s}})$ is replaced by $\exp(-\kappa RE_b/2N_0)$.

$n^C$ and $n^M$ are the largest number of error events for the convolutional code and multi-$h$ CPM modulator, respectively. The terms $A^{h_i}_{l,\kappa,n_m}$ and $A^C_{w,l,n_c}$ can be obtained by using transfer functions as described in the next section.

### 5.3.2 Transfer Function of Multi-$h$ CPM

Denote the transfer function for modulation index $h_i$ by the $(Q+1)\times(Q+1)$ state transition matrix $\mathbf{A}(L,I,D)|_{h_i}$. The state transition matrix can be formed from the corresponding difference-state transition diagram [126]. Although we use a 2-$h$ CPM scheme with $H_2 = (2/4, 3/4)$ as an example, the extension to other cases is straightforward. Figs. 34(b) and (c) show the phase-difference state transition diagrams for $h_1 = 2/4$ and $h_2 = 3/4$, respectively. The transition paths are labelled with $m \cdot I^{w(i\to j)}D^{d(i\to j)}L$ $(\gamma)$ where $w(i \to j) = 0$ if $\gamma = 0$ and $w(i \to j) = 1$ if $\gamma \neq 0$, $d(i \to j)$ denotes the normalized squared Euclidean distance (NSED) for a given transition, and $m$ is a multiplicity factor given by $(M - |\gamma|/2)/M \in \{1/M, 2/M, \ldots, 1\}$. For a non-existing state transition, a zero is assigned to the corresponding transition paths. By dividing the zero state into the start and end states, the transition matrices $\mathbf{A}(L,I,D)|_{h_1}$ and $\mathbf{A}(L,I,D)|_{h_2}$ for 2-$h$ CPM with $H_2 = (2/4, 3/4)$ are

$$\mathbf{A}(L,I,D)|_{h_1} = \begin{pmatrix} 0 & 0 & ID^{d_3}L & 0 & 0 \\ 0 & D^{d_3}L & 0 & \frac{1}{2}I(D^{d_1}+D^{d_2})L & 0 \\ 0 & 0 & D^{d_4}L & 0 & ID^{d_3}L \\ 0 & \frac{1}{2}I(D^{d_1}+D^{d_2})L & 0 & D^{d_3}L & 0 \\ 0 & 0 & 0 & 0 & 0 \end{pmatrix}, \tag{49}$$

and

$$\mathbf{A}(L,I,D)|_{h_2} = \begin{pmatrix} 0 & \frac{1}{2}ID^{d_2}L & 0 & \frac{1}{2}ID^{d_2}L & 0 \\ 0 & D^{d_3}L & \frac{1}{2}ID^{d_1}L & 0 & \frac{1}{2}ID^{d_2}L \\ 0 & \frac{1}{2}ID^{d_1}L & D^{d_4}L & \frac{1}{2}ID^{d_1}L & 0 \\ 0 & 0 & \frac{1}{2}ID^{d_1}L & D^{d_3}L & \frac{1}{2}ID^{d_2}L \\ 0 & 0 & 0 & 0 & 0 \end{pmatrix}, \tag{50}$$

respectively, where the exponents of $D$ in $\mathbf{A}(L,I,D)|_{h_1}$ are $d_1 = 1 - \pi/2$, $d_2 = 1 + \pi/2$, $d_3 = 1$, and $d_4 = 2$, and the exponents of $D$ in $\mathbf{A}(L,I,D)|_{h_2}$ are $d_1 = 1 - \sin(3\pi/2)/(3\pi/2)$,

$d_2 = 1 + \sin(3\pi/2)/(3\pi/2)$, $d_3 = 1$, and $d_4 = 2$.

For binary 2-$h$ CPM schemes, the transfer functions when $h_i$ $(i = 1, 2)$ are the initial deviation corresponding to the upper-right corner entry of $\mathbf{A}_M(L, I, D)|_{h_i}$, such that

$$T_M(L, I, D)|_{h_i} = \{\mathbf{A}_M(L, I, D)|_{h_i}\}_{(1,Q+1)}, \tag{51}$$

where

$$\begin{aligned} \mathbf{A}_M(L, I, D)|_{h_1} &= \mathbf{A}|_{h_1} + \mathbf{A}|_{h_1}\mathbf{A}|_{h_2} + \mathbf{A}|_{h_1}\mathbf{A}|_{h_2}\mathbf{A}|_{h_1} + \mathbf{A}|_{h_1}\mathbf{A}|_{h_2}\mathbf{A}|_{h_1}\mathbf{A}|_{h_2} + \cdots \\ &= (\mathbf{I} - \mathbf{A}|_{h_1}\mathbf{A}|_{h_2})^{-1}(\mathbf{A}|_{h_1} + \mathbf{A}|_{h_1}\mathbf{A}|_{h_2}), \end{aligned} \tag{52}$$

where the $i$-th term in the righthand side of (52) represents a possible state transition at time $iT_s$, and $\mathbf{A}_M(L, I, D)|_{h_2}$ can be calculated by exchanging $h_1$ and $h_2$ in (52).

The transfer functions in terms of the input weights and error event lengths are

$$T_M(L, I)|_{h_1} = \frac{I^2L^3(2 - 3L^2 + IL - IL^2 + I^2L + I^2L^2 + I^3L^2)}{2 - 4L^2 + 2L^4 - 2IL^2 + 2IL^4 - I^2L^4 - I^3L^4}, \tag{53}$$

and

$$T_M(L, I)|_{h_2} = \frac{I^2L^3(1 + I + IL - IL^2 + I^2L - 2L^2)}{2 - 4L^2 + 2L^4 - 2IL^2 + 2IL^4 - I^2L^4 - I^3L^4}. \tag{54}$$

In (48), $A^{h_i}_{l,\kappa,n_m}$ is the number of error events for the multi-$h$ CPM modulator with the initial deviation of $h_i$, and is obtained from the transfer function $T_M(I, L)_{h_i} = \sum_j \sum_k A^{h_i}_{j,k} I^j L^k$.

Finally, the transfer function of the 4-state non-recursive convolutional encoder with generator polynomial $(7, 5) = (1 + D + D^2, 1 + D^2)$ is $T_C(L, I)_{(7,5)} = \frac{IL^3}{1-IL(1+L)}$, with free distance $d_f = 5$. In (48), $A^C_{w,l,n_c}$ is the number of error events for the convolutional code and $T_C(L, I) = \sum_w \sum_l A^C_{w,l} I^w L^l$.

### 5.3.3 Convergence Analysis Based on Input and Output Extrinsic Information

Convergence analysis approache [27] provides an useful framework to evaluate the error performance in the water-fall region, which shows different behavior from the error-floor region. The probability density functions $p(\lambda)$ for input and output extrinsic information for the iterative multi-$h$ CPM demodulator and decoder is tracked by calculating the histogram of $\lambda$. Assuming a Gaussian and symmetric density approximation, the statistics of $p(\lambda)$

depend on its mean $\nu = E[\lambda]$ and variance $\sigma^2 = \text{var}[\lambda]$. Then the input and output SNR (not channel $E_b/N_0$) for the quality of the extrinsic information is defined as $\text{SNR} \triangleq \nu^2/\sigma^2 = \nu/2$ [27]. Let us denote the output SNRs of the multi-$h$ CPM demodulator and convolutional decoder by $\text{SNR}_{M,o}$ and $\text{SNR}_{C,o}$, respectively. They are non-linear functions of the input SNRs, denoted by $\text{SNR}_{M,i}$ and $\text{SNR}_{C,i}$, respectively, and $E_b/N_0$. Therefore, $\text{SNR}_{M,o} = f_M(\text{SNR}_{M,i}, E_b/N_0)$ and $\text{SNR}_{C,o} = f_C(\text{SNR}_{C,i})$, where $f_M(\cdot)$ and $f_C(\cdot)$ denote the multi-$h$ CPM demodulation and convolutional decoding functions, respectively[3].

## *5.4 Numerical Results and Discussions*

Rate-1/2, 2- and 4-state non-recursive convolutional codes with generator polynomials $(3, 1)_8$ and $(7, 5)_8$, respectively, are used as the channel code. Full-response binary multi-$h$ CPM with a rectangular frequency shaping pulse having the various modulation index sets listed in Table 2 are considered. The proposed schemes are compared with serially concatenated MSK, since the mean modulation indexes of the multi-$h$ CPM schemes are about 1/2. Note that the minimum NSED of MSK is equal to 2 and the first inevitable merge occurs at $T_s$. The information block length is $N_u = 1000$ bits and the number of decoding iterations is 15.

**Table 2:** Parameters of various multi-$h$ CPM schemes.

| MIS | Minimum NSED | $\bar{h}$ | $K$ | $\eta$ | $Q$ |
|---|---|---|---|---|---|
| $H_2$=(2/4, 3/4) | 2.79 | 0.625 | 2 | 3 | 4 |
| $H_2$=(4/8, 5/8) | 3.55 | 0.563 | 2 | 3 | 8 |
| $H_3$=(4/8, 5/8, 6/8) | 3.79 | 0.625 | 3 | 4 | 8 |

**Table 3:** Spectral property of various binary multi-$h$ CPMs. $BW_{RMS}$: RMS bandwidth, $BW_{99}$: 99% power containment bandwidth, $BW_{90}$: 90% power containment bandwidth, $BW_{ML}$: main-lobe bandwidth.

| MHPM | $\bar{h}$ | $BW_{RMS}$ | $BW_{99}$ | $BW_{90}$ | $BW_{ML}$ |
|---|---|---|---|---|---|
| $H_2$=(2/4, 3/4) | 0.625 | 0.64 | 1.68 | 0.95 | 1.5 |
| $H_2$=(4/8, 5/8) | 0.563 | 0.56 | 1.34 | 0.86 | 1.4 |
| $H_3$=(4/8, 5/8, 6/8) | 0.625 | 0.63 | 1.66 | 0.93 | 1.4 |
| MSK ($h$=1/2) | 0.5 | 0.5 | 1.20 | 0.79 | 1.5 |

[3]These nonlinear functions are calculated by Monte Carlo simulation.

### 5.4.1 Error Performance on AWGN Channels

Fig. 35 shows the bit error rate performance on an AWGN channel. Observe that $H_2 = (2/4, 3/4)$ provides the best performance and outperforms MSK by 0.4 dB. It was reported in [131] that the spectral properties of $H_2 = (2/4, 3/4)$ are very similar to MSK, as summarized in Table 3. Observe also that $H_2 = (2/4, 3/4)$ outperforms $H_2 = (4/8, 5/8)$ despite having a smaller minimum NSED and a smaller number of phase states. From Table 2 that the mean modulation indices of 3-$h$ CPM with $H_3 = (4/8, 5/8, 6/8)$ and 2-$h$ CPM with $H_2 = (2/4, 3/4)$ are both equal to 0.625. Surprisingly, 2-$h$ CPM with $H_2 = (2/4, 3/4)$ outperforms 3-$h$ CPM with $H_3 = (4/8, 5/8, 6/8)$ despite having a larger minimum NSED. We conclude that a larger minimum NSED and a larger number of phase states do not necessary improve the BER performance. Finally, observe that the simpler 2-state convolutional code outperforms the 4-state convolutional code in the water-fall region despite having a smaller free distance. However, 2-state code has a lower error-floor than the 4-state code, such that the former is inferior to the latter at moderate-to-high $E_b/N_0$ region. The above results will be further explained by convergence analysis.

### 5.4.2 Convergence Analysis

We assess the effect of the constituent multi-$h$ CPM modulator and convolutional code in the water-fall region through convergence analysis, as shown in Fig. 36. Fig. 36(a) shows that the multi-$h$ CPM schemes have a higher initial value of $\mathrm{SNR}_{M,o}$ and a steeper slope than MSK. This explains why the multi-$h$ CPM schemes outperform MSK, as shown in Fig. 35. Multi-$h$ CPM with $H_2 = (2/4, 3/4)$ has a higher initial value of $\mathrm{SNR}_{M,o}$ than multi-$h$ CPM with $H_3 = (4/8, 5/8, 6/8)$, resulting in better performance as shown in Fig. 35.

Fig. 36(b) shows the input and output SNR for multi-$h$ CPM with $H_2 = (2/4, 3/4)$ at different $E_b/N_o$. Note that the initial value of the upper $f_M$ curves when $SNR_{M,i} = 0$ increases as $E_b/N_o$ increases. The upper curve for $f_M$ and lower curve for $f_C^{-1}$ will touch at $E_b/N_o = \gamma_t$, where $\gamma_t$ represents the minimum $E_b/N_o$ threshold for convergence in the iterative demodulation and decoding process. Since $\gamma_t$ for the 2-state code is lower than that for the 4-state code, the 2-state code exhibits superior performance in the water-fall

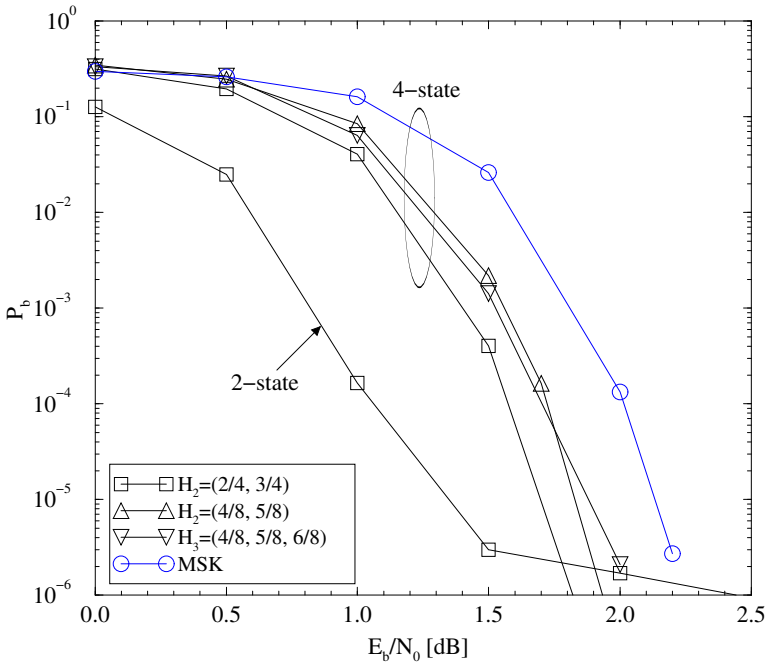


**Figure 35:** Performance of various serially concatenated multi-$h$ CPM schemes on an AWGN channel.

region, as shown in Fig. 35.

### 5.4.3 Effect of Fading Correlation on Performance

Multi-$h$ CPM with $H_2 = (2/4, 3/4)$ and MSK are compared for independent and correlated fading channels, as shown in Fig. 37. S-random interleaver [29] with $S = 16$ is used for the simulations. The multi-$h$ CPM scheme outperforms MSK by about 1 dB. It is observed that the simulation results show similar behavior as the upper bound results. However, since the upper bound is calculated using a truncated bound that does not count all the error events, it results in an optimistic bound. Finally, the BER improvement from channel coding diminishes and more pronounced error-floor at high $E_b/N_0$ occurs with increased fading correlation.

## *5.5 Conclusions*

We have proposed a serially concatenated coded multi-$h$ CPM with iterative demodulation and decoding along with the concept of the generalized turbo-like coded modulation. We

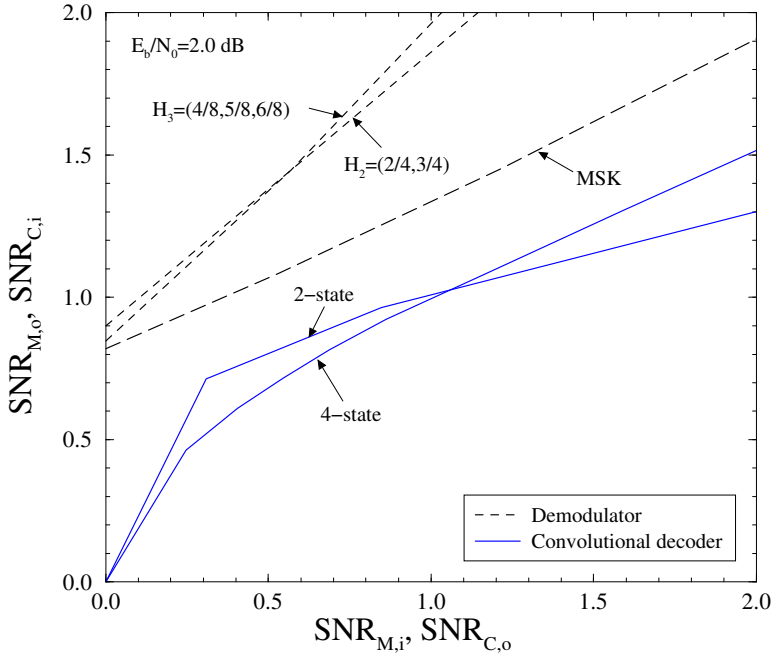


(a)

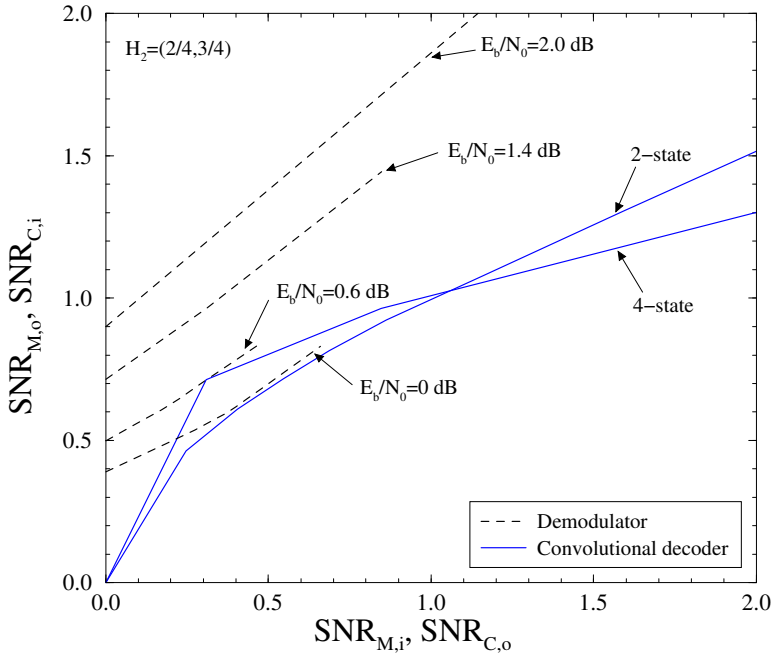


(b)

**Figure 36:** Convergence analysis for the iterative receiver on an AWGN channel. (a) Input and output SNR for different multi-$h$ CPM schemes at $E_b/N_0 = 2.0$ dB. (b) Input and output SNR for multi-$h$ CPM with $H_2 = (2/4, 3/4)$.

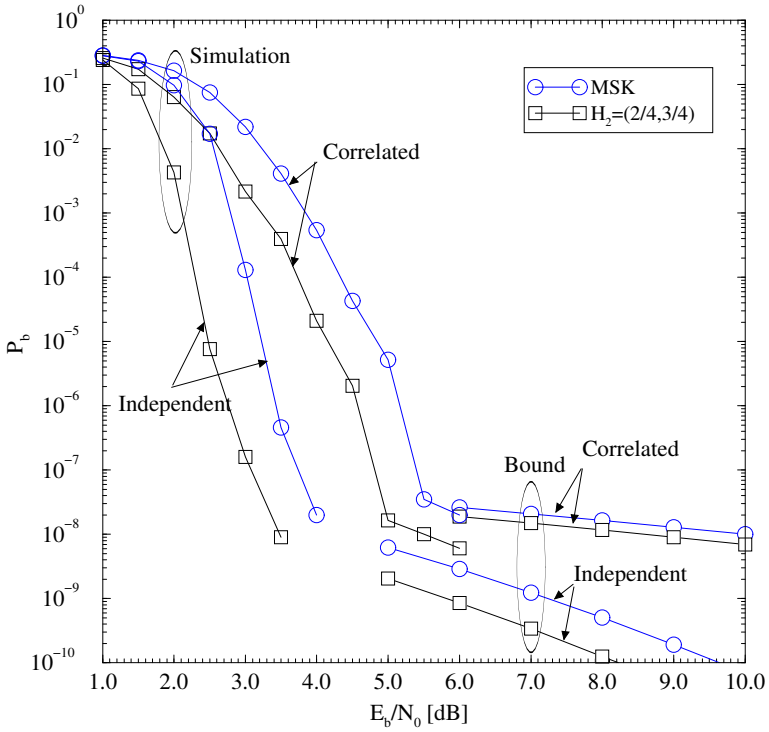


**Figure 37:** Union-Chernoff bounds on BER for independent and correlated flat Rayleigh fading channels. Serially concatenated 2-$h$ CPM with $H_2 = (2/4, 3/4)$ and a 4-state convolutional code are considered. In case of the correlated fading channel, $f_m T_s = 0.01$.

have shown that a channel code with larger minimum distance, or a multi-$h$ CPM modulator with a larger number of phase states do not necessary provide better BER performance. Candidate choices for the modulation index set can be evaluated by using convergence characteristics and the multi-$h$ modulator should be matched to the channel code. We have also evaluated performance in the error-floor region through union-Chernoff bounding techniques.

# CHAPTER VI

# TURBO HYBRID-ARQ FOR W-CDMA

High-quality data transmission through wireless channels becomes a very important requirement to support the QoS of various multimedia services. Turbo codes typically operate in block mode and are, therefore, well suited for packet-data transmission, and have been chosen as one of the channel coding schemes for the 3G IMT-2000 standards [21]. Relatively long delays due to iterative decoding and retransmission can be tolerated in packet data transmission.

Generally, FEC coding systems offer good throughput performance, but their reliability is limited. To overcome the limited reliability of decoded packets, a FEC code can be combined with an ARQ scheme to form a hybrid-ARQ scheme. The ARQ portion of such a system provides very high reliability while the FEC portion, by correcting as many erroneous packets as possible, in advance reduces the frequency of retransmission requests [81]. When convolutional or block codes are used as a FEC code, various techniques have been suggested for combining the retransmitted packets to improve the performance. One such technique is maximum likelihood combining [22], where a maximum likelihood rule is used to combine the retransmissions. Another technique is code combining or Type-III ARQ [58], where the code is punctured during one transmission and some or all of the punctured bits are transmitted during the retransmission.

Recently, several Type-I turbo-coded ARQ (TC-ARQ) schemes by using CRC-based TC-ARQ [95] and stability-based TC-ARQ [52] schemes for packet-data transmission were proposed. The TC-ARQ schemes employ multiple encoders, decoders, and interleavers to diversify retransmission, and utilize the soft-information in case of the iterative decoding of retransmitted data. At low-to-moderate SNR region, such TC-ARQ schemes can significantly decrease the FER.

In this chapter, we propose a hybrid-ARQ scheme based on the use of a concatenated RS-turbo code to provide strong burst-error correction capability as well as low-error probability by removing the residual errors resulting from a suboptimal turbo decoding. Turbo principle with a packet combining technique is utilized [65]. The BER and FER performances of W-CDMA system for multipath fading channels are investigated.

## *6.1 Concatenated RS-Turbo Coded Hybrid-ARQ*

To effectively combat burst errors that occur frequently in wireless channel, a shortened RS code is concatenated with parallel turbo code. A rate-1/3 turbo code consists of the parallel concatenation of two convolutional codes with a S-random concatenation interleaver. Each randomly selected integer is compared to $S$ previously selected integers. If the current selection is equal to any $S$ previous selections within a distance of $\pm S$, then the current selection is rejected. This process is repeated until all $N$ integers are selected. While the searching time increases with $S$, we can obtain good interleaving pattern in a reasonable time by choosing $S < \sqrt{N/2}$ [29]. The two identical RSC codes are of memory length 3 (i.e., 8-state), with the code generator polynomials in octal $g = (15/13)$, which is specified in the cdma2000 standard [123]. Iterative decoding with Max-Log-MAP SISO decoders is used for its fast decoding and easy implementation due to low complexity [50], [107]. If a proper scaling of the signal prior to quantization is performed, a negligible degradation of the error performance can be incurred with 8-bit quantization compared to that of floating point calculation. Thus, the demodulated signal output is quantized. The fixed point decoding algorithm that is needed in a real-time turbo decoder can avoid destructive overflow problem [134].

For the Simple turbo-coded ARQ in [95], the transmitter sends the same packet during every retransmission until the packet is deemed to be correctly decoded. The receiver ignores previous transmissions, and decodes the received sequence for each transmission independently. Clearly, this scheme is simple but inferior. The performance of this scheme can be enhanced significantly with a minimal increase in complexity and storage requirements.

In the following, the turbo hybrid-ARQ with average packet combining (APC) will be

described. If the packet is deemed erroneous at the receiver, the LLR outputs of the SISO decoder are stored and a retransmission is requested. The retransmitted data sequence can be interleaved using a different turbo interleaver other than the one used during the first transmission, and encoded using the same turbo encoder, and then transmitted.

The stored LLR outputs from the previous transmission are treated as *a priori* information, $L_{a\ priori}$, and added to the extrinsic information in each stage of the decoding. At the $m$-th iteration, the LLRs generated by the SISO decoders for data bit $a_k$ are

$$L_1^{(m)}(a_k) = L_{\text{sys}}(a_k) + L_{a\ priori}(a_k) + L_{\text{ext2}}^{(m-1)}(a_k) + L_{\text{ext1}}^{(m)}(a_k) \quad (55)$$

$$L_2^{(m)}(a_k) = L_{\text{sys}}(a_k) + L_{a\ priori}(a_k) + L_{\text{ext1}}^{(m)}(a_k) + L_{\text{ext2}}^{(m)}(a_k) \quad (56)$$

$$L_{\text{ext1}}^{(m)} = f(L_{\text{sys}}, L_{a\ priori}, L_{\text{ext2}}^{(m-1)}) \quad (57)$$

$$L_{\text{ext2}}^{(m)} = f(L_{\text{sys}}, L_{a\ priori}, L_{\text{ext2}}^{(m)}), \quad (58)$$

where $L_{\text{sys}}(a_k) = (2/\sigma^2)y_{s_k}$ is the LLR due to the systematic component, and $L_{\text{ext1}}^{(m)}(a_k)$ and $L_{\text{ext2}}^{(m)}(a_k)$ are the extrinsic information for each bit generated at the $m$th decoding stage by DEC1 and DEC2, respectively. Note that $f(\ \cdot\ )$ denotes the MAP decoding unit. The iterative procedure is started with the initial condition $L_{\text{ext2}}^{(0)}(a_k) = 0$. The bit decisions at stage $m$ are made based on $L_2^{(m)}(a_k)$.

Because the APC scheme can yield significant gain in error performance for severely corrupted wireless channels [117], the APC method is applied to the turbo hybrid-ARQ system to improve the system capacity and reliability. Assume that $L$ copies, $Y^{(1)}, ..., Y^{(L)}$, have been received and recognized to be unreliable. These packets are combined into a single packet, $\hat{C}^{(L)}$, by taking the average of the demodulated soft decision values of each repeated packet symbol. It is noted that previously received packets are available in the receiver using a buffer.

$$\hat{c_j}^{(L)} = \frac{1}{L}\sum_{i=1}^{L} {y_j}^{(i)}, \quad (59)$$

where ${y_j}^{(i)} = {x_j}^{(i)} + {n_j}^{(i)}$, ${x_j}^{(i)} = \pm 1$ and ${n_j}^{(i)}$ is the Gaussian random variable with variance ${\sigma_i}^2$.

Since the additional interleaver in turbo hybrid-ARQ encoder acts as an additional channel interleaver and the turbo encoder structure has to be modified whenever retransmission is requested, it causes more complexity and delay from additional encoding and interleaving. Therefore, we can remove the additional interleaver except for the turbo interleaver. The stored SISO LLR output, $L_p(u)$, from the previous transmission is compared with the deinterleaved LLR of the extrinsic information, $L_2(u;O)$, from the second SISO decoder (SISO DEC2). If the absolute value of the deinterleaved LLR is less than absolute value of $L_p(u)$, $|L_p(u)|$, then $L_p(u)$ is added to the extrinsic information to form more reliable LLR, $L_1(u;I)$ at the next iteration. During the initial iteration stage, $L_p(u)$ is used instead of initial zero value. Note that since the addition of $L_p(u)$ at medium-to-low SNR region is a little constructive, it is not necessary to add it. The turbo hybrid-ARQ decoder is shown in Fig. 38.

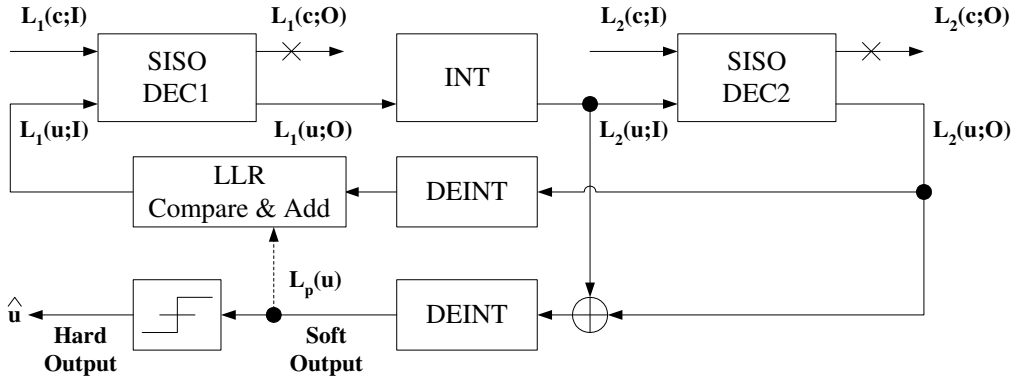


**Figure 38:** The structure of the turbo hybrid-ARQ decoder.

## *6.2 W-CDMA System with Turbo Hybrid-ARQ*

### 6.2.1 System Description

W-CDMA has been proposed as a promising 3G multiple access scheme for the IMT-2000 [21] systems because it can support large capacity and high data rate transmission [2]. Turbo coding also provides an adaptive and reliable mobile multimedia data transmission, especially delay tolerant packet transmission [91]. In many cases, CDMA is supported by

a FEC code such as convolutional and turbo codes. In this section, we describe W-CDMA system with turbo hybrid-ARQ scheme and investigate the error performance in W-CDMA system. Fig. 39 illustrates a block diagram of the 3G W-CDMA system with turbo hybrid-ARQ. The binary information data is initially RS encoded by shortened RS encoder. Since wireless channels usually give rise to burst errors, an outer RS coding is employed in order to detect and correct the burst errors effectively as well as to perform parity check for retransmission decision. Then, the RS encoded data is encoded by turbo encoder. For flexible and fast turbo decoding, a flexible iteration method is employed. In this method, if no frame error is detected after $M$ iterations, iterative decoding stops since more iterative decoding is not necessary. Then, the turbo encoded data is block interleaved by a channel interleaver before QPSK modulation.

The QPSK data symbols are mapped over multiple slots and some non-information bearing null data are appended to the modulated data to fill all slots completely. Each frame is 10 ms in time length and consists of 15 slots. For coherent detection and power control, 4 pilot symbol data is inserted into every slot. Because we perform the symbol level simulation, we omit the spreading block. However, the simulated channel model contains multipath taps to resolve the multipath components. At the receiver, matched filter resolves the frequency-selective Rayleigh fading channel into multiple flat fading paths. Channel estimation is performed on each resolved path using the pilot symbols. The output of the matched filter associated with each resolved path is multiplied by the complex conjugate of its corresponding channel estimate before being combined using coherent Rake receiver to exploit multipath diversity. The Rake combined output is equal to the soft decision output and is demodulated and then channel deinterleaved. The deinterleaved data is iteratively decoded and, if there still exists any error in the decoded frame, it can repeat the decoding up to the prescribed number of the maximum iteration. If the decoded frame cannot be corrected at the end of the maximum iteration, the turbo hybrid-ARQ receiver requests another retransmission by sending a NAK message through an error-free feedback uplink channel. If the number of retransmission exceeds the maximum number of retransmission request, it declares a decoding failure.

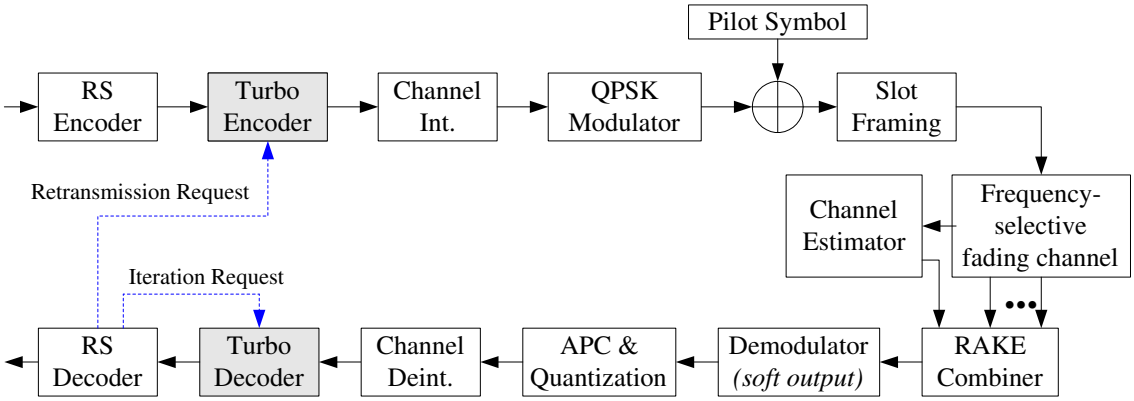


**Figure 39:** W-CDMA system with the turbo hybrid-ARQ scheme.

The simulated frequency-selective fading channel uses IMT-2000 Vehicular channel A/B model [87] at the carrier frequency of 2 GHz. Within one channel environment, channel A is the low delay spread case that occurs frequently and channel B is the median delay spread that also occurs frequently. The relative received power of the channel model is shown in Table 4. It is also noted that the propagation delays are known. A closed loop fast transmit power control (TPC) with update rate of 1,500 Hz and 1 dB power step is used. Note that no power control command error is assumed, yet a power control delay is considered.

**Table 4:** IMT-2000 Vehicular channel A/B models.

| Channel A | Channel B |
|---|---|
| Average Power (dB) | Average Power (dB) |
| 0.0 | -2.5 |
| -1.0 | 0.0 |
| -9.0 | -12.8 |
| -10.0 | -10.0 |
| -15.0 | -25.2 |
| -20.0 | -16.0 |

### 6.2.2 Channel Estimation and Rake Reciever

Although coherent detection can be used to increase link capacity under fast fading, channel estimation for coherent detection is difficult to implement. To avoid degradation by employing the channel estimation filters based on linear interpolation, low-order Gaussian

interpolation, Wiener filtering, and pilot symbol-assisted coherent orthogonal filtering [6], a channel estimation technique using time-multiplexed pilot symbols that operates well throughout the range of slow-to-fast fading was proposed for 3G W-CDMA system. The pilot symbols that are inserted at the beginning of each slot are periodically multiplexed with the sequence of transmitted data, and the pilot symbols and data symbols following pilot symbols constitute a slot as shown in Fig. 40 (a). The used channel estimation filter is called the weighted multi-slot averaging (WMSA) channel estimation filter because it uses pilot symbols throughout multiple slots. It was shown that the performance for the time-multiplexed pilot channel is slightly better than that of the parallel pilot channel [6]. In this section, we investigate channel estimation technique based on WMSA filters in [6], and simulate the error performance.

The binary information data for a user to be transmitted is turbo-encoded. The turbo encoded data is block interleaved by a channel interleaver before QPSK modulation. The QPSK data symbols are mapped over multiple slots and non-information bearing null data are appended as necessary to the modulated data to fill all slots completely. Each frame is 10 ms, $T_{frame}$, in duration and consists of 15 slots (i.e., $T_{slot}$ = 10 ms/15 $\approx$ 0.667 ms) with symbol period of $T_s = \frac{T_{slot}}{(N_d+N_p)}$ where $N_p$ and $N_d$ are denoted as the number of pilot and data symbols in each slot, respectively. For coherent detection and fast TPC, known unmodulated 4 pilot symbols are inserted into at the beginning of every slot as shown in Fig. 40 (a). Namely, pilot symbols and data symbols are time-multiplexed in each slot. Note that Fig. 40 (b) illustrates the frame structure using an alternative parallel pilot channel. Because we perform symbol level simulation for simplicity, the chip-spreading block is omitted.

The $k$-th user's turbo-encoded data signal $b_k(t)$ is modulated onto the phase-coded carrier $c_k(t)$, which is given by

$$c_k(t) \quad = \quad \sqrt{2P}a_k(t)e^{(\omega_c t+\theta_k)}, \tag{60}$$

where $P$, $\theta_k$, and $\omega_c = 2\pi f_c$ stand for common signal power, the phase of the $k$-th carrier, and the center frequency, respectively, and $a_k(t)$ represents spreading sequence which is

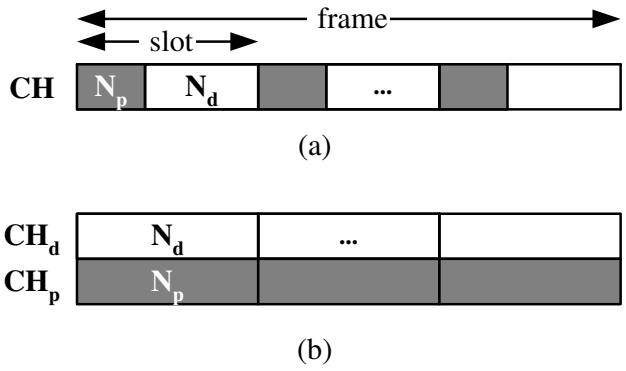


**Figure 40:** Frame and slot structures of W-CDMA system. (a) Time-multiplexed channel structure. (b) Parallel channel structure.

assigned to the $k$-th user if used. Thus, the transmitted signal $s_k(t)$ for the $k$-th user is given by

$$s_k(t) = \sqrt{2P}a_k(t)b_k(t)e^{(\omega_c t+\theta_k)}. \quad (61)$$

However, the simulated channel model contains resolvable multipath components. AWGN with power spectral density of $N_0$. At the receiver, a matched filter resolves the multipath Rayleigh fading channel into multiple flat fading paths. Channel estimation for coherent detection based on WMSA is performed on each resolved path using the time-multiplexed pilot symbols with encoded data symbols [6]. The received composite signal $r_{k,l}(t)$ with $L$ multipaths ($l = 0, 1, ..., L-1$) for $K$ users ($k = 0, 1, ..., K-1$) is given by

$$r_{k,l}(t) = \sum_{k=0}^{K-1}\sum_{l=0}^{L-1} u_k(t-\tau_{k,l})\alpha_{k,l}(t) + n(t), \quad (62)$$

where $u_k(t)$ is low-pass equivalent transmitted waveform for the $k$-th user, $\tau_{k,l}$ is time-varying propagation delay for $l$-th path and the $k$-th user, $\alpha_{k,l}(t)$ is time-varying fading gain for $l$-th path and the $k$-th user assuming $\sum_{l=0}^{L-1} E[|\alpha_{k,l}(t)|^2] = 1$, and $n(t)$ is AWGN.

The output of the matched filter, a bank of synchronous correlators, associated with each resolved path is multiplied by the complex conjugate of its corresponding channel estimate before being combined using a coherent Rake receiver. The coherent Rake receiver using the WMSA channel estimation filters is shown in Fig. 41.

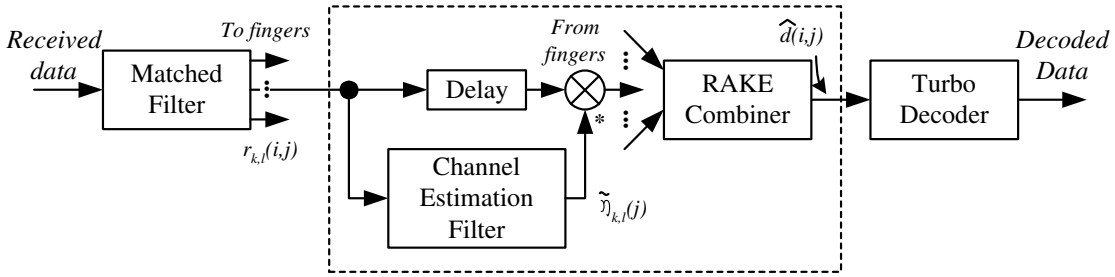


**Figure 41:** Coherent Rake receiver using the WMSA channel estimation filters.

Since 4 fingers are used in our simulation, the strongest 4 paths among all multipaths can be tracked using maximal ratio combining (MRC). The $k$-th user is assumed to be a desired user and the matched filter output at the $i$-th symbol position of the $j$-th slot for the $l$-th path can be obtained by

$$r_{k,l}(i,j) = \sqrt{2P}\alpha_{k,l}(i,j)e^{[\omega_c t+\theta(i,j)]} + n_{k,l}(i,j), \tag{63}$$

where $r_{k,l}(i,j) = r_{k,l}(iT_s + jT_{slot})$, $\alpha_{k,l}(i,j) = \alpha_{k,l}(iT_s + jT_{slot})$, $\theta(i,j) = \theta[i + j(N_d + N_p)]$, and $n_{k,l}(i,j)$ is the corresponding noise as defined by

$$n_{k,l}(i,j) = \frac{1}{T}\int_{iT+jT_{slot}+\tau_{k,l}}^{(i+1)T+jT_{slot}+\tau_{k,l}} n(t)u(t-\tau_{k,l})dt. \tag{64}$$

For MRC-based coherent Rake combining, the values of $\eta_{k,l}(i,j) = \sqrt{2P}\xi_{k,l}(i,j)$ need to be estimated by the WMSA channel estimation filter. The channel estimate to be used for coherent Rake combining is denoted as $\tilde{\eta}_{k,l}$. Then, coherent Rake combined soft-output at the $i$-th data position of the $j$-th slot for the $k$-th user can be calculated by multiplying $r_{k,l}(i,j)$ by the complex conjugates of $\tilde{\eta}_{k,l}(i,j)$ is given by

$$\hat{r}_{k,l}(i,j) = \sum_{l=0}^{L-1} \tilde{\eta}^*_{k,l}(i,j)r_{k,l}(i,j),\ i = N_p, N_{p+1}, ..., N_p + N_d - 1 \tag{65}$$

where $\tilde{\eta}^*_{k,l}(i,j)$ is the complex conjugate of the channel estimation output.

First, instantaneous channel estimation at the time position is performed using the $N_p$ pilot symbols belonging to the $n$-th slot as

$$\hat{\eta}_{k,l}(j) = \frac{1}{N_p}\sum_{i=0}^{N_p-1} r_{k,l}(i,j). \tag{66}$$

The fading variation over the interval of $N_p$ pilot symbols is negligible, so $\hat{\eta}_{k,l}(j)$ is approximated to

$$\hat{\eta}_{k,l}(j) \approx \sqrt{2P}\xi_{k,l}(i=0,j) + n_{k,l}(j), \tag{67}$$

where $n_{k,l}(j)$ is a complex-valued Gaussian noise with variance of $(N_0/T)/N_p$. Therefore, the SNR of the channel estimate increases $N_p$ times from the received SNR per symbol. In the case of slow fading, the channel gain remains almost the same over a period of several slots, so we can coherently add the several consecutive channel estimates in order to extend the observation interval. We apply a linear filter having $2M$ taps to extend the observation period to $2M$ slots. The filter output is expressed as

$$\tilde{\eta}_{k,l}(j) = \sum_{i=0}^{M-1} \beta_i \hat{\eta}_{k,l}(j-i) + \sum_{i=0}^{M} \beta_{i-1} \hat{\eta}_{k,l}(j+i), \tag{68}$$

where $\beta_i$ is the real-valued weighting factor (or linear filter tap coefficient). The filter output $\tilde{\eta}_{k,l}(j)$ is used as the channel estimate at all time positions of the $n$-th slot, so the channel estimate $\tilde{\eta}_{k,l}(i,j)$ is reduced to $\tilde{\eta}_{k,l}(j)$ where $i = N_p, N_{p+1}, ..., N_p + N_d - 1$. The weighting factor $\beta_i$'s are summarized in Table 5.

**Table 5:** Weighting factors for the WMSA channel estimation.

| Number of slots ($M$) | Weighting factors ($\beta$) |
|---|---|
| 6 | $\beta_0 = 1, \quad \beta_1 = 0.8, \quad \beta_2 = 0.3$ |
| 4 | $\beta_0 = 1, \quad \beta_1 = 0.6$ |

By using larger number of multiple slots and by selecting the appropriate weighting factors $\beta_i$'s, more accurate channel estimation is achieved. If the fading is very slow, the $2M$-tap WMSA channel estimator increases the SNR of the channel estimate by a factor of $\gamma$ which is defined by

$$\gamma = N_p \frac{\left(\sum_{i=0}^{M-1} \beta_i\right)^2}{\sum_{i=0}^{M-1} \beta_i^2}. \tag{69}$$

Although we consider a single user case ($K = 0$) in this work, multiple access interference (MAI) can be approximated as Gaussian noise for a large number of users. Thus, results can be extended to a multiuser environment by substituting $N_0$ with $N_0 + I_0$, where $N_0$ and $I_0$ represents the variances of Gaussian noise and MAI, respectively.

Finally, the Rake combined soft-output is demodulated and quantized, and passed through the channel deinterleaver. The deinterleaved data is iteratively decoded by SISO decoders by looking up a puncturing pattern, and if there exists any error in the decoded frame at the end of each iteration, iterations can continue decoding up to the prescribed maximum number of iterations. Then, the FER performance are evaluated according to the number of averaging slots used for WMSA channel estimation.

## *6.3 Numerical Results and Discussions*

In this section, we present simulation results of the turbo hybrid-ARQ system. Table 6 summarizes the main simulation parameters.

**Table 6:** Simulation parameters for W-CDMA system.

| | |
|---|---|
| Simulation link | Forward link (BS to MS) |
| Data rate | 32 kbps (320 bits/frame) |
| Frame period | 10 ms (1 frame = 16 slots) |
| Modulation | QPSK |
| Channel interleaving | Block interleaver |
| IMT-2000 channel model | Freq.-selective Rayleigh fading, 2 GHz, 100 km/h ($f_D$=185 Hz) |
| Power control | Step size = 1 dB, No PC command error |
| Rake combining | Max. ratio combining, 4 fingers |
| FEC codes | Shortened RS(40,32) over GF(256), Rate-1/3 turbo code with $g = (15/13)_8$ and 8-state, S-random interleaver, Decoding iteration up to 12 |
| Hybrid-ARQ | Max. retransmission up to 3 |

### 6.3.1 Error and Latency Performances of the Turbo HARQ Scheme

Fig. 42 compares the BER and FER performances of the turbo hybrid-ARQ systems. We can observe that the turbo hybrid-ARQ scheme which is based on concatenated RS-turbo code and the average packet combining technique at the receiver offers a significant decrease in both BER and FER at low SNR region over the simple turbo-coded ARQ and non-ARQ scheme in severe frequency-selective fading channel.

As shown in Fig. 43, the gain difference resulting from different number of maximum

retransmission is negligible. Thus, the maximum retransmission number of 3 is enough to avoid excessive ARQ delay as well as to obtain reasonable gain when the turbo hybrid-ARQ scheme is used.

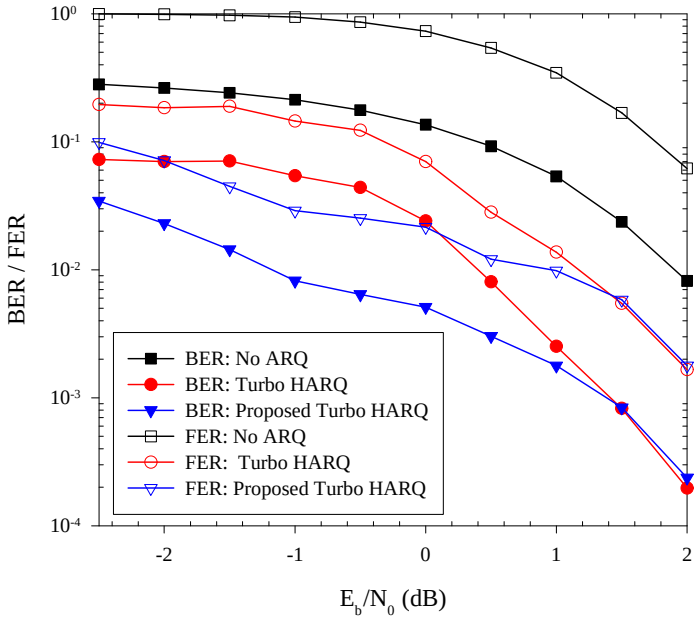


**Figure 42:** BER and FER performances of the turbo hybrid-ARQ W-CDMA system.

### 6.3.2 Performance in the W-CDMA System

The FER performances for different vehicle speed (or maximum Doppler frequency) are compared in Fig. 44. The IMT-2000 Vehicular channel B model is used. As the vehicle speed gets slower, the frame error rate abruptly decreases at relatively high SNR region. We believe that this result is due to the power control becoming more effective and APC giving constructive effect to combine packets with the decrease in the maximum Doppler frequency at the region of high SNR.

Finally, Fig. 45 shows BER and FER performances as the number of decoding iteration increases from 1 to 20 at fixed SNRs. At relatively low SNR of -1 dB, the BER decreases from $7 \times 10^{-2}$ to $5 \times 10^{-3}$ as much as almost an order of 10 as the number of decoding iteration increases from 10 to 20. As expected, although we can obtain larger gain by doing

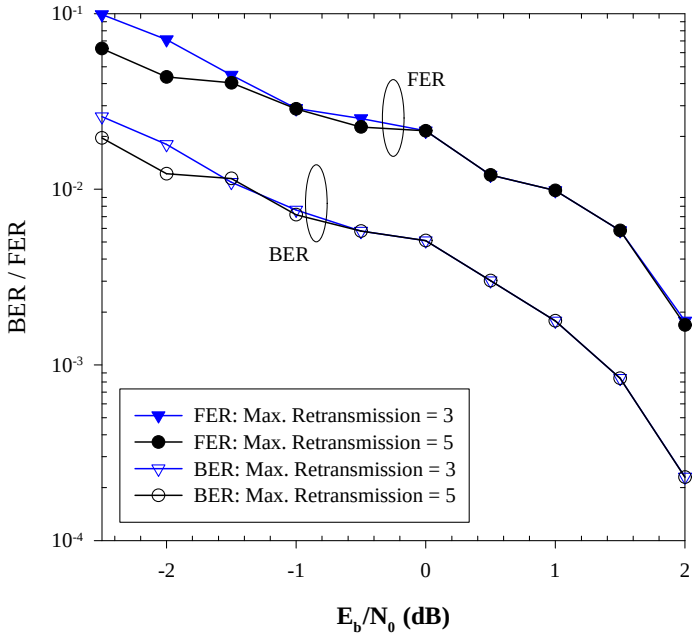


**Figure 43:** BER and FER performances of different numbers of ARQ retransmission.

more iterative decoding at low SNR region in particular, this causes larger decoding delay such that some services may not tolerate the latency.

## *6.4 Conclusions*

We have proposed a full-retransmission Type-I turbo hybrid-ARQ scheme employing the concatenated RS-turbo code and a simple yet effective average packet combining technique to improve the BER and FER performances as well as to decrease the average number of decoding iterations for packet-data transmission of W-CDMA system. Concatenated RS-turbo code provides strong burst-error correction capability as well as low-error probability by removing the residual errors resulting from a suboptimal turbo decoding. We have shown that the turbo hybrid-ARQ scheme exploiting the soft outputs and turbo principle can improve the error performance in multipath fading channels, outperforming the conventional turbo HARQ techniques at low SNR region. Therefore, we can maximize the capacity and design more robust packet-data communication.

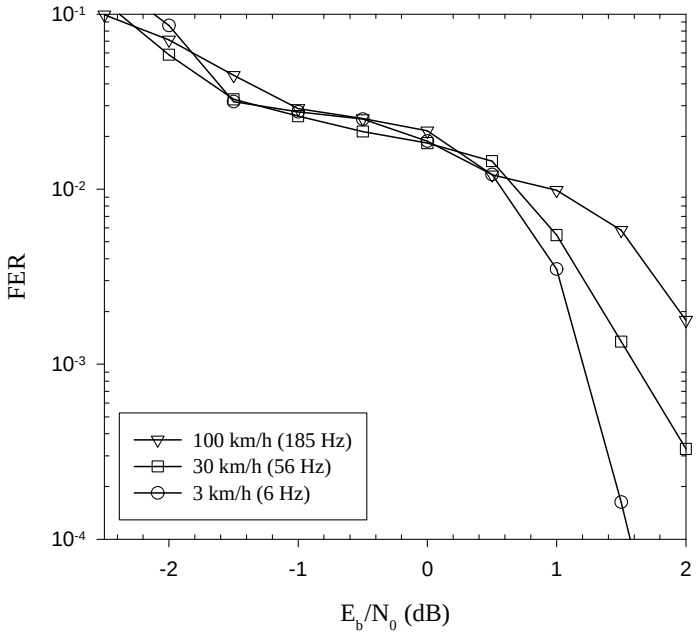


**Figure 44:** FER performance for different vehicle speeds. IMT-2000 Vehicular channel B model is used.

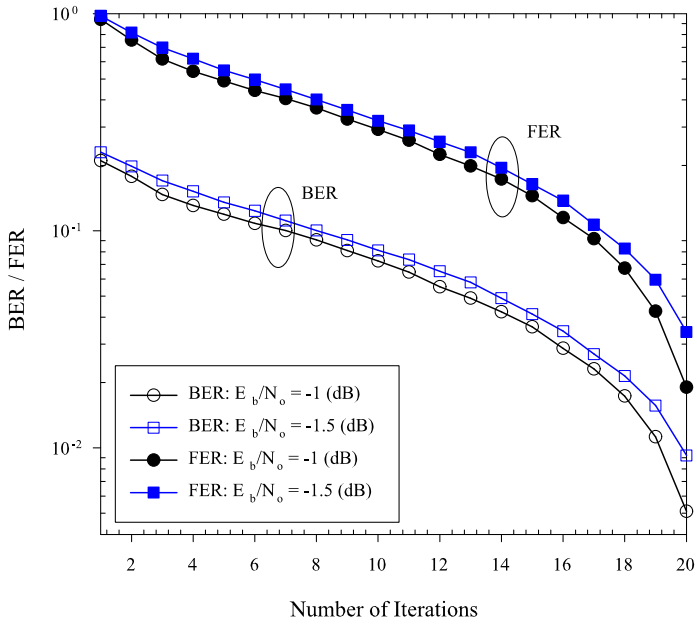


**Figure 45:** BER and FER performances according to the number of decoding iterations.

# CHAPTER VII

# RATE COMPATIBLE PUNCTURED TURBO-LIKE CODES

In this chapter, we propose rate compatible punctured turbo-like codes using PCCC and SCCC and their puncturing methods to support adaptive code rate and incremental redundancy retransmission for packet-data networks. In addition, we propose Type-II RCPT-HARQ and RCPS-HARQ schemes that provide excellent performance in reliability and throughput.

## *7.1 Rate Compatible Punctured Turbo Codes*

FEC codes such as convolutional and turbo codes generally require the selection of a fixed coding rate that is well adapted to the channel characteristics. However, in some cases, a more adaptive and versatile coding scheme is needed to meet unequal error protection requirements or/and to cope with unknown or time varying channel conditions. Rate compatible punctured turbo codes can meet these needs. Motivated by the RCPC codes, RCPT codes with code rates of 1/3 and 1/2 were introduced in [10] and the performance of the RCPT codes on AWGN and flat Rayleigh fading channels was discussed in [57].

The FER performance of turbo-like codes usually improves with the increase in the block length due to the beneficial interleaving gain in contrast to the convolutional codes. Therefore, it is promising to use turbo-like codes to transmit a non-real time long packet-data. Furthermore, by employing a rate compatible punctured turbo hybrid-ARQ (RCPT-HARQ) protocol, we can achieve a more reliable packet-data transmission scheme. However, we need to select and adjust the puncturing patterns, incremental step, and repetition number according to the given service requirements and channel conditions. Recently, the use of RCPT codes in a HARQ system on a non-stationary Gaussian channel was proposed in [109]. In [76], rate compatible turbo codes were applied to a Type-II HARQ system

to obtain high reliability and throughput performance at low SNR region. As a practical application, an adaptive packet soft handoff scheme using punctured turbo coding was proposed in [63].

Since RCPT coding provides excellent unequal-error protection, which means rate variation within a packet is possible due to the code compatibility, and rate adaptation capabilities to a time-varying fading channel, we can easily achieve a good throughput performance without increasing the system complexity and block length. Since RCPT coding requires a single rate-$1/n$ turbo encoder and iterative decoder pair, and the transmitter and receiver need only share a puncturing table, a versatile coded system with minimal complexity can be designed. Furthermore, by employing the Type-II RCPT-HARQ protocol, more flexible and higher throughput packet-data transmission is possible.

### 7.1.1 Concatenated RS-RCPT Codes

We propose a flexible and powerful FEC coding based on the use of a concatenated RS-turbo code and rate compatible puncturing technique. Because RCPT codes can offer unequal error protection similar to conventional RCPC codes [48], we can easily achieve good bit and frame error rate performance without increasing the system complexity and interleaver size. The RCPT codes can be designed in a way similar to RCPC codes. That is, the rate-$1/n$ convolutional encoder and soft decision Viterbi decoder are substituted by a rate-$1/n$ turbo encoder and a turbo decoder, respectively. In our scheme, an outer RS code is used to correct the burst-errors and to fix the deficiency of the iterative decoder due to the instability and convergence problem, reducing error-floor by removing residual errors. Note that a CRC check is used to perform retransmission decisions and to stop iterations in the turbo decoder. According to our simulation results, concatenated RS-turbo codes outperform concatenated RS-convolutional codes by 1.5 to 2 dB. For the comparison with similar complexity, rate-1/3 turbo codes with constraint length $K$=4 and 4 iterations and convolutional codes with $K$=9 are used.

The RCPT encoder output consists of the systematic component $x_s$ and the two parity components $x_{1p}$ and $x_{2p}$, as shown in Fig. 46. The systematic and parity bits of turbo

encoder are then punctured according to a specified puncturing pattern. The punctured data consists of the punctured systematic component $y_s$ and the two punctured parity components $y_{1p}$ and $y_{2p}$. We classify the puncturing rules into two classes; *systematic puncturing* punctures only the parity bits, while *non-systematic puncturing* punctures the systematic bits as well. The puncturing patterns for the systematic and non-systematic puncturing cases are shown in Fig. 47 (a) and (b), respectively. The original unpunctured code rate is set to $1/n$, where $n = 3$. A '1' and '0' in the puncturing table represents transmitted and punctured code bit positions, respectively. The punctured data is then multiplexed to form serial sequences to transmit. The puncturing table consists of three sub-blocks each having $P$ bits, where the three sub-blocks specify the puncturing patterns for the systematic, Parity 1 and Parity 2 components, and $P$ stands for the puncturing period.

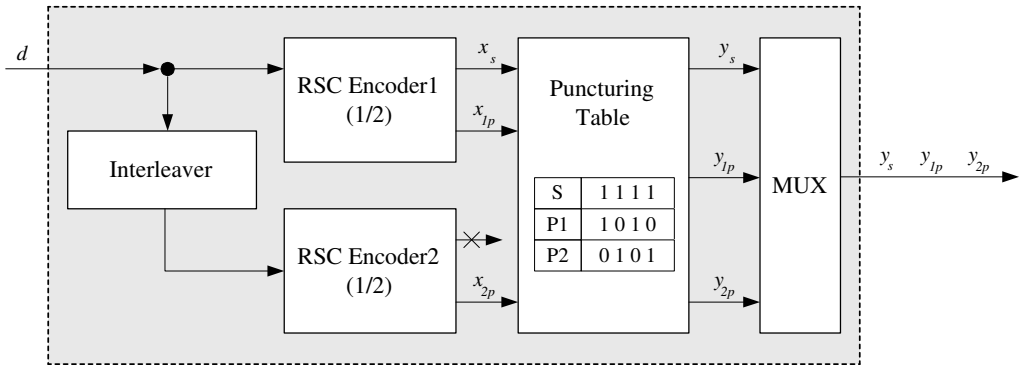


**Figure 46:** RCPT encoder with a puncturing table.

For each index $k$, we define an $n \times P$ binary puncturing table, denoted by $PT_k$, where $k = 0, 1, ..., (n-1)P$. For systematic puncturing $PT_0$ must contain $P$ ones in the first row. $PT_{k+1}$ must have ones in the same positions as $PT_k$ plus an additional one and, finally, $PT_{(n-1)P}$ becomes a puncturing table of all ones. For example, let us form an RCPT code with $n = 3$, $P = 4$ and $k = 0, 1, 2, 4, 8$ which consists of two rate-1/2 RSC encoders. For this case, the RCPT code can choose any code rate from among rates 1, 4/5, 2/3, 1/2, and 1/3. We can set the index $k$ and its incremental value according to channel conditions and to meet delay constraints (e.g., $k = 2, 4, 8$). Therefore, the overall code rate of the RS-RCPT

coded system with an outer shortened RS $(N_o, K_o)$ code is given by

$$\hat{R}_k = \frac{K_o}{N_o} \cdot R_k = \frac{K_o}{N_o} \cdot \frac{P}{P+k}, \tag{70}$$

where the $k$ is the puncturing index. Note that the number of encoded information bits will vary due to the variable puncturing. Since $E_b/N_0$ is not constant for the RS-RCPT coded system, unlike a fixed rate FEC system, we should compare the different RS-RCPT coded systems at different $E_s/N_0$.

| Puncturing Table | $PT_0$ | $PT_1$ | $PT_2$ | $PT_4$ | $PT_8$ |
|---|---|---|---|---|---|
| Systematic | **1 1 1 1** | 1 1 1 1 | 1 1 1 1 | 1 1 1 1 | 1 1 1 1 |
| Parity 1 | 0 0 0 0 | **1** 0 0 0 | 1 0 0 0 | 1 0 **1** 0 | 1 **1** 1 1 |
| Parity 2 | 0 0 0 0 | 0 0 0 0 | 0 0 0 **1** | 0 **1** 0 1 | 1 1 **1** 1 |
| Index | *k=0* | *k=1* | *k=2* | *k=4* | *k=8* |
| Code Rate | $R_0$=*1* | $R_1$=*4/5* | $R_2$=*2/3* | $R_4$=*1/2* | $R_8$=*1/3* |

**(a)**

| Puncturing Table | $PT_0$ | $PT_1$ | $PT_2$ | $PT_4$ | $PT_8$ |
|---|---|---|---|---|---|
| Systematic | **1 1 1 0** | 1 1 1 0 | 1 1 1 0 | 1 1 1 0 | 1 1 1 **1** |
| Parity 1 | 0 0 0 **1** | 0 0 0 1 | 0 **1** 0 1 | 0 1 0 1 | **1** 1 **1** 1 |
| Parity 2 | 0 0 0 0 | **1** 0 0 0 | 1 0 0 0 | 1 0 **1** **1** | 1 **1** 1 1 |
| Index | *k=0* | *k=1* | *k=2* | *k=4* | *k=8* |
| Code Rate | $R_0$=*1* | $R_1$=*4/5* | $R_2$=*2/3* | $R_4$=*1/2* | $R_8$=*1/3* |

**(b)**

**Figure 47:** Rate compatible puncturing tables for RCPT codes ($n$=3, $P$=4 and $k$=0, 1, 2, 4, 8). (a) Systematic puncturing. (b) Non-systematic puncturing.

### 7.1.2 Puncturing Methods and RCPT-HARQ Protocol

The RCPT codes have practical utility and versatility in that the system requires a single rate-$1/n$ encoder and decoder. The rate compatible puncturing rule limits the puncturing pattern such that all of the code bits of a high rate punctured code must be included in the lower rate codes (i.e., the high rate codes should be used in the lower rate codes). The

transmitter and receiver only share a puncturing table to determine which code bits to transmit, and the receiver may simply insert erasures for the code bits that have not yet been received. Therefore, the transmitter need only transmit supplemental code bits to get to the next lowest rate code.

RS-RCPT-HARQ protocol falls into incremental redundancy codes, in that more bits are incrementally transmitted to adaptively meet the error performance requirements of the system. If the decoded frame has detectable errors after a prescribed maximum number of decoding iterations, the receiver sends a NAK message to the transmitter through a feedback channel to request the next transmission. If the number of retransmissions exceeds the maximum number of retransmissions allowed, a decoding failure is declared. We ignore the effects of finite memory buffer at the receiver and feedback errors on the system performance for simplicity. Fig. 48 shows a flowchart for the concatenated RS-RCPT-HARQ protocol. In case of the retransmissions, we use a packet combining scheme to combine the received frames.

We investigate the throughput and error performance of the RS-RCPT-HARQ scheme for some families of puncturing tables. It is necessary that at least some non-systematic parity bits be transmitted so that iterative decoding is possible. Because all decoding modules share the systematic bits, puncturing the systematic bits of turbo codes gives more loss than the case of puncturing the non-systematic bits. Given a turbo encoder and a fixed puncturing period, $P$, we consider five puncturing methods for selecting puncturing tables corresponding to the highest rate of the RCPT code:

- *Method I (Systematic Puncturing)*: In the initial transmission ($k = 0$), transmit all $P$ systematic code bits. If an error is detected at the receiver, then transmit two code bits from the non-systematic sub-blocks ($k = 2$).

- *Method II (Non-systematic Puncturing)*: In the initial transmission ($k = 0$), transmit $P-1$ positions of systematic code bits and 1 code bit from the non-systematic sub-blocks. If errors are detected at the receiver, the remaining portion of systematic and parity sub-blocks ($k = 2$) are transmitted.

- *Method III (Non-systematic Puncturing)*: In the initial transmission ($k = 0$), puncture

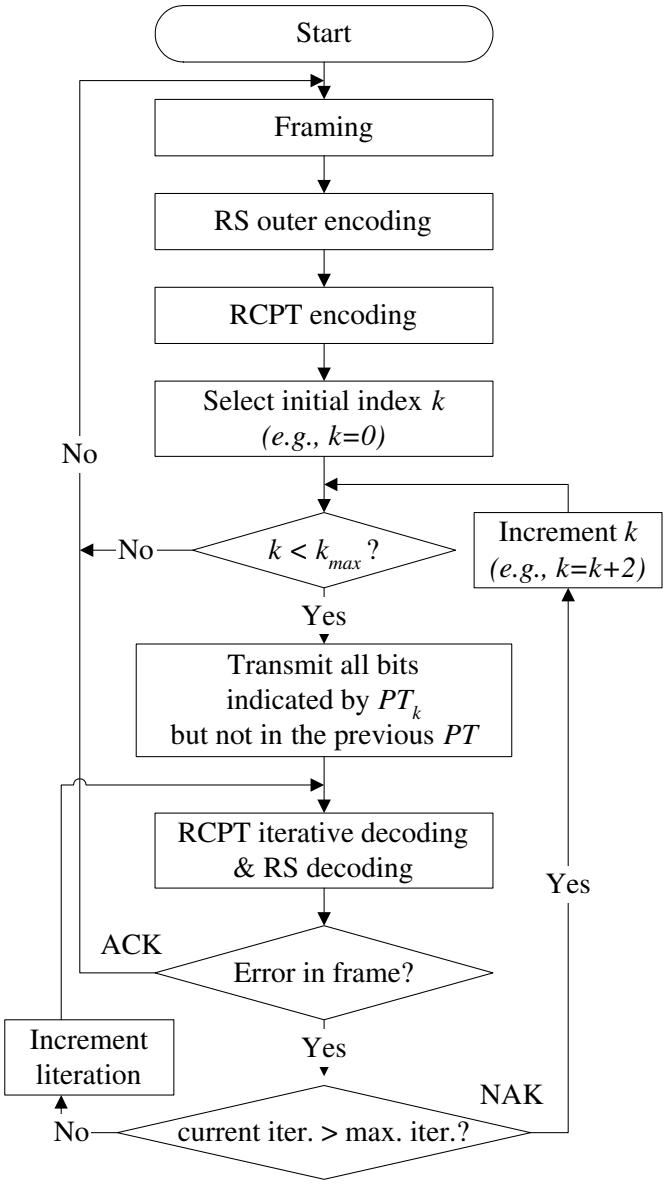


**Figure 48:** Flowchart for the RS-RCPT-HARQ protocol.

more than 1 systematic code bit and transmitting instead 1 or more code bits of non-systematic sub-blocks.

• *Method IV (Systematic Puncturing)*: In the initial transmission ($k = 1$), transmit $P$ systematic code bits and 1 non-systematic code bit sub-blocks instead of setting $k = 0$. If any error is detected, then transmit additional non-systematic code bits sub-blocks (e.g., $k = 3$).

• *Method V (Non-systematic Puncturing)*: In the initial transmission ($k = 1$), transmit $P - 1$ systematic code bits and two non-systematic code bits. If any error is detected, then transmit additional non-systematic code bits (e.g., $k = 3$).

From our preliminary simulations, the Method III is first excluded because it always performed worse than the Method II. The performance of the Method III method is dramatically worse for a puncturing period $P$=4, since half of the systematic bits are punctured in the initial transmission. In case of $P$=8, we may obtain a performance very close to that of the Method II by puncturing two positions of systematic bits, but the throughput will be still better with the Method II. Generally, if a combination of the puncturing period and the frame size is large enough, it may be advantageous to puncture more than one systematic position in the initial transmission. For the Method I, we transmit at rates $R_0 = 8/8, R_3 = 8/11, ...$, whereas for Method II, we transmit at rates $R_1 = 8/9, R_2 = 8/10, ....$

To achieve more reliability at the sacrifice of additional delay, we repeat the protocol two additional times and use a code combining scheme to combine received frames for the puncturing tables of the PH8 family (i.e., the maximum number of transmissions becomes 9). Fig. 49 shows five puncturing tables of the PH8 family. PH8A and PH8B transmit according to rates $R_k$ with $k$=0,4,8 (Methods I and II, respectively) for each protocol loop, while PH8C, PH8D and PH8E transmit according to rates $R_k$ with $k$=2,5,8, $k$=4,6,8 and $k$=1,5,8, respectively. PH8A falls into the Method I puncturing method that is generated by systematic puncturing. From the second transmission, puncturing positions of Parity 1 and 2 sub-blocks are equally distributed. PH8B falls into the Method II puncturing method

that is generated by non-systematic puncturing (i.e., one position of the systematic sub-block is punctured and one position of the parity sub-blocks is transmitted) and puncturing positions in parity sub-blocks are not equally distributed from the second transmission. PH8C and PH8D falls into the Method IV and are generated by systematic puncturing (i.e., additional one position and two positions of parity sub-blocks are transmitted at the first transmission, respectively). Finally, PH8E is a Method V that is generated by non-systematic puncturing (i.e., one position of systematic sub-block is punctured and additional two positions of parity sub-blocks are transmitted at the first transmission).

### 7.1.3 Numerical Results and Discussions

Binary information data is initially encoded by a shortened RS $(40, 32)$ code over GF(256). The RS encoded data is again encoded by a rate-1/3 RCPT encoder with a puncturing table having $P$=4. Two identical 8-state RSC codes with the code generator polynomials, $g = (1 + D + D^3/1 + D^2 + D^3)$, and an S-random turbo interleaver where $S$ is $\lfloor\sqrt{N/2}\rfloor$, where $N$ is the concatenation interleaver size, are used. The RCPT encoded data is block interleaved by a channel interleaver before QPSK modulation in same way as the W-CDMA system in Chapter VI. The simulated frequency-selective fading channel uses the ITU IMT-2000 Vehicular channel A/B model [87] and the ETSI UMTS Phase 2 channel model [35] at carrier frequency of 2 GHz and mobile velocity of 30 km/h.

Fig. 50 compares the BER and FER performances of the RS-RCPT coded system for different code rates. Note that a concatenation interleaver size of 320 bits and $S = 12$ is used for the simulations. As the RCPT code rate decreases from $R_0 = 1$ down to $R_8 = 1/3$, we can obtain an additional coding gain of around $3 \sim 4$ dB for the next lowest code rate at FER $= 10^{-3}$. The BER curves show a similar trend as the FER.

Figs. 51 and 52 compare the FER performance of the RS-RCPT coding system for different puncturing patterns with $R_4 = 1/2$ (denoted as P9) and $R_2 = 2/3$ (denoted as PA), respectively. To choose a good puncturing pattern for the RCPT code, we compare puncturing tables for $R_4 = 1/2$ and $R_2 = 2/3$. For the case of $R_4 = 1/2$, the P9 and P9-1 puncturing tables are better than the others. Because the puncturing positions are

**PH8A: Systematic**

| Puncturing Table | $PT_0$ | $PT_4$ | $PT_8$ | Same as Protocol Loop 1 | Same as Protocol Loop 1 |
|---|---|---|---|---|---|
| Systematic | 1 1 1 1 | 0 0 0 0 | 0 0 0 0 | | |
| Parity 1 | 0 0 0 0 | 1 0 1 0 | 0 1 0 1 | | |
| Parity 2 | 0 0 0 0 | 0 1 0 1 | 1 0 1 0 | | |
| Index | *k=0* | *k=4* | *k=8* | | |
| Code Rate | $R_0$=*1* | $R_4$=*1/2* | $R_8$=*1/3* | | |
| | **Protocol Loop 1** | | | **Loop 2** | **Loop 3** |

**PH8B: Non-systematic**

| Puncturing Table | $PT_0$ | $PT_4$ | $PT_8$ | Same as Protocol Loop 1 | Same as Protocol Loop 1 |
|---|---|---|---|---|---|
| Systematic | 1 1 1 0 | 0 0 0 1 | 0 0 0 0 | | |
| Parity 1 | 0 0 0 1 | 0 1 0 0 | 1 0 1 0 | | |
| Parity 2 | 0 0 0 0 | 1 0 1 0 | 0 1 0 1 | | |
| Index | ***k=0*** | ***k=4*** | ***k=8*** | | |
| Code Rate | $R_0$=*1* | $R_4$=*1/2* | $R_8$=*1/3* | | |
| | **Protocol Loop 1** | | | **Loop 2** | **Loop 3** |

**PH8C: Systematic**

| Puncturing Table | $PT_2$ | $PT_5$ | $PT_8$ | Same as Protocol Loop 1 | Same as Protocol Loop 1 |
|---|---|---|---|---|---|
| Systematic | 1 1 1 1 | 0 0 0 0 | 0 0 0 0 | | |
| Parity 1 | 1 0 0 0 | 0 0 1 0 | 0 1 0 1 | | |
| Parity 2 | 0 0 0 1 | 0 1 1 0 | 1 0 0 0 | | |
| Index | ***k=2*** | ***k=5*** | ***k=8*** | | |
| Code Rate | $R_2$=*2/3* | $R_5$=*4/9* | $R_8$=*1/3* | | |
| | **Protocol Loop 1** | | | **Loop 2** | **Loop 3** |

**PH8D: Systematic**

| Puncturing Table | $PT_4$ | $PT_6$ | $PT_8$ | Same as Protocol Loop 1 | Same as Protocol Loop 1 |
|---|---|---|---|---|---|
| Systematic | 1 1 1 1 | 0 0 0 0 | 0 0 0 0 | | |
| Parity 1 | 1 0 1 0 | 0 1 0 0 | 0 0 0 1 | | |
| Parity 2 | 0 1 0 1 | 0 0 1 0 | 1 0 0 0 | | |
| Index | ***k=4*** | ***k=6*** | ***k=8*** | | |
| Code Rate | $R_4$=*1/2* | $R_6$=*2/5* | $R_8$=*1/3* | | |
| | **Protocol Loop 1** | | | **Loop 2** | **Loop 3** |

**PH8E: Non-systematic**

| Puncturing Table | $PT_1$ | $PT_5$ | $PT_8$ | Same as Protocol Loop 1 | Same as Protocol Loop 1 |
|---|---|---|---|---|---|
| Systematic | 1 1 1 0 | 0 0 0 1 | 0 0 0 0 | | |
| Parity 1 | 1 0 0 0 | 0 0 1 1 | 0 1 0 0 | | |
| Parity 2 | 0 0 1 0 | 0 1 0 0 | 1 0 0 1 | | |
| Index | ***k=1*** | ***k=5*** | ***k=8*** | | |
| Code Rate | $R_1$=*4/5* | $R_5$=*4/9* | $R_8$=*1/3* | | |
| | **Protocol Loop 1** | | | **Loop 2** | **Loop 3** |

**Figure 49:** Five puncturing tables of PH8 family.

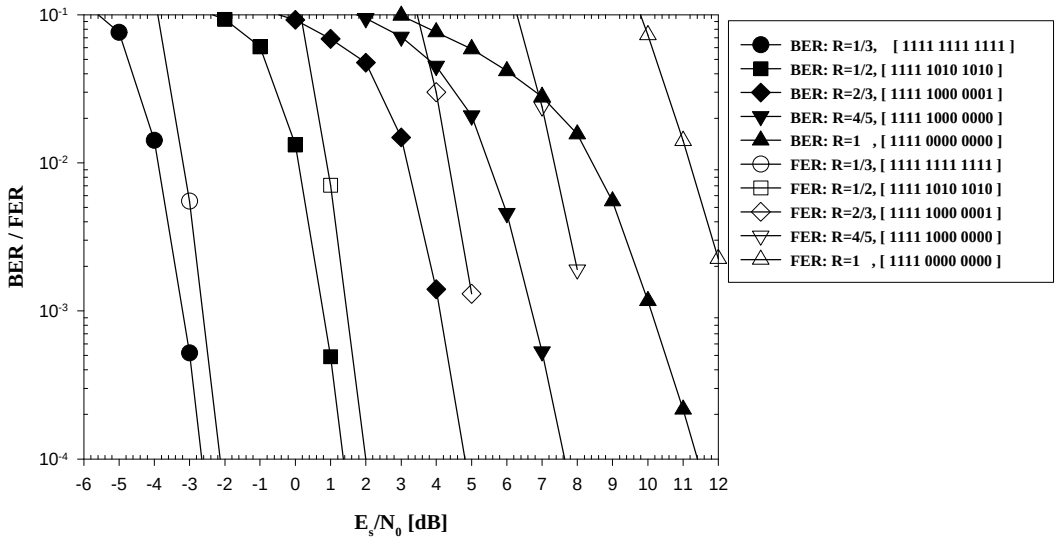


**Figure 50:** BER and FER performances for different code rates ($R_k$=1/3 to 1).

uniformly marked on Parity 1 and Parity 2 sub-blocks, the iterative decoding of the RCPT code becomes more effective. The P9-3 and P9-5 puncturing tables perform worse than the others since puncturing is done on Parity 1 or Parity 2 sub-block only. In addition, the performance with the non-systematic puncturing tables P9-4 and P9-6, is satisfactory, but they degrade as much as 0.1 dB and 0.2 dB compared to the puncturing tables P9 at FER=$10^{-3}$, respectively. This is because the additional assigned bits on the parity sub-blocks compensate for the loss from puncturing systematic bits. For the case of $R_2 = 2/3$, the performance behavior is very similar as the case with $R_4 = 1/2$ except for the case of PA-5. The degradation results from the non-systematic puncturing of two positions on the systematic sub-block at the higher code rate. Therefore, we should avoid using these puncturing patterns for higher code rate system since excessive non-systematic puncturing easily produces many errors.

Figs. 53 and 54 compare the FER and throughput performances for the PH8 family, respectively. The throughput is defined as the average code rate required for error-free information transmission for the puncturing types. Note that the ETSI UMTS Phase-2 channel with mobile velocity of 3 km/h are used for the simulations. We achieve larger

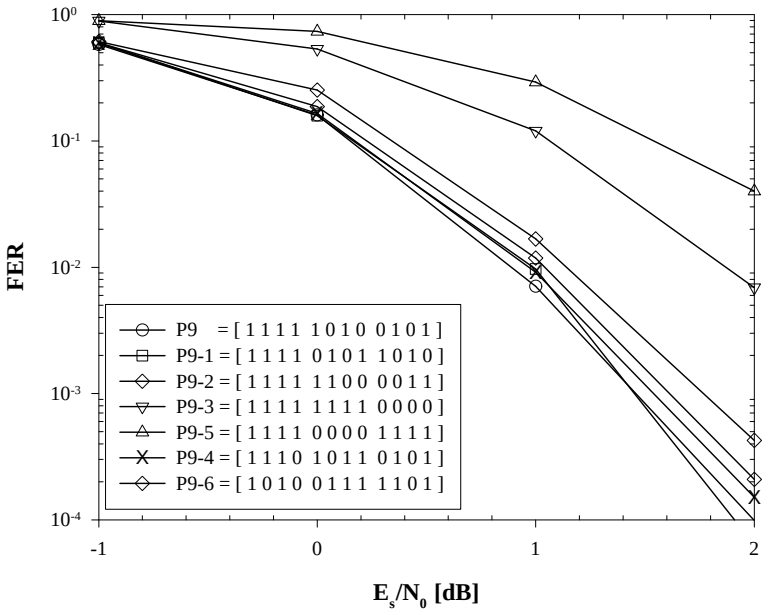


**Figure 51:** FER performance for different puncturing tables with $R$=1/2 (P9 family).

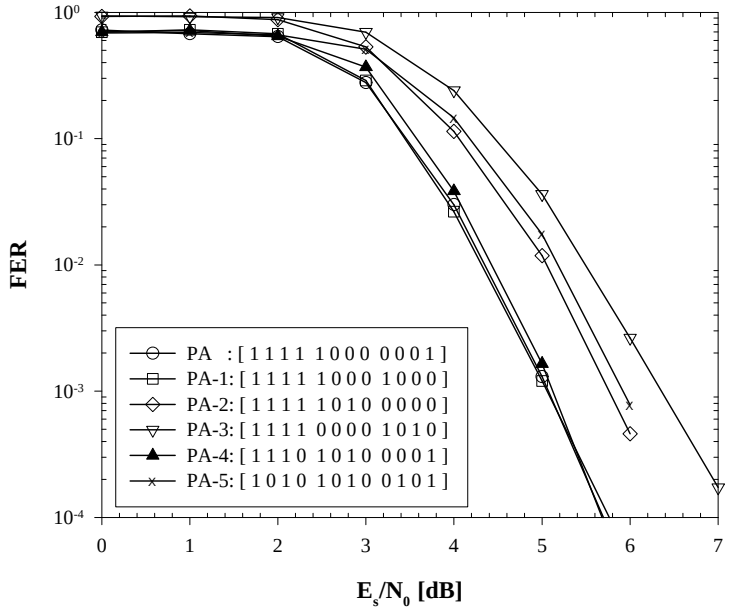


**Figure 52:** FER performance for different puncturing tables with $R$=2/3 (PA family).

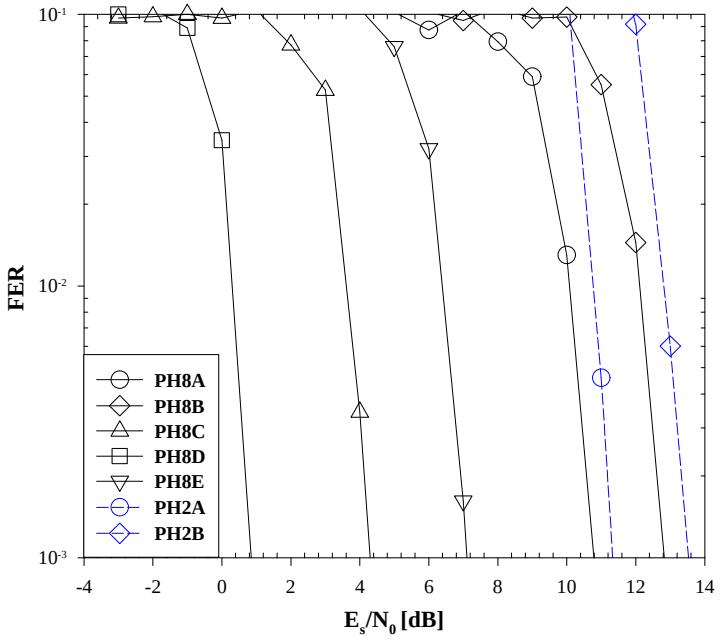


**Figure 53:** FER performance of puncturing tables of PH2 and PH8 families.

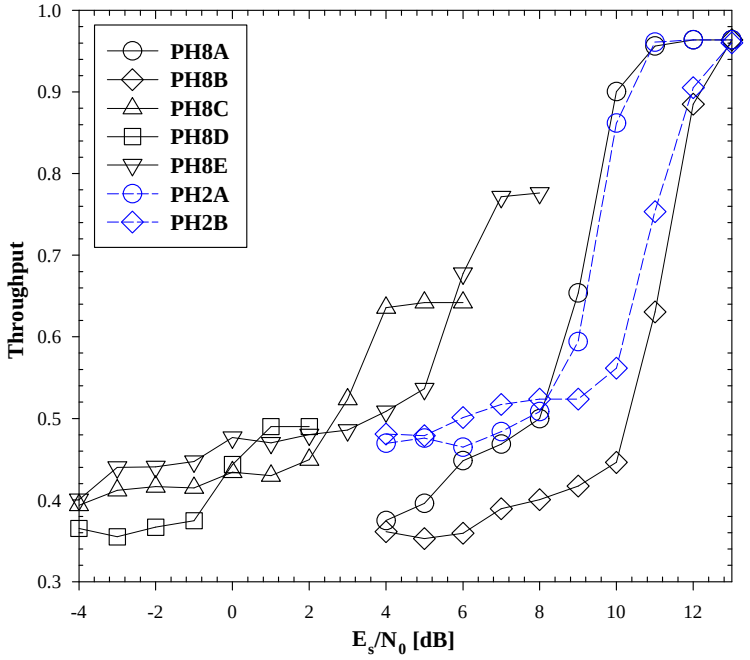


**Figure 54:** Throughput performance of puncturing tables of PH2 and PH8 families.

coding gain (i.e., PH8D > PH8C > PH8E > PH8A) with the increase in the initial $k$. However, throughput decreases. According to the comparison of the FER between the PH8A and PH2A (and between the PH8B and PH2B), we achieve larger coding gain by employing hybrid-ARQ and protocol repetition. Note that the PH2A (Method I) and the PH2B (Method II) correspond to the first protocol loop of the PH8A and PH8B shown in Fig. 49, respectively. Since the protocol repetition gives rise to more delay and degraded throughput, we need to adjust the initial $k$, incremental step and repetition number according to given service requirements and channel conditions. The PH8B (Method II) gives the worst FER and throughput performance at the region of medium-to-high SNRs. Note that throughput is defined as the rate of average received total code bits to information data bits to get error-free frames and undecoded frames are excluded for the throughput calculation.

### 7.1.4 Conclusions

To support an adaptive and reliable transmission of packet- and voice-data in hostile mobile radio channel, we have proposed the concatenated RS-RCPT codes with a variable code rate up to one. We have proposed the RS-RCPT encoder/decoder and puncturing methods and investigated the error and throughput performances in W-CDMA system for multipath fading channels. We have shown that concatenated RS-RCPT codes can correct the burst-errors and fix the deficiency of the iterative decoder due to the instability and convergence problem, reducing error-floor by removing residual errors. In addition, to design versatile retransmission systems using RS-RCPT codes, we have proposed a class of incremental redundancy Type-II RS-RCPT-HARQ scheme. Finally, since there exists a trade-off between error rate and throughput performances, we should select and adjust the initial value of $k$, incremental step, and repetition number according to the QoS requirements and channel conditions.

## 7.2 Rate Compatible Punctured SCCC

High-speed data services in mobile communications, such as mobile Internet access and mobile broadcasting, will require a powerful error control coding scheme. Such services support high data rate and asymmetric transmission such as the 3GPP W-CDMA HSDPA (High Speed Downlink Packet Access) [1] and 3GPP2 cdma2000 HDR (High Data Rate) or 1xEV-DO/1xEV-DV [123, 11, 116] systems. Packet-data transmission typically requires very low BER/FER down to $10^{-8}/10^{-5}$ and varying latency ranging from 10 to 80 ms. To provide different code rates and QoS requirements for hostile wireless channels, an adaptive error control coding scheme must be used to mitigate time-varying wireless channel impairments.

Iterative decoding-based PCCC, otherwise known as turbo coding, can provide excellent coding gains. However, PCCC has a BER/FER flooring effect in the region of moderate-to-high SNR, i.e., flattening effect of the BER/FER, due to a small number of low weight codewords [99], while SCCC, an another important class of turbo-like codes, shows little error flooring problem even with small interleavers [13]. In case of PCCC, BER decreases approximately as $N^{-1}$, while in case of SCCC, it typically decreases as $N^{-3}$, where $N$ is the concatenation interleaver length. The error-floor effect is a main obstacle to very high reliability packet transmission. Therefore, SCCC provides better FER performance than PCCC in the region of moderate-to-high SNR, and is better suited for offering error-free packet transmission [13]. Moreover, SCCC is less sensitive to interleaver design than PCCC and makes a more natural code concatenation and a simpler decoder possible. SCCC is more attractive in that it can be extended to serially concatenated coded modulation schemes such as BICM.

Rate compatible punctured codes such as RCPC codes [48] and PCCC-based rate compatible punctured turbo codes [10], [57], [109], [61] have been shown to provide different levels of error protection and adaptability to unknown and time-varying channels at the expense of a small structural change. By combining the high reliability error correcting capability of SCCC together with a rate compatible puncturing method, we can achieve adaptive packet-data transmission as well as high reliability due to the interleaving gain and

low error-floor. In this chapter, we propose a scheme denoted as rate compatible punctured SCCC (RCPS) and investigate the error performance on an AWGN and multipath fading channel for W-CDMA system. Since the RCPS codes have different encoder structure from the RCPP codes, we need to devise different puncturing methods from that of the RCPP codes [62]. Comparative results with the RCPP and RCPP-HARQ are also given. In addition, we propose a concatenated RS-RCPS coding scheme for additional error correction. Furthermore, by employing an RCPS-HARQ technique based on incremental redundancy retransmission, we can also obtain similar throughput performance as RCPP-HARQ[1].

### 7.2.1 RCPS Codes and Puncturing Methods

A serial concatenated codes have a probability of error that decreases exponentially as the frame size increases while the decoding complexity increases linearly [37]. In our work, rate-1/3 SCCC and PCCC with similar complexity are considered. The schematic structure of the SCCC encoder is shown in Fig. 55 (a). The SCCC encoder consists of outer and inner convolutional encoders (including a puncturer, if applicable) with a bitwise concatenation interleaver between them. The source data sequence $u_O$ is first encoded by the outer rate-2/3 encoder. Since the puncturing of the systematic bits causes BER performance degradation for RSC encoders, rate-2/3 is obtained by puncturing the parity bits. Then the output data $c_O$ is interleaved. Finally, the interleaved data $u_I$ is encoded by the inner encoder with rate-1/2. The output of the inner encoder $c_I$ is transmitted through the channel. The detailed encoder structure of SCCC with constraint length $K$=3 (4-state) is shown in Fig. 55 (b). Note that inner encoder must be recursive to achieve the interleaver gain [13]. Although outer encoder can be non-recursive, an RSC encoder is used here for both inner and outer encoders.

At the receiver, the additive SISO decoding algorithm that is extended from LOG-MAP algorithm in [3] is used for iterative decoding of SCCC. PCCC can be decoded by using SCCC's additive SISO modules with minor modifications.

RCPS can be designed in a way similar to RCPP by modifying puncturing scheme,

[1]RCPP is the same as RCPT codes in the thesis.

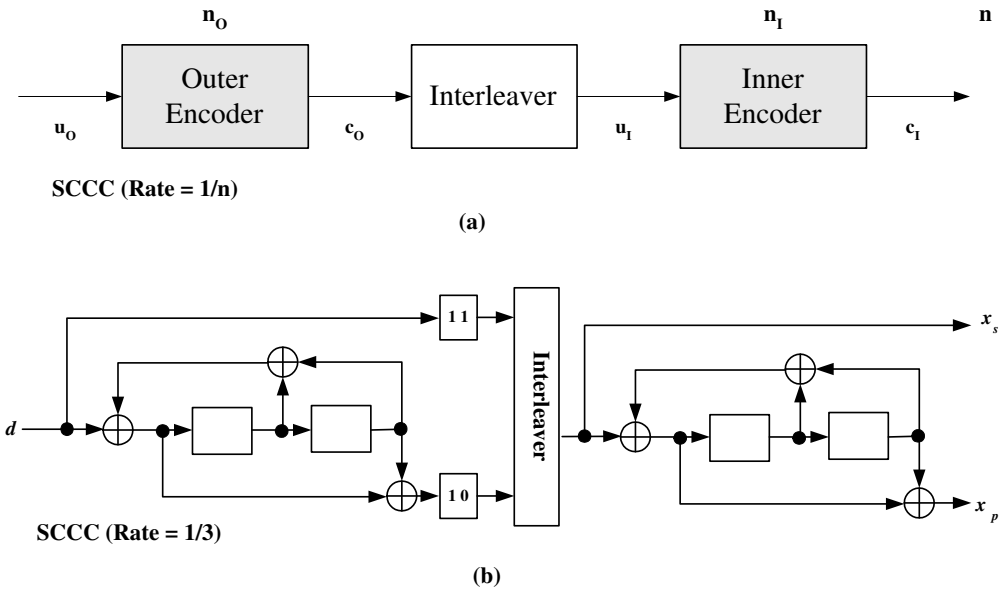


**Figure 55:** Encoder structures of SCCC. (a) General structure. (b) SCCC with rate-1/3, 4-state.

encoder and decoder. The inner encoder of RCPS output consists of the systematic component $x_s$ and the parity component $x_p$. The systematic and parity bits of the RCPS inner encoder are then punctured according to a specified puncturing pattern. The punctured data consists of the punctured systematic component $y_s$ and the punctured parity component $y_p$. The puncturing rules can be classified into two classes; systematic puncturing which punctures only the parity bits, and non-systematic puncturing which punctures both the systematic and parity bits. Because all decoding modules share the systematic bits, puncturing the systematic bits of SCCC degrades FER performance more than the case of puncturing the parity bits. Therefore, only systematic puncturing will be considered for RCPS and RCPP because it performs better than non-systematic puncturing [57].

The original unpunctured code rate of the RCPS is set to $1/n = 1/3$, where the inner and outer code rates are $1/n_O = 2/3$ and $1/n_I = 1/2$, respectively. The puncturing table consists of the systematic and parity sub-blocks each having $P$ bits, where the two sub-blocks specify the puncturing patterns for the systematic and parity components, and $P$ stands for the puncturing period. For each puncturing index $k_s$, we define an $n_I \times P$ binary

puncturing table, $PT_{k_s}$, where puncturing index $k_s = 0, 1, ..., (n_I - 1)P$ that can be set according to channel conditions. For systematic puncturing $PT_0$ must contain $P$ ones in the first row. $PT_{k_s+1}$ must have ones in the same positions as $PT_{k_s}$ plus an additional one and, finally, $PT_{(n_I-1)P}$ becomes a puncturing table of all ones. The overall rate of the RCPS code is $R_{k_s} = n_O \cdot \frac{P}{P+k_s}$. For example, let us form a family of RCPS with $n_I = 2$, $P = 4$ and $k_s = 0, 1, 2, 3, 4$. In this case, we choose any code rate, $R_{k_s}$, among rates 2/3, 8/15, 4/9, 8/21, and 1/3, as shown in Fig. 56. Note that the highest code rate of the RCPS is 2/3 unlike 1 of the RCPP due to the different encoder structure.

| | | | | | | | | | | | | | | | | | | | |
|---|---|---|---|---|---|---|---|---|---|---|---|---|---|---|---|---|---|---|---|
| Systematic | **1** | **1** | **1** | **1** | 1 | 1 | 1 | 1 | 1 | 1 | 1 | 1 | 1 | 1 | 1 | 1 | 1 | 1 | 1 | 1 |
| Parity | 0 | 0 | 0 | 0 | **1** | 0 | 0 | 0 | 1 | 0 | **1** | 0 | 1 | **1** | 1 | 0 | 1 | 1 | 1 | **1** |
| | $T_0$ | | | | $T_1$ | | | | $T_2$ | | | | $T_3$ | | | | $T_4$ | | | |
| Index | $k_s$=0 | | | | $k_s$=1 | | | | $k_s$=2 | | | | $k_s$=3 | | | | $k_s$=4 | | | |
| Code Rate | $R_0$=2/3 | | | | $R_1$=8/15 | | | | $R_2$=4/9 | | | | $R_3$=8/21 | | | | $R_4$=1/3 | | | |

**Figure 56:** Puncturing table for the RCPS codes using the systematic puncturing.

### 7.2.2 RCPS-HARQ Protocol

If the decoded frame has detectable errors after a prescribed maximum number of decoding iterations, the receiver sends a NAK message to transmitter through a feedback channel to request a retransmission. If the number of retransmissions exceeds the maximum number of retransmissions allowed, a decoding failure is declared. In case of retransmissions, a packet combining scheme that combines the received frames can be employed.

Type-II RCPS-HARQ scheme can achieve high reliability and throughput performance. The RCPS-HARQ falls into the category of incremental redundancy codes, in that more bits are incrementally transmitted to adaptively meet the error performance requirements. Therefore, the transmitter only need to transmit supplemental code bits to get to the next lowest rate code.

**RCPS-HARQ ($PT_S$)**

| Transmission Trial | 1st | 2nd | 3rd |
|---|---|---|---|
| systematic | 1 1 1 1 | 1 1 1 1 | 1 1 1 1 |
| parity | 0 0 0 0 | 1 0 1 0 | 1 1 1 1 |
| code rate | $R_1$=2/3 | $R_2$=4/9 | $R_3$=1/3 |
| | $t_1$=4 | $t_2$=2 | $t_3$=2 |

**RCPP-HARQ ($PT_P$)**

| Transmission Trial | 1st | 2nd | 3rd |
|---|---|---|---|
| systematic | 1 1 1 1 | 1 1 1 1 | 1 1 1 1 |
| parity 1 | 1 0 0 0 | 1 1 1 0 | 1 1 1 1 |
| parity 2 | 0 0 0 1 | 1 0 0 1 | 1 1 1 0 |
| code rate | $R_1$=2/3 | $R_2$=4/9 | $R_3$=1/3 |
| | $t_1$=6 | $t_2$=3 | $t_3$=3 |

**Figure 57:** Puncturing tables for the RCPS-HARQ ($PT_s$) and RCPP-HARQ ($PT_p$).

### 7.2.3 Numerical Results and Discussions

A frame size of 640 bits, BPSK modulation, S-random interleaver with $S$=21, and maximum 4 iterations are used for simulation on an AWGN channel. For purpose of comparison, the complexity of the 8-state PCCC [61] is known to be nearly close to the 4-state SCCC. The code generator polynomials for RCPS and RCPP are $g_S = (1, 5/7)$ and $g_P = (1, 13/15)$ in octal, respectively. A 16 parity-bit CRC code is used for error detection of each frame and for stopping iterations of the turbo decoder. The CRC encoded information data is fed into RCPS encoder. when an RS code is used, the CRC encoded data is encoded again by the inner shortened RS $(80, 64)$ code over GF(256) with code rate-0.8 for correcting the burst-errors. Then the encoded data is BPSK modulated to be transmitted.

The FER performance of the RCPS and RCPP codes with same code rate-1/3 (i.e., no puncturing) on an AWGN channel is compared in Fig. 58. The RCPS outperforms the RCPP below FER=$10^{-3}$ due to PCCC's error-floor effect on that region. On the contrary,

for the concatenation with RS code, the FER of the RCPP is slightly better than that of RCPS. It is desirable that RS-RCPP show little error-floor effect unlike RCPP. However, both RS-RCPS and RS-RCPP are still better than RCPS due to the burst-error correcting capability of the RS code.

For the rate-2/3 and 4/9 puncturing cases, the FER performance of RCPS and RCPP are compared in Fig. 59. In case of rate-1/3 and 4/9, RCPS outperforms RCPP by 0.3 to 0.6 dB at FER=$10^{-4}$, respectively. However, in case of rate-2/3, the RCPP is much better than the RCPS because the RCPS has no parity bit to be transmitted. It is desirable that at least some non-systematic parity bits be transmitted so that iterative decoding is possible.

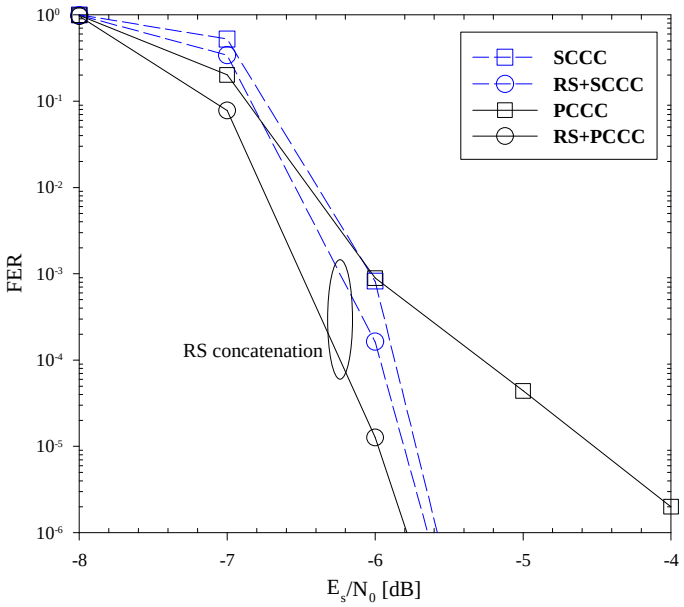


**Figure 58:** FER performance of the SCCC, PCCC, RS-SCCC, and RS-PCCC. AWGN channel and rate-1/3.

The proposed RCPS is applied to W-CDMA system that is described in the RCPT code case, where the RCPP encoder/decoder is substituted with RCPS encoder/decoder. Same simulation parameters as in the previous chapter are used except for the channel model. Because most high-data-rate wireless application is designed for indoor nomadic users, the multipath fading channel that is specified by the ITU's IMT-2000 Indoor channel A model

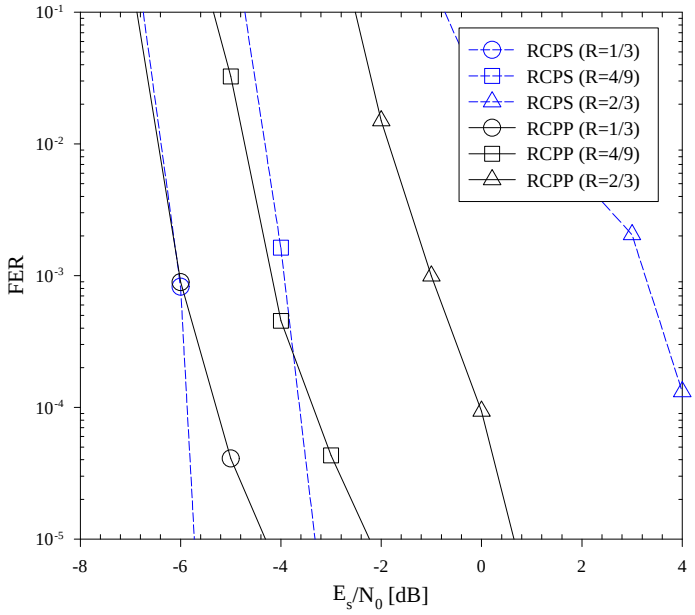


**Figure 59:** FER performance of the RCPS and RCPP codes for different code rates. AWGN channel, and rate-1/3, 4/9, and 2/3.

at carrier frequency of 2 GHz and mobile velocity of 0 km/h is used.

Fig. 60 compares the FER performance of the W-CDMA systems with the RCPS and RCPP code for different code rates in multipath fading channel. Let us define *crosspoint* as the point where RCPS begin to outperform RCPP for given same code rate. As the code rate increases from rate-1/3 to 4/9, the crosspoint occurs in lower FER region (i.e., from $5 \times 10^{-3}$ to $10^{-4}$).

Fig. 61 compares the FER performance of the RCPS-HARQ and the RCPP-HARQ systems for the $PT_s$ and $PT_p$ puncturing tables that are shown in Fig. 57 on an AWGN channel (i.e., the maximum numbers of transmission is three). The RCPS-HARQ outperforms the RCPP-HARQ by 0.3 dB at FER= $10^{-4}$ in terms of FER performance. Therefore, RCPS-HARQ is more suitable for packet transmission than RCPP-HARQ, if low FER is required. In terms of throughput performance, the RCPS-HARQ is slightly lower than the RCPP-HARQ, as shown in Fig. 62.

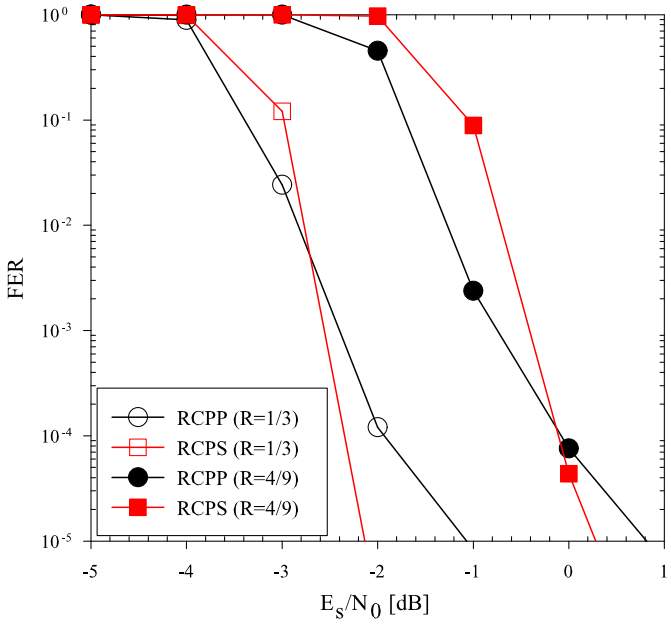


**Figure 60:** FER performances of the W-CDMA systems with the RCPS and RCPP codes for different code rates. IMT-2000 Indoor channel A model is used.

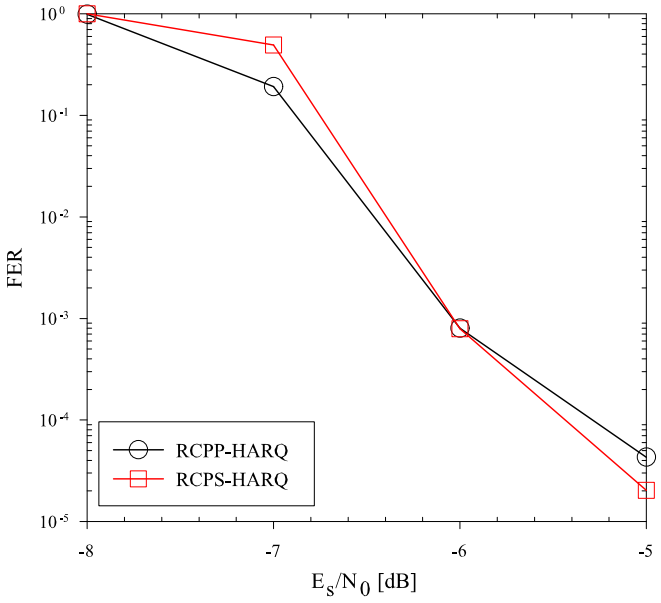


**Figure 61:** FER performance of the RCPS-HARQ ($PT_s$) and RCPP-HARQ ($PT_p$) systems on an AWGN channel.

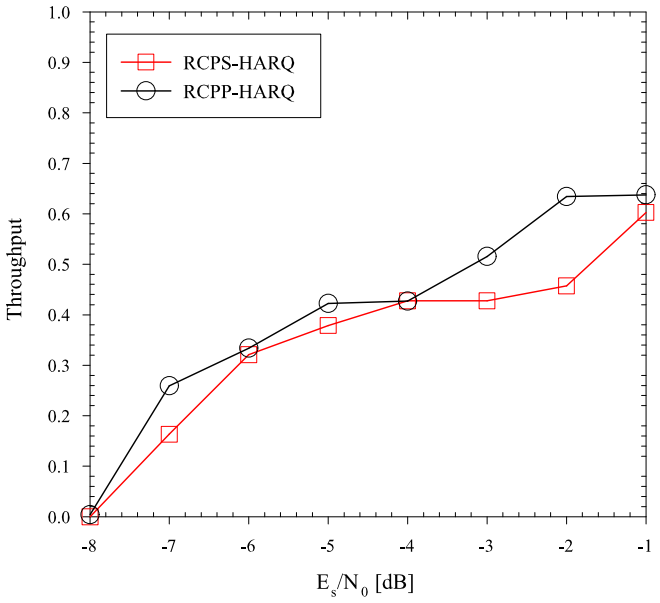


**Figure 62:** Throughput performance of the RCPS-HARQ ($PT_s$) and RCPP-HARQ ($PT_p$) systems on an AWGN channel.

### 7.2.4 Conclusions

We have proposed the RCPS codes using an SCCC, an another important class of turbo-like codes that is widely used, to accommodate different code rates and very low FER requirements for high-speed packet-data transmission. We have also proposed the puncturing methods that are well matched to the RCPS codes and shown that the RCPS codes provide lower FER than that of the RCPP codes in the region of moderate-to-high SNR. We have investigated the performance of the RCPS and RS-RCPS codes on an AWGN and multipath fading channels. Comparative results with the RCPP codes have also been presented. In addition, we have proposed a Type-II RCPS-HARQ scheme using incremental redundancy retransmission to achieve a lower FER than that of RCPP-HARQ at the slight cost of throughput.

# CHAPTER VIII

# CONCLUDING REMARKS

## *8.1 Summary of Contributions*

In this thesis, we have presented advanced error control schemes using turbo-like codes, turbo-like coded modulations, turbo hybrid-ARQ schemes, and rate compatible puncturing techniques for commercial and tactical spread-spectrum communications, especially for CDMA cellular systems and DS and FH anti-jam systems. ML bounding techniques and convergence analysis have also been utilized because they offer good benchmarks for the error performance comparison and evaluation of the suboptimal iterative receivers and help us to construct effective turbo-like coding schemes.

The main contributions and results of the thesis are as follows.

In Chapter III, we have proposed a power and bandwidth efficient DS concatenated coded CPM system. Block-wise interleaving has been shown to outperform chip-wise interleaving. A mixed concatenated coded CPM system with a proper mixture ratio has been shown to improve the anti-jamming performance. Finally, the error-floor phenomenon for MCC in the case of a large mixture ratio has been explained by the poor decoding convergence through the convergence analysis.

In Chapter IV, we have presented the coherent and non-coherent anti-jam serially concatenated slow FH-CPM systems. Through simulation and ML bound analysis, we have showed the anti-jamming performance in the presence of the PBNJ. Consequently, we have drawn some important design considerations with regard to the outer convolutional codes and the inner CPMs as well as FH parameters. We have also shown that better anti-jamming capability is achieved as the decoding iteration increases. And, the MSDD-based non-coherent iterative receiver exploiting channel memory performs close to the coherent one with increase in the observation interval. In addition, it has been shown that an outer code with larger state does not necessary provide better anti-jamming performance at low

$E_b/N_J$ as opposed to the bound analysis at high $E_b/N_J$. Furthermore, we have presented a novel iterative jamming estimation technique combined with the anti-jam iterative receiver for the serially concatenated slow FH-CPM system. We have compared the anti-jamming performance in the presence of partial and no jamming information.

In Chapter V, we have proposed serially concatenated multi-$h$ CPM with iterative demodulation and decoding. We have shown that a channel code with larger minimum distance, or a multi-$h$ CPM modulator with a larger number of phase states do not necessary provide better BER performance. Candidate choices for the modulation index set can evaluated by using convergence characteristics and the multi-$h$ modulator should be matched to the channel code. We have also evaluated performance in the error-floor region through union-Chernoff bounding techniques.

In Chapter VI, we have proposed a Type-I turbo hybrid-ARQ scheme using a concatenated RS-turbo code and a packet combining technique for W-CDMA system to improve the error and decoding latency performances. For coherent W-CDMA system, we have considered the fast power control and Rake receiver with a multipath fading channel estimation technique.

Finally, in Chapter VII, we have proposed rate compatible punctured turbo-like codes using PCCC and SCCC to offer versatile coded systems. Puncturing methods and strategy have been classified and compared in terms of the error and throughput performances. In addition, we have proposed Type-II RCPT-HARQ and RCPS-HARQ schemes using incremental redundancy retransmission for improving reliability and throughput.

## *8.2 Suggestions for Future Research*

We propose the following suggestions for future research.

- *Turbo-like coded space-time modulation for spread-spectrum*

  To achieve higher data rates, the multiple-input multiple-output (MIMO) wireless communication systems can theoretically increase capacity by up to a factor equaling the number of transmit and receive antennas. In addition, powerful turbo-like coding and low-complexity iterative detection can dramatically improve the spread-spectrum

systems subject to hostile jamming/interference and, thus, improve the LPI/LPD performance. Therefore, spread-spectrum systems based on low-complexity turbo-like coded space-time modulation schemes that properly exploit the turbo principle for concatenated codes and recursive differential space-time modulation (DSTM) is a promising topic for research.

- *Anti-jam spread-spectrum systems with graphical codes*

  Recently, graphical codes such as LDPC and tree codes showed comparable error performance to turbo codes. However, anti-jam spread-spectrum systems using these codes are yet to be studied in details. In addition, it will be useful to use the analysis frameworks of graphical codes to analyze the performance.

- *Turbo hybrid-ARQ schemes for MIMO systems and adaptive modulation and coding*

  Turbo hybrid-ARQ schemes that are extended to MIMO environments will be interesting. Further, hybrid-ARQ schemes with an adaptive modulation or adaptive power control technique have a potential to improve the overall system performance.

# APPENDIX A

# UNION BOUNDS ON THE PERFORMANCE OF ML DECODING FOR SCCC

Although the bound on the performance of ML decoding of turbo-like codes, which use a suboptimal decoder, becomes prohibitively complex for very long codes and diverges in low SNR region, the ML bound is still an invaluable practical tool for the design and analysis and sets a benchmark for the comparison of the practical suboptimal decoding methods. The most commonly used upper bound on the error probability of a digital communication system is union bound. For the calculation of the union bound for a binary block code, one only needs to have the input-output weight enumerating function (or distance spectrum) of the code.

In this appedix, we present the union bound on performance for the serially concatenated convolutional code (SCCC) with coherent detection on an AWGN channel. The SCCCs include RA codes, serially concatenated DPSK, and serially concatenated CPM. We use the transfer function bounding approach in [13] to obtain the ensemble input-output weight enumerating function (IOWEF). The performance of the SCCC can be approximated by that of the equivalent block code whose IOWEF labels the branch of the hyper-trellis joining the zero states of outer- and inner-code trellises[1].

Consider an SCCC $C_s$ with the overall rate $R = m/p$ consists of the outer convolutional code $C_o$ with rate $R^o = m/n$, and the inner convolutional code $C_i$ with rate $R^i = n/p$, joined by an interleaver of length $N$. The weight enumerating function (WEF) of the code is defined as [126]

$$A(H) \triangleq \sum_{d=0}^{p} A_d H^d, \tag{71}$$

where $A_d$ represents the number of codewords with Hamming weight $d$ and $H$ is a dummy

[1]Terminated convolutional codes are used.

variable and is referred to as the WEF coefficient. Note that the WEF provides the weight distribution which only depends on the codewords. The more detailed IOWEF is defined as [126]

$$A(W,H) \triangleq \sum_{w=0}^{m}\sum_{d=0}^{p} A_{w,d}W^w H^d \tag{72}$$

$$= \sum_{w=0}^{m} W^w A(w,H) \tag{73}$$

$$= \sum_{d=0}^{p} H^d A(W,d), \tag{74}$$

where $A_{w,d}$ represents the number of codewords with weight $d$ associated with an information words of weight $w$ and is referred to as the IOWEF coefficient or the input-output weight spectrum, and the conditional input weight enumerating function (CIWEF) is $A(W,d) \triangleq \sum_{w=0}^{m} A_{w,d}W^w$. And, the conditional output weight enumerating function (COWEF) is $A(w,H) \triangleq \sum_{d=0}^{p} A_{w,d}H^d$ and enumerates the weight distribution of codewords generated by information words of a given weight $w$. The relationship between $A(w,H)$ and $A(W,H)$ is

$$A(w,H) = \frac{1}{w!}\frac{\partial^w A(W,H)}{\partial W^w}\bigg|_{W=0}. \tag{75}$$

The pairwise error probability, denoted by $P_{pw}(d)$, between a codeword of weight $d$ and the all-zero codeword on an AWGN channel is given by

$$P_{pw}(d) = Q\left(\sqrt{d\frac{2RE_b}{N_0}}\right) = \frac{1}{2}\mathrm{erfc}\left(\sqrt{d\frac{RE_b}{N_0}}\right) < e^{-d\frac{RE_b}{N_0}}, \tag{76}$$

where $Q(x) \triangleq \frac{1}{\sqrt{2\pi}}\int_x^\infty e^{-\lambda^2/2}d\lambda = \frac{1}{2}\mathrm{erfc}(x/\sqrt{2})$.

Therefore, we can obtain a closed-form upper bound on BEP under ML soft-decision decoder by assuming all-zero transmitting sequence as below

$$P_b \triangleq \sum_{w=1}^{m} P_b(w) \le \sum_{d=d_m}^{N/R^i}\sum_{w=w_m^o}^{NR^o} \frac{w}{NR^o}A_{w,d}P_{pw}(d), \tag{77}$$

where $w_m^o$ is the minimum weight of an input sequence generating an error event of the outer code, $d_m$ of a length-$N$ compound error event is the minimum weight of the codewords for the SCCC, $A_{w,d}$ represents the ensemble IOWEF for the SCCC. Note that

$B_d \triangleq \sum_{w=w_m^o}^{NR^o} \frac{w}{NR^o} A_{w,d}$ represents the bit error multiplicity for error events[2] and is dependent on $d$. The Chernoff bounds for BEP and WEP are given by

$$P_b \leq \sum_{d=d_m}^{N/R^i} \sum_{w=w_m^o}^{NR^o} \frac{w}{NR^o} A_{w,d} H^d = \frac{1}{NR^o} \frac{\partial A(W,H)}{\partial W}\Big|_{W=1}, \tag{78}$$

and

$$P_w \leq \sum_{d=d_m}^{N/R^i} \left( \sum_{w=w_m^o}^{NR^o} A_{w,d} \right) H^d = A(W,H)|_{W=1}, \tag{79}$$

respectively. Also, (77) can be rewritten using (74) and (76) as

$$P_b < \sum_{w=w_m^o}^{NR^o} \frac{w}{NR^o} A(w,H)|_{H=e^{-RE_b/N_0}}. \tag{80}$$

In addition, the ensemble IOWEF $A_{w,d}$ can be obtained by calculating $A^o_{w,l}$ and $A^i_{l,d}$ and assuming the *uniform interleaver* of length $N$ as

$$A_{w,d} = \sum_{l=0}^{N} \frac{A^o_{w,l} \cdot A^i_{l,d}}{\binom{N}{l}}. \tag{81}$$

The probabilistic uniform interleaving is devised in [13] to map a given input sequence of length $N$ and weight $l$ into its all distinct $\binom{N}{l}$ permutations with equal probability of $1/\binom{N}{l} = l!(N-l)!/N!$. The premise is that there is at least one interleaver, which performs better than the average. The weight enumerating function of sequences of the convolutional code that concatenate $j$ error events with total input information weight $l$ is given by $A(l,H,j) = \sum_d A_{l,d,j} H^d$, where $A_{l,d,j}$ represents the number of sequences of weight $d$, input weight $l$, and number of concatenated error events $j$. The coefficient $A_{l,d}$ can be upper-bounded as $A_{l,d} \leq \sum_{j=1}^{n_M} \binom{N/n}{j} A_{l,d,j}$, where $n_M$ is the largest number of error events concatenated in a codeword of weight $d$ and generated by a weight $l$ information sequence. With $j = n^o$ and $j = n^i$ for the outer and inner code, respectively, we can rewrite $A_{w,d}$[3] as

$$A_{w,d} \leq \sum_{l=d_f^o}^{N} \sum_{n^o=1}^{n_M^o} \sum_{n^i=1}^{n_M^i} \frac{\binom{N/n}{n^o}\binom{N/n}{n^i}}{\binom{N}{l}} A^o_{w,l,n^o} A^i_{l,d,n^i}, \tag{82}$$

where $d_f^o$ is the free distance of the outer code[4].

[2] It is sometimes called the bit-normalized weight enumerating function (BNWEF).

[3] Clearly, $A_{0,0} = 1$ by linearity.

[4] $d_f^o$ is set as the lower limit because there can be no less than $d_f^o$ ones in the $N$-symbol outer code sequence.

Since the error-floor is mostly affected by a few codewords of low-weight, a *truncated* bound considering only the low-weight codewords can be used for an approximation [133], [38], [119].

Note that we can further bound the binomial functions using

$$\frac{N^n}{n^n n!} < \frac{(N-n+1)^n}{n!} < \binom{N}{n} < \frac{N^n}{n!}. \tag{83}$$

Finally, substitution of these bounds in (82) yields the bound in the form all-zero transmitting sequence as below

$$P_b \leq \sum_{d=d_m}^{N/R^i} P_{pw}(d) \sum_{w=w_m^o}^{NR^o} \sum_{l=d_f^o}^{N} \sum_{n^o=1}^{n_M^o} \sum_{n^i=1}^{n_M^i} N^{\beta_M - 1} \frac{l^l l!}{n^{n^o+n^i-1} n^o! n^i!} \frac{w}{NR^o} A^o_{w,l,n^o} A^i_{l,d,n^i}, \tag{84}$$

where $\beta_M = n^o + n^i - l$.

For very high values of SNR, $P_w$ and $P_b$ are given by

$$P_b \leq \frac{1}{2} \frac{w_{free}}{k} \mathrm{erfc}\left(\sqrt{d_{free} R \frac{E_b}{N_0}}\right), \tag{85}$$

and

$$P_w \leq \frac{1}{2} N_{free} \mathrm{erfc}\left(\sqrt{d_{free} R \frac{E_b}{N_0}}\right), \tag{86}$$

where $d_{free}$, $N_{free}$, and $w_{free}$ denote the free distance of the code, its multiplicity, and its information bit multiplicity, respectively. Note that $N_{free} = A_d^{free}$ and $w_{free} = B_d^{free}$.

# APPENDIX B

# TRANSFER CHARACTERISTICS FOR THE JAMMING CHANNEL

In this appendix, we derive the extrinsic information transfer characteristics for the pulse jamming channel. The channel LLR-values assuming known JSI $\mathbf{z}$ at the receiver are calculated as

$$\begin{aligned} L &= \log\left[\frac{P(y|x=+1,z)}{P(y|x=-1,z)}\right] \\ &= \frac{\exp\left\{-\frac{(y-1)^2}{2\sigma_z^2}\right\}/\sqrt{2\pi\sigma_z^2}}{\exp\left\{-\frac{(y+1)^2}{2\sigma_z^2}\right\}/\sqrt{2\pi\sigma_z^2}} \\ &= 2y/\sigma_z^2, \end{aligned} \tag{87}$$

where $\mathbf{y} = \mathbf{x} + \mathbf{n}_J$ with the transmitted binary symbols $x \in \{\pm 1\}$ and $\mathbf{n}_J$ is the AWGN and jamming noise vector. Thus, (87) can be rewritten as

$$L = \frac{2}{\sigma_z^2} \cdot (x + n_J), \tag{88}$$

where variable $n_J$ is Gaussian distributed with mean zero and variance $\sigma_z^2 = N_0/2 + z \cdot N_J/2\rho$. Furthermore, (88) can be represented as $L = \nu_L \cdot x + n_L$, where mean $\nu_L = 2/\sigma_z^2$ and variance $\sigma_L^2 = 4/\sigma_z^2$. Hence, the conditional PDF for the LLR-value $L$ is calculated as

$$p(\lambda|X=x) = \frac{1}{\sqrt{2\pi\sigma_L^2}} \exp\left\{-\frac{(\lambda - \nu_L \cdot x)^2}{2\sigma_L^2}\right\}. \tag{89}$$

# REFERENCES


[1] 3GPP, "High speed downlink packet access (HSDPA)," TR 25.855, 3rd Generation Partnership Project, Jun. 2001.

[2] Adachi, F., Sawahashi, M., and Suda, H., "Wideband DS-CDMA for next-generation mobile communications systems," *IEEE Commun. Mag.*, vol. 36, pp. 56–69, Sept. 1998.

[3] Ambroze, A., Wade, G., and Tomlinson, M., "Iterative MAP decoding for serial concatenated convolutional codes," *IEE Proc. Commun.*, vol. 145, pp. 53–59, Apr. 1998.

[4] Anderson, J. B., Aulin, T., and Sundberg, C.-E., *Digital Phase Modulation*. New York: Plenum Press, 1986.

[5] Anderson, J. B. and Taylor, D. P., "A bandwidth-efficient class of signal-space codese," *IEEE Trans. Inform. Theory*, vol. 24, pp. 703–712, Nov. 1978.

[6] Andoh, H., Sawahashi, M., and Adachi, F., "Channel estimation filter using time-multiplexed pilot channel for coherent Rake combining in DS-CDMA mobile radio," *IEICE Trans. Commun.*, vol. E81-B, pp. 1517–1526, Jul. 1998.

[7] Asano, D. K., Hayashi, T., and Kohno, R., "Modulation and processing gain tradeoffs in DS-CDMA spread spectrum systems," in *Proc. IEEE ISSSTA '98*, (Sun City, South Africa), pp. 9–13, Sept. 1998.

[8] Aulin, T. and Sundberg, C.-E., "On the minimum Euclidean distance for a class of signal space codes," *IEEE Trans. Inform. Theory*, vol. 28, pp. 43–55, Jan. 1982.

[9] Bahl, L. R., Cocke, J., Jelinek, F., and Raviv, J., "Optimal decoding of linear codes for minimizing symbol error rate," *IEEE Trans. Inform. Theory*, vol. 20, pp. 284–287, Mar. 1974.

[10] Barbulescu, A. S. and Pietrobon, S. S., "Rate compatible turbo-codes," *IEE Electron. Letters*, vol. 31, pp. 535–536, Mar. 1995.

[11] Bender, P., Black, P., Grob, M., Padovani, R., Sindhushyana, N., and Viterbi, S., "CDMA/HDR: A bandwidth efficient high speed wireless data service for nomadic users," *IEEE Commun. Mag.*, vol. 38, pp. 70–77, Jul. 2000.

[12] Benedetto, S., Divsalar, D., Montorsi, G., and Pollara, F., "Algorithm for continuous decoding of turbo codes," *IEE Electron. Letters*, vol. 32, pp. 314–315, Feb. 1996.

[13] Benedetto, S., Divsalar, D., Montorsi, G., and Pollara, F., "Serial concatenation of interleaved codes: Performance analysis, design, and iterative decoding," *IEEE Trans. Inform. Theory*, vol. 44, pp. 909–926, May 1998.

[14] Benedetto, S. and Montorsi, G., "Design of parallel concatenated convolutional codes," *IEEE Trans. Commun.*, vol. 44, pp. 591–600, May 1996.

[15] Benedetto, S. and Montorsi, G., "Unveiling turbo codes: Some results on parallel concatenated coding schemes," *IEEE Trans. Info. Theory*, vol. 42, pp. 409–428, Mar. 1996.

[16] Berlekamp, E. R., "The technology of error correction codes," *Proc. IEEE*, vol. 68, pp. 564–593, May 1980.

[17] Berrou, C. and Glavieux, A., "Near optimum error correcting coding and decoding: turbo-codes," *IEEE Trans. Commun.*, vol. 44, pp. 1261–1271, Oct. 1996.

[18] Berrou, C., Glavieux, A., and Thitimajshima, P., "Near shannon limit error-correcting coding and decoding: Turbo codes," in *Proc. IEEE ICC '93*, (Geneva, Switzerland), pp. 1064–1070, May 1993.

[19] Brendler, J. A., "Tactical military communications," *IEEE Commun. Mag.*, vol. 30, pp. 67–72, Jan. 1992.

[20] Cain, J. B., Clark, G. C., and Geist, J. M., "Punctured convolutional codes of rate $(n-1)/n$ and simplified maximum likelihood decoding," *IEEE Trans. Inform. Theory*, vol. 25, pp. 97–100, Jan. 1979.

[21] Callendar, M. H. and et al., "Special issue on IMT-2000: Standards efforts of the ITU," *IEEE Personal Commun.*, vol. 4, Aug. 1997.

[22] Chase, D., "Code combining - a maximum-likelihood decoding approach for combining an arbitrary number of noisy packets," *IEEE Trans. Commun.*, vol. 33, pp. 385–393, May 1985.

[23] Cover, T. M. and Thomas, J. A., *Elements of Information Theory*. New York: John Wiley & Sons, 1991.

[24] Dai, H. and Poor, V., "Turbo multiuser detection for coded DMT VDSL systems," *IEEE J. Select. Areas Commun.*, vol. 20, pp. 351–362, Feb. 2002.

[25] Divsalar, D., "A simple tight bound on error probability of block codes with application to turbo codes," *JPL TMO Progress Report*, pp. 1–35, Nov. 1999.

[26] Divsalar, D., Dolinar, S., and Pollara, F., "Improving turbo-like codes using iterative decoder analysis," in *Proc. IEEE ISIT '01*, (Washington, DC), p. 100, Jun. 2001.

[27] Divsalar, D., Dolinar, S., and Pollara, F., "Iterative turbo decoder analysis based on density evolution," *IEEE J. Select. Areas Commun.*, vol. 19, pp. 891–907, May 2001.

[28] Divsalar, D., Jin, H., and McEliece, R. J., "Coding theorems for turbo-like codes," in *Proc. 36th Annual Allerton Conf. on Commun., Control, and Comp.*, (Urbana, IL), pp. 201–210, Sept. 1998.

[29] Divsalar, D. and Pollara, F., "Turbo codes for PCS applications," in *Proc. IEEE ICC '95*, (Seattle, WA), pp. 54–59, Jun. 1995.

[30] Divsalar, D. and Pollara, S., "Low-rate turbo codes for deep-space communications," in *Proc. IEEE ISIT '95*, (Whistler, Canada), p. 35, Sept. 1995.

[31] Dolinar, S. and Divsalar, D., "Weight distributions for turbo codes using random and nonrandom permutations," *JPL TDA Progress Report*, pp. 56–65, Aug. 1995.

[32] Drukarev, A. and Costello, Jr., D., "A comparison of block and convolutional codes in ARQ error control schemes," *IEEE Trans. Commun.*, vol. 30, pp. 2449–2455, Nov. 1982.

[33] Duman, T. M., *Turbo codes and turbo coded modulation systems: Analysis and performance bounds*. PhD thesis, Northeastern University, Boston, MA, May 1998.

[34] Duman, T. M. and Salehi, M., "New performance bounds for turbo codes," *IEEE Trans. Commun.*, vol. 46, pp. 717–723, Jun. 1998.

[35] ETSI, *UMTS SMG2 L1 Documents*. 1998-1999.

[36] Fonseka, J. P. and Davis, G. R., "Combined coded/multi-h CPFSK signaling," *IEEE Trans. Commun.*, vol. 38, pp. 1708–1715, Oct. 1990.

[37] Forney, G. D., *Concatenated Codes*. Boston, MA: MIT Press, 1966.

[38] Fossorier, M. P. C., Lin, S., and Costello, Jr., D. J., "On the weight distribution of terminated convolutional codes," *IEEE Trans. Inform. Theory*, vol. 45, pp. 1646–1648, Jul. 1999.

[39] Frank, C. D. and Pursley, M. B., "Concatenated coding for frequency-hop spread-spectrum with partial-band interference," *IEEE Trans. Commun.*, vol. 44, pp. 377–387, Mar. 1996.

[40] Gagnon, F. and Haccoun, D., "Bounds on the error performance of coding for nonindependent rician-fading channels," *IEEE Trans. Commun.*, vol. 40, pp. 351–360, Feb. 1992.

[41] Gallager, R. G., *Low-Density Parity-Check Codes*. Boston, MA: MIT Press, 1963.

[42] Gallager, R. G., "A simple derivation of the coding theorem and some applications," *IEEE Trans. Inform. Theory*, vol. 11, pp. 3–18, Jan. 1965.

[43] Gamal, H. E. and A. R. Hammons, J., "Analyzing the turbo decoder using the Gaussian approximation," *IEEE Trans. Inform. Theory*, vol. 47, pp. 671–686, Feb. 2001.

[44] Gamal, H. E. and Geraniotis, E., "Iterative channel estimation and decoding for convolutionally coded anti-jam FH signals," *IEEE Trans. Commun.*, vol. 50, pp. 321–331, Feb. 2002.

[45] Gertsman, M. J. and Lodge, J. H., "Symbol-by-symbol MAP demodulation of CPM and PSK signals on rayleigh flat-fading channels," *IEEE Trans. Commun.*, vol. 45, pp. 788–799, Jul. 1997.

[46] Glisic, S., Nikolic, Z., Milosevic, N., and Pouttu, A., "Advanced frequency hopping modulation for spread spectrum WLAN," *IEEE J. Select. Areas Commun.*, vol. 18, pp. 16–29, Jan. 2000.

[47] Graser, S. J., "Techniques for improving power and bandwidth efficiency of UHF MILSATCOM waveforms," in *Proc. IEEE MILCOM '01*, (Washington, DC), pp. 653–657, Oct. 2001.

[48] Hagenauer, J., "Rate-compatible punctured convolutional codes (RCPC codes) and their applications," *IEEE Trans. Commun.*, vol. 36, pp. 389–400, Apr. 1988.

[49] Hagenauer, J., Offer, E., and Papke, L., "Iterative decoding of binary block and convolutional codes," *IEEE Trans. Info. Theory*, vol. 42, pp. 429–445, Mar. 1996.

[50] Hagenauer, J., Robertson, P., and Papke, L., "Iterative (turbo) decoding of systematic convolutional codes with the MAP and SOVA algorithm," in *Proc. ITG '94*, (Munich, Germany), pp. 21–29, Sept. 1994.

[51] Hall, E. K. and Wilson, S., "Design and performance analysis of turbo codes on Rayleigh fading channels," *IEEE J. Select. Areas Commun.*, vol. 16, pp. 160–174, Feb. 1998.

[52] Hamorsky, J., Wachsmann, U., Huber, J. G., and Cizmar, A., "Hybrid automatic repeat request scheme with turbo codes," in *Proc. 1st Int. Symp. on Turbo Codes and Related Topics*, (Brest, France), pp. 247–250, Sept. 1997.

[53] Ho, P. and Kim, J. H., "Pilot symbol-assisted detection of CPM schemes operating in fast fading channels," *IEEE Trans. Veh. Technol.*, vol. 44, pp. 337–347, Mar. 1996.

[54] IS-95, *Mobile Station-Base Station Compatibility Standard for Dual-Mode Wide-Band Spread Spectrum Cellular System.* TIA/EIA, Jul. 1993.

[55] Jin, H., *Analysis and design of turbo-like codes.* PhD thesis, California Institute of Technology, Pasadena, CA, May 2001.

[56] Jin, H. and McEliece, R. J., "Coding theorems for turbo code ensembles," *IEEE Trans. Inform. Theory*, vol. 48, pp. 1451–1461, Jun. 2002.

[57] Jung, P. and Plechinger, J., "Performance of rate compatible punctured turbo-codes for mobile radio applications," *IEE Electron. Letters*, vol. 33, pp. 2102–2103, Dec. 1997.

[58] Kallel, S., "Complementary punctured convolutional (CPC) codes and their applications," *IEEE Trans. Commun.*, vol. 43, pp. 2005–2009, Jun. 1995.

[59] Kang, J. H. and Stark, W. E., "Turbo codes for non-coherent FH-SS with partial band interference," *IEEE Trans. Commun.*, vol. 46, pp. 1451–1458, Nov. 1998.

[60] Kaplan, G. and Shamai (Shitz), S., "Achievable performance over the correlated Rician channel," *IEEE Trans. Commun.*, vol. 42, pp. 2967–2978, Nov. 1994.

[61] Kim, H. and Stüber, G. L., "Rate compatible punctured turbo coding for W-CDMA," in *Proc. IEEE Int. Conf. Personal Wireless Commun. (ICPWC) '00*, (Hyderabad, India), pp. 143–147, Dec. 2000.

[62] Kim, H. and Stüber, G. L., "Rate compatible punctured SCCC," in *Proc. IEEE Veh. Technol. Conf. (VTC) '01 Fall*, (Atlantic City, NJ), pp. 2399–2403, Sept. 2001.

[63] Kim, H. and Stüber, G. L., "An adaptive packet soft handoff scheme based on punctured turbo coding," in *Proc. IEEE Int. Symp. Wireless Personal Multimedia Commun. (WPMC) '02*, (Honolulu, HI), pp. 57–61, Oct. 2002.

[64] Kim, H. and Stüber, G. L., "Turbo-like coded multi-h continuous phase modulation," in *Proc. IEEE MILCOM '04*, (Monterey, CA), Oct. 2004.

[65] Kim, H., Stüber, G. L., and Narayanan, K. R., "Turbo-coded ARQ and its application to wideband CDMA system," in *Proc. IEEE Int. Conf. Telecommun. (ICT) '00*, (Acapulco, Mexico), pp. 852–856, May 2000.

[66] Kim, H., Tan, J., Stüber, G. L., and Narayanan, K. R., "Performance of direct-sequence concatenated coded CPM under pulse jamming," in *Proc. ARL CTA Commun. and Networks Symp. '03*, (College Park, MD), May 2003.

[67] Kim, H., Zhao, Q., Stüber, G. L., and Narayanan, K. R., "Anti-jamming performance of slow FH-CPM signals with concatenated coding and jamming estimation," in *Proc. IEEE MILCOM '03*, (Boston, MA), pp. 1120–1125, Oct. 2003.

[68] Kim, J. Y. and Poor, H. V., "Turbo-coded packet transmission for an optical CDMA network," *IEEE J. Lightwave Technol.*, vol. 18, pp. 1905–1916, Dec. 2000.

[69] Kschischang, F. R., Frey, B. J., and Loeliger, H.-A., "Factor graphs and the sum-product algorithm," *IEEE Trans. Inform. Theory*, vol. 47, pp. 498–519, Feb. 2001.

[70] Kuhn, V., "Evaluating the performance of turbo codes and turbo-coded modulation in a DS-CDMA environment," *IEEE J. Select. Areas Commun.*, vol. 17, pp. 2138–2147, Dec. 1999.

[71] Lam, Y. M. and Wittke, P. H., "Frequency-hopped spread-spectrum transmission with band-efficient modulations and simplified non-coherent sequence estimation," *IEEE Trans. Commun.*, vol. 38, pp. 2184–2196, Dec. 1990.

[72] Lane, W. D. and Bush, A. M., "Spread-spectrum multi-$h$ modulation," *IEEE J. Select. Areas Commun.*, vol. 8, pp. 728–742, Jun. 1990.

[73] Lee, C.-S., Vlahoyiannatos, S., and Hanzo, L., "Satellite based turbo-coded, blind-equalized 4-QAM and 16-QAM digital video broadcasting," *IEEE Trans. Broadcasting*, vol. 46, pp. 23–33, Mar. 2000.

[74] Lee, W. C. Y., "Overview of cellular CDMA," *IEEE Trans. Veh. Technol.*, vol. 40, pp. 291–302, May 1991.

[75] Leeuwin, K., Belfiore, J. C., and Kaleh, G. K., "Chernoff bound of trellis-coded modulation over correlated fading channels," *IEEE Trans. Commun.*, vol. 42, pp. 2506–2511, Aug. 1994.

[76] Li, J. and Imai, H., "Performance of hybrid-ARQ protocols with rate compatible turbo codes," in *Proc. 1st Int. Symp. on Turbo Codes and Related Topics*, (Brest, France), pp. 188–191, Sept. 1997.

[77] Li, J., Narayanan, K. R., and Georghiades, C. N., "Generalized product accumulate codes: analysis and performance," in *Proc. IEEE GLOBECOM '01*, (San Antonio, TX), pp. 975–979, Nov. 2001.

[78] Li, W., Dubey, V. K., and Law, C. L., "The performance of turbo coding over power-controlled fading channel in ka-band leo satellite systems," *IEEE Trans. Veh. Technol.*, vol. 52, pp. 1032–1043, Jul. 2003.

[79] Li, X. and Ritcey, J. A., "Trellis-coded modulation with bit interleaving and iterative decoding," *IEEE J. Select. Areas Commun.*, vol. 17, pp. 715–724, Apr. 1998.

[80] Lin, S. and Costello, Jr., D. J., *Error Control Coding - Fundamentals and Applications*. New Jersey: Prentice-Hall, 1983.

[81] Lin, S., Costello, Jr., D. J., and Miller, M. J., "Automatic repeat request error control schemes," *IEEE Trans. Commun.*, vol. 32, pp. 5–17, Dec. 1984.

[82] Lin, S. and Yu, P. S., "A hybrid ARQ scheme with parity retransmission for error control of satellite channels," *IEEE Trans. Commun.*, vol. 30, pp. 1701–1719, Jul. 1982.

[83] Lodge, J. and Moher, M., "Maximum likelihood sequence estimation of CPM signals transmitted over rayleigh flat-fading channels," *IEEE Trans. Commun.*, vol. 38, pp. 787–794, Jun. 1990.

[84] Lok, T. M. and Lehnert, J. S., "DS/SSMA communication system with trellis coding and CPM," *IEEE J. Select. Areas Commun.*, vol. 12, pp. 716–722, May 1994.

[85] Lu, B., Wang, X., and Li, Y., "Iterative receivers for space-time block-coded OFDM systems in dispersive fading channels," *IEEE Trans. Wireless Commun.*, vol. 1, pp. 213–225, Apr. 2002.

[86] Lucas, R., Bossert, M., and Breitbach, M., "On iterative soft-decision decoding of linear binary block codes and product codes," *IEEE J. Select. Areas Commun.*, vol. 16, pp. 276–296, Feb. 1998.

[87] M.1225, R., *Guideline for Evaluation of Radio Transmission Technologies for IMT-2000*. Switzerland: ITU-R, 1997.

[88] MacKay, D. J. C., "Good error correcting codes based on very sparse matrices," *IEEE Trans. Inform. Theory*, vol. 45, pp. 399–431, Mar. 1998.

[89] Mandelbaum, D. M., "Adaptive-feedback coding scheme using incremental redundancy," *IEEE Trans. Inform. Theory*, vol. 20, pp. 388–389, May 1974.

[90] McPheters, L. L., McLaughlin, S. W., and Narayanan, K. R., "Precoded PRML, serial concatenation, and iterative (turbo) decoding for digital magnetic recording," *IEEE Trans. Magnetics*, vol. 35, pp. 2325–2327, Sept. 1999.

[91] Melis, B. and Romano, G., "Application of turbo codes in the up-link of a DS-CDMA system," in *Proc. 1st Int. Symp. on Turbo Codes and Related Topics*, (Brest, France), pp. 243–246, Sept. 1997.

[92] Metzner, J. J., "Improvements in block-retransmission schemes," *IEEE Trans. Commun.*, vol. 27, pp. 525–532, Feb. 1979.

[93] MIL-STD-188-181B, *Interoperability Standard for Single-Access 5-kHz and 25-kHz UHF Satellite Communications Channels*. U.S. Department of Defense Interface Standard, Mar. 1999.

[94] Moqvist, P. and Aulin, T. M., "Serially concatenated continuous phase modulation with iterative decoding," *IEEE Trans. Commun.*, vol. 49, pp. 1901–1915, Nov. 2001.

[95] Narayanan, K. R. and Stüber, G. L., "A novel ARQ technique using the turbo coding principle," *IEEE Commun. Letters*, vol. 1, pp. 49–51, Mar. 1997.

[96] Narayanan, K. R. and Stüber, G. L., "A serial concatenation approach to iterative demodulation and decoding," *IEEE Trans. Commun.*, vol. 47, pp. 956–961, Jul. 1999.

[97] Narayanan, K. R. and Stüber, G. L., "Performance of trellis-coded CPM with iterative demodulation and decoding," *IEEE Trans. Commun.*, vol. 49, pp. 676–687, Apr. 2001.

[98] Peleg, M., Sason, I., Shamai (Shitz), S., and Elia, A., "On interleaved, differentially encoded convolutional codes," *IEEE Trans. Inform. Theory*, vol. 45, pp. 2572–2582, Nov. 1999.

[99] Perez, L. C., Seghers, J., and Costello, Jr., D. J., "A distance spectrum interpretation of turbo codes," *IEEE Trans. Inform. Theory*, vol. 42, pp. 1698–1709, Nov. 1996.

[100] Peterson, R. L., Ziemer, R. E., and Borth, D. E., *Introduction to Spread Spectrum Communications*. New Jersey: Prentice-Hall, 1995.

[101] Pfister, H. D. and Siegel, P. H., "The serial concatenation of rate-1 codes through uniform random interleavers," *IEEE Trans. Inform. Theory*, vol. 49, pp. 1425–1438, Jun. 2003.

[102] Ping, L. and Wu, K. Y., "Concatenated tree codes: a low-complexity, high-performance approach," *IEEE Trans. Inform. Theory*, vol. 47, pp. 791–799, Feb. 2001.

[103] Poltyrev, G., "Bounds on the decoding error probability of binary linear codes via their spectra," *IEEE Trans. Inform. Theory*, vol. 40, pp. 1284–1292, Jul. 1994.

[104] Qiu, X. and Chawla, K., "On the performance of adaptive modulation in cellular systems," *IEEE Trans. Commun.*, vol. 47, pp. 884–895, Jun. 1999.

[105] Richardson, T. and Urbanke, R., "The capacity of low density parity check codes under message passing decoding," *IEEE Trans. Inform. Theory*, vol. 47, pp. 599–618, Feb. 2001.

[106] Rimoldi, B., "A decomposition approach to CPM," *IEEE Trans. Inform. Theory*, vol. 34, pp. 260–270, Mar. 1988.

[107] Robertson, P., Villebrun, E., and Hoeher, P., "A comparison of optimal and sub-optimal MAP decoding algorithms operating in the log domain," in *Proc. IEEE ICC '95*, (Seattle, WA), pp. 1009–1013, Jun. 1995.

[108] Robertson, P. and Worz, T., "Bandwidth-efficient turbo trellis-coded modulation using punctured component codes," *IEEE J. Select. Areas Commun.*, vol. 16, pp. 206–218, Feb. 1998.

[109] Rowitch, D. N. and Milstein, L. B., "On the performance of hybrid FEC/ARQ systems using rate compatible punctured turbo (RCPT) codes," *IEEE Trans. Commun.*, vol. 48, pp. 948–959, Jun. 2000.

[110] Sason, I. and Shamai (Shitz), S., "Improved upper bounds on the ML decoding error probability of parallel and serial concatenated turbo codes via their ensemble distance spectrum," *IEEE Trans. Inform. Theory*, vol. 46, pp. 24–47, Jan. 2000.

[111] Sason, I. and Shamai (Shitz), S., "On improved bounds on the decoding error probability of block codes over interleaved fading channels, with applications to turbo-like codes," *IEEE Trans. Inform. Theory*, vol. 47, pp. 2275–2299, Sept. 2001.

[112] Shamai (Shitz), S. and Sason, I., "Variations on the gallager bounds, connections, and applications," *IEEE Trans. Inform. Theory*, vol. 48, pp. 3029–3051, Dec. 2002.

[113] Shannon, C. E., "A mathematical theory of communication," *Bell Sys. Technol. J.*, vol. 27, pp. 379–423 and 623–656, Jul. and Oct. 1948.

[114] Simon, M. and Divsalar, D., "Maximum-likelihood block detection of non-coherent continuous phase modulation," *IEEE Trans. Commun.*, vol. 41, pp. 90–98, Jan. 1993.

[115] Simon, M. K., Omura, J. K., Scholtz, R. A., and Levitt, B. K., *Spread Spectrum Communications*. Maryland: Computer Science, 1985.

[116] Soong, A. C. K., Oh, S.-J., Damnjanovic, A. D., and Yoon, Y. C., "Forward high-speed wireless packet data service in IS-2000 - 1xEV-DV," *IEEE Commun. Mag.*, vol. 41, pp. 170–177, Aug. 2003.

[117] Souissi, S. and Wicker, S. B., "A diversity combining DS/CDMA system with convolutional encoding and Viterbi decoding," *IEEE Trans. Veh. Technol.*, vol. 44, pp. 304–312, May 1995.

[118] Stüber, G. L., *Principles of Mobile Communication*. Boston, MA: Kluwer, 1996.

[119] Takeshita, O. Y., Fossorier, M. P. C., and Costello, Jr., D. J., "A new technique for computing the weight spectrum of turbo-codes," *IEEE Commun. Letter*, vol. 3, pp. 251–253, Aug. 1999.

[120] Tanner, R. M., "A recursive approach to low complexity codes," *IEEE Trans. Inform. Theory*, vol. 27, pp. 533–547, Sept. 1981.

[121] ten Brink, S., "Convergence of iterative decoding," *IEE Electron. Letters*, vol. 35, pp. 806–808, May 1999.

[122] ten Brink, S., "Convergence behavior of iteratively decoded parallel concatenated codes," *IEEE Trans. Commun.*, vol. 49, pp. 1727–1737, Oct. 2001.

[123] TIA/EIA, *The cdma2000 (IS-2000) Standard*. Mar. 1999.

[124] Torrieri, D. J., "Frequency hopping with multiple frequency-shift keying and hard decisions," *IEEE Trans. Commun.*, vol. 32, pp. 574–582, May 1984.

[125] Viterbi, A. J., *CDMA: Principles of Spread Spectrum Communications*. Boston, MA: Addison-Wesley, 1995.

[126] Viterbi, A. J. and Omura, J. K., *Principles of Digital Communications and Coding*. New York: McGraw-Hill, 1979.

[127] Viterbi, A. M. and Viterbi, A. J., "Improved union bound on linear codes for the input-binary AWGN channel, with applications to turbo codes," in *Proc. IEEE ISIT '98*, p. 29, Aug. 1998.

[128] Wiberg, N., *Codes and decoding on general graphs*. PhD thesis, University of Linkoöping, Sweden, Apr. 1996.

[129] Wicker, S. B., *Error Control Systems for Digital Communication and Storage*. New Jersey: Prentice-Hall, 1995.

[130] Wilson, S., Highfill, J., and Hsu, C.-D., "Error bounds for multi-$h$ phase codes," *IEEE Trans. Commun.*, vol. 28, pp. 660–665, Jul. 1982.

[131] Wilson, S. G. and Gaus, R. C., "Power spectral of multi-$h$ phase codes," *IEEE Trans. Commun.*, vol. 29, pp. 250–256, Mar. 1981.

[132] Win, M. Z. and Scholtz, R. A., "Ultra-wide bandwidth time-hopping spread-spectrum impulse radio for wireless multiple-access communications," *IEEE Trans. Commun.*, vol. 48, pp. 679–689, Apr. 2000.

[133] Wolf, J. K. and Viterbi, A. J., "On the weight distribution of linear block codes formed from convolutional codes," *IEEE Trans. Commun.*, vol. 44, pp. 1049–1051, Sept. 1996.

[134] Wu, Y. and Woerner, D., "The influence of quantization and fixed point arithmetic upon the BER performance of turbo codes," in *Proc. IEEE VTC '99 Spring*, (Houston, TX), pp. 1683–1687, May 1999.

[135] Xiong, F. and Bhatmuley, S., "Performance of MHPM in Rician and Rayleigh flat fading mobile channels," *IEEE Trans. Commun.*, vol. 45, pp. 279–283, Mar. 1997.

[136] Yamamoto, H. and Itoh, K., "Viterbi decoding algorithm for convolutional codes with repeat request," *IEEE Trans. Inform. Theory*, vol. 26, pp. 540–547, Sept. 1980.

[137] Yang, F., Leung, H., Bi, G., and Ye, M., "Concatenated trellis coding and full response CPM for wireless DS/SSMA communications," in *Proc. IEEE VTC '99 Fall*, (Amsterdam, Netherlands), pp. 2576–2580, Sept. 1999.

[138] Yiin, L. and Stüber, G. L., "Non-coherently detected trellis-coded partial response CPM on mobile radio channels," *IEEE Trans. Commun.*, vol. 44, pp. 967–975, Aug. 1996.

# VITA

Hasung Kim received the B.S. and M.S. degrees from Korea University, Seoul, Korea, in 1994 and 1996, respectively, and the Ph.D. degree from the Georgia Institute of Technology, Atlanta, Georgia, in 2004, all in electrical engineering. From 1996 to 1998, he was with research laboratories of KT (Korea Telecom), the largest telecom company in Korea, as a research engineer where he worked in the area of CDMA/W-CDMA physical layer and mobile network/switching. His research interests include coding and modulation, communication theory, spread-spectrum communications, CDMA and W-CDMA systems, radio resource management, mobile networking and switching, and radio propagation and channel modeling.